Experimental Investigations of Plasmon Induced Catalytic Reactions using TERS

Dissertation

(kumulativ)

zur Erlangung des akademischen Grades

doctor rerum naturalium (Dr. rer. nat.)

FRIEDRICH-SCHILLER-
UNIVERSITÄT
JENA

Vorgelegt dem Rat der Chemisch-Geowissenschaftlichen

Fakultät der Friedrich-Schiller-Universität

von Pushkar Singh, M. Sc. Physik

geboren am 01.12.1976 in Almora (Indien)

Gutachter:

1. **Prof. Dr. Volker Deckert, Institut für Physikalische Chemie**

2. **apl. Prof. Dr. Wolfgang Fritzsche, IPHT Jena**

Datum der Verteidigung: **04. 09. 2020**

Table of contents

1 Zusammenfassung 1

2 Research Background 7

2.1 Motivation 7

2.2 From Microscopy to Nanoscopy 8

2.2.1 Electron Microscopy 9

2.2.2 Scanning Probe Microscopy 10

2.3 Raman Spectroscopy 16

2.4 Surface Enhanced Raman Spectroscopy 18

2.5 Tip-Enhanced Raman Spectroscopy 20

2.6 Development of a new multicolor TERS setup 23

3 Research Summary 27

3.1 Plasmonic differences at the micro- and nanoscale 28

3.2 Plasmon induced protonation 31

3.3 Plasmon induced deprotonation 35

3.4 Plasmonic dissociation at single molecule level 38

3.5 References 42

4 Publications 49

4.1 Differences in single and aggregated nanoparticle plasmon spectroscopy. 49

4.2 Local protonation control using plasmonic activation 55

4.3 Plasmon induced deprotonation of 2-mercaptopyridine 61

4.4 Single molecule level plasmonic catalysis - a dilution study of p-nitrothiophenol on gold dimmers 71

4.5 Further Publications 81

4.6 Acknowledgement 83

4.7 Further Outlook 85

1 Zusammenfassung

Diese Arbeit konzentriert sich auf die Untersuchung plasmoninduzierter, katalytischer Reaktionen wie Protonierung, Deprotonierung und Dissoziation von kleinen, organischen Moleküle. Das molekulare Verständnis der chemischen Reaktionen ist sehr wichtig in Bezug auf den zugrundeliegenden Mechanismen. Zwei verschiedene Techniken, SERS und TERS, wurden eingesetzt, um Einsicht in Plasmonen-katalysierte Reaktionen zu erhalten, indem Temperatur, atmosphärische Bedingungen, pH, Konzentration, Laserwellenlänge und Laserleistung verändert wurden. Weiterhin wurde eine systematische Studie durchgeführt um zu untersuchen, ob die Anzahl der betrachteten Moleküle in SERS und TERS eine wichtige Rolle spielt. Darüber hinaus wird der Einfluss von chemischen Wechselwirkungen zwischen der Spitze und der Probe bewertet.

In dem Technik-basierten Kapitel wird die Entwicklung eines multicolor TERS-Setup vorgestellt. Bei dieser Konfiguration werden unterschiedliche Wellenlängen verwendet, um selektiv die Resonante bzw. nicht-Resonante-Raman-Streuung zu untersuchen. Ein Vergleich der Ergebnisse dieser beiden Techniken kann eine tiefere Einsicht in die molekularen Eigenschaften der untersuchten Probenspektren geben.

Unterschiede zwischen SERS- und TERS-Spektren

Mehrere Studien haben über Variationen der Bandposition und zeitabhängige Eigenschaften in TERS berichtet. Dieses Phänomen wurde auf Änderungen in der molekularen Orientierung in Bezug auf die Wechselwirkung mit der Spitze und chemische Interaktionen zwischen Spitze und Probe. Solch große Fluktuationen wurden bei SERS nie beobachtet, und bisher fehlt eine systematische Studie zum Vergleich von SERS- und TERS-Spektren. In dieser Arbeit wurde ein direkter Vergleich von Bandpositionsvariationen und der daraus folgenden Halbwertsbreiten-(FWHM) Variationen sowie der zeitabhängigen Messungen dieser beiden Techniken durchgeführt. Experimentell zeigte sich, dass für die größere Bandposition Variationen und reproduzierbar kleineren FWHM von TERS-Spektren eine viel geringere Anzahl von Molekülen in Kombination mit chemischen Wechselwirkungen zwischen der Spitze und der Probe in TERS für diese Variationen verantwortlich war.

Plasmon induzierte Protonierungsreaktion

In dieser Arbeit wurde 4-Mercaptopyridin (4-MPY) als Modellsystem für eine plasmoninduzierte Protonierungsreaktion ausgewählt. Vor der tatsächlichen TERS-Messung musste die Probe homogen auf einem passenden Substrat immobilisiert werden. Es ist weithin bekannt, dass Gold- und Silberoberflächen am besten dafür geeignet sind, da sie für die Bildung einer selbstorganisierten Monoschicht von Thiolen förderlich sind [1-3]. Im Prinzip kann die Adsorption von 4-MPY an Metalloberflächen durch drei potentielle Stellen erfolgen.Diese sindhöchstwahrscheinlich: (1) über den Schwefel, (2) über den Stickstoff oder (3) über die π-Elektronen des Rings. Die erhaltenen SERS- und TERS-Raman-Spektren bestätigten die Bildung einer chemischen Ag-S- bzw. Au-S-Bindung. Die anschließende durch Licht in Anwesenheit von Silbernanopartikeln aktiviert Protonierung von 4-MPY produziert 4-MPY^{+}-H und wurde unter Normalbedingungen mittels SERS und TERS verfolgt. Experimente unter Argon zeigen, dass als Protonenquelle entweder atmosphärischer Wasserstoff oder Wasser dient. Die Studie zeigte weiterhin, dass die Intensität des Oberflächenplasmons ein Schlüsselfaktor für die Initiierung der Protonierungsreaktion ist. Eine schnellere Protonierung unter TERS im Vergleich zu SERS zeigte, dass die Feldbeschränkung im Gap-Modus, welche durch zwei Metalloberflächen (Gold-Nanoplättchen zur Probenimmobilisierung und silberbeschichtete Spitze zur plasmonischen Anregung) erzeugt wird, zu einer zusätzlichen Verstärkung führt. Die Reaktionsgeschwindigkeit kann durch die Anregungswellenlänge (grün oder rot) sowie die atmosphärischen Bedingungen gesteuert werden.

Plasmon induzierte Deprotonierungsreaktion

In Verbindung mit den Ergebnissen der plasmoninduzierten Protonierung wurde der Einfluss der Substitutionsstelle in Pyridin auf die Protonierungssuszeptibilität untersucht. Für dieses Experiment wurde 2-Mercaptopyridin (2-MPY) gewählt. 2-MPY unterscheidet sich von 4-MPY nur durch die Position der Thiolgruppe, die nicht entgegengesetzt, sondern direkt benachbart zum Stickstoff im Pyridinring ist. Es wird gezeigt, dass das Substitutionsmodell (ortho vs. para) entscheidend für das unterschiedliche chemische Verhalten von 2-MPY und 4-MPY ist. Im Kontrast zu 4-MPY konnte eine Monoschicht von 2-MPY auf Silbernanopartikeln in SERS unter Umgebungsbedingungen nicht protoniert werden, was einer anderen Bindung von 2-MPY an die Silbernanopartikel zugerechnet wurde. Daraufhin wurde 2-MPY vor den Raman-Experimenten bei pH 1,3 protoniert und das protonierte Molekül (2-MPY + -H) wurde sodann durch Oberflächenplasmonen deprotoniert. Um Heizeffekte zu eliminieren, wurde eine temperaturabhängige Untersuchung durchgeführt, die zeigte, dass die Deprotonierungsreaktion temperaturunempfindlich war. Ähnlich wie bei der Plasmonen-induzierten Protonierungsreaktion wurde eine schnellere Deprotonierungsreaktion in TERS-Experimenten im Vergleich zu SERS beobachtet, was auf einen großen und reproduzierbaren Feldeinschluss zwischen der TERS-Spitze und der Goldoberfläche hinweist.

Plasmon induzierte Dissoziationsreaktion

In früheren Studien wurde gezeigt, dass eine selbstorganisierte Monoschicht von p-Nitrothiophenol (p-NTP) unter Eiinfluss von Oberflächenplasmonen in SERS zu 4,4-Dimercaptoazobenzol (DMAB) dimerisiert. Wenn die Konzentration jedoch niedrig genug ist, um Clusterbildung und Selbstorganisation zu verhindern, sollte der Abstand der an den Nanopartikeln adsorbierten p-NTP-Moleküle zu groß für eine intermolekulare Reaktion werden und eine Reaktion sollte nicht stattfinden. Dann muss jedes detektierte SERS-Signal von einem einzelnen oder wenigen, isolierten und nicht wechselwirkenden, getrennten Molekülen stammen. Dieses "Gedankenexperiment" wurde mit isolierten Goldnanopartikeldimeren als Substrate für die SERS-Messungen durchgeführt. Bei einer sehr niedrigen Konzentration (10^{-9} M) wurde in den folgenden SERS-Experimenten eine Dissoziation von p-NTP-Molekülen zu Thiophenol (TP) beobachtet. Außerdem deutet eine stufenförmige Änderung der Signalintensität während des Prozesses sehr stark an, dass die Dissoziationsreaktion von p-NTP zu TP auf oder nahe des Einzelmoleküllevels auftrat.

Aufbau eines mehrfarbigen TERS-Instruments

In Resonanz-Raman-Streuexperimenten sollte die Anregungswellenlänge nahe an eines erlaubten, elektronischen Übergangs des Moleküls liegen. Dieser Prozess erhöht die Streuintensität um einen Faktor von bis zu 10^6 und liefert Informationen über den angeregten Zustand. In der Standard-Raman-Spektroskopie wird eine Anregungswellenlänge gewählt, die weit von jedem elektronischen Übergang entfernt ist, und somit werden Informationen über den elektronischen Grundzustand gesammelt. Ein Vergleich der Spektren dieser beiden Techniken kann sinnvoll sein, um ein tieferes Verständnis des zu untersuchenden Moleküls zu erhalten. Dafür wurde ein Multicolor-TERS-Setup entwickelt, bei dem fünf verschiedene Laserlinien von Violett (405 nm) bis Rot (660 nm) eingebaut wurden. Insbesondere die Integration eines Strahlteilers in Form eines einzigen Doppelprismas ermöglicht einen schnellen Austausch von Anregungswellenlängen ohne die Notwendigkeit einer Laser-Justage. Dieses Element macht das System einzigartig im Vergleich zu Standard-TERS-Aufbauten.

Abstract

This thesis is focused on the investigation of plasmon induced catalytic reactions like protonation, deprotonation and dissociation of small organic molecules. The molecular understanding of chemical reactions is very important with respect to the underlying mechanisms. Two different techniques, SERS and TERS, were used to get insight into plasmon catalyzed reactions by changing temperature, atmospheric conditions, pH, concentration, laser wavelength and laser power. In addition, to explore if the number of molecules under investigation in SERS and TERS plays an important role, a systematic study was performed. Furthermore, the influence, of chemical interactions between the tip and the sample is assessed.

In the technique based chapter, the development of a multicolour TERS setup will be introduced. With such a setup, different wavelengths will be used to selectively probe the resonance and non-resonance Raman scattering, respectively. A comparison of the results from these two techniques can provide a deeper insight into the molecular properties of the investigated sample spectra.

Differences between SERS and TERS spectra

Several studies have reported signal position variations and time dependent properties in TERS. This phenomenon was attributed to changes in the molecular orientation with respect to the tip and chemical tip-sample interactions. Such large fluctuations were never observed in SERS and so far, a systematic study comparing SERS and TERS spectra is missing. In the present work a direct comparison of peak position variations and full-width-half-maximum (FWHM) variations due to the position and the time dependent measurements of these two techniques has been performed. Experimentally, the larger peak position variation and reproducibly smaller FWHM of TERS spectra indicated that a much lower number of molecules combined with chemical interactions between tip and sample in TERS was responsible for these variations.

Plasmon induced protonation reaction

In this study 4-mercaptopyridine (4-MPY) was chosen as a model system for a plasmon induced protonation reaction. Prior to the actual TERS measurement the sample had to be homogeneously immobilized on an appropriate substrate. It is commonly known that gold and silver surfaces are most suitable since they allow for the formation of a self-assembled monolayer of thiols [1-3]. In principle, the adsorption of 4-MPY on metal surfaces can occur by

three potential sites and most likely: (1) via the sulphur, (2) via the nitrogen or (3) via the aromatic π-electrons of the ring. The obtained SERS and TERS Raman spectra confirmed the formation of a chemical Ag-S and Au-S bond, respectively. The subsequent protonation of 4-MPY producing 4-MPY$^+$-H, activated by light in the presence of silver nanoparticles was monitored under ambient conditions using SERS and TERS. Experiments under argon show that the proton source was either atmospheric hydrogen or water. The study further indicated that the intensity of the surface plasmon is a key factor to initiate the protonation reaction. A faster protonation under TERS conditions compared to SERS showed that the field confinement in the gap-mode, generated by two metal surfaces (gold-nanoplates for sample immobilization and silver coated tip for plasmonic excitation) leads to an additional enhancement. The reaction turnover rate can be controlled by the excitation wavelength (green versus red) and the atmospheric conditions.

Plasmon induced deprotonation reaction

In conjunction with the results obtained in the plasmon induced protonation, the influence of the substitution site in pyridine on the protonation susceptibility was monitored. For this experiment 2-mercaptopyridine (2-MPY) was chosen. 2-MPY differs from 4-MPY only by the thiol group position, which is not opposite but directly adjacent to the nitrogen in the pyridine ring. It will be demonstrated that the substitution pattern (ortho vs. para) is decisive for the different chemical behaviour of 2-MPY and 4-MPY. In contrast to 4-MPY, a monolayer of 2-MPY on silver nanoparticles could not be protonated in SERS under ambient conditions, which was ascribed to a different binding of 2-MPY on the silver nanoparticles. Consequently, prior to Raman experiments, 2-MPY was protonated at pH 1.3 and the protonated molecule (2-MPY$^+$-H) was deprotonated by surface plasmons. To eliminate heating effects, a temperature dependent study was performed which indicated that the deprotonation reaction was temperature insensitive. Similar to the plasmon induced protonation reaction, a faster deprotonation reaction in TERS experiments compared to SERS was observed pointing to a large and reproducible field confinement between the TERS tip and the gold surface.

Plasmon induced dissociation reaction

In previous studies, it was found that a self-assembled monolayer of p-nitrothiophenol (p-NTP) dimerizes to 4, 4-dimercaptoazobenzene (DMAB) under surface plasmon conditions in SERS. However, if the concentration was low enough to prevent clustering and self-assembly, the distance of p-NTP molecules adsorbed on the nanoparticles should become too large for an intermolecular reaction and a reaction should not occur. Then, any detected SERS signal must originate from a single or only a few isolated and non-interacting separated molecules. This “Gedankenexperiment” was realized using isolated gold nanoparticle dimers as substrates for the

SERS measurements. At a very low concentration (10^{-9} M) in the following SERS experiments a dissociation of p-NTP molecules to thiophenol (TP) was observed. In addition, a step-like signal intensity change during the process strongly indicates that the dissociation reaction of p-NTP to TP occurred at or close to a single molecule level.

Setting up a multicolor TERS instrument

In resonance Raman scattering experiments, the excitation wavelength should be close to an allowed electronic transition of the molecule. This process increases the scattering intensity up to 10^6 and provides information about excited state modes. In standard Raman spectroscopy an excitation wavelength far away from any electronic transition is chosen and hence information about ground state modes is collected. A comparison of the spectra from these two techniques can be useful to gain a deeper understanding of the molecule under investigation. For this purpose, a multicolor TERS setup was developed where five different lasers lines ranging from violet (405 nm) to red (660 nm) were incorporated. Particularly, the integration of a single double prism based beam splitter allows for a quick exchange of excitation wavelengths without the necessity of laser realignment. This element renders the system unique compared to standard TERS setups.

2 Research Background

2.1 Motivation

Surface plasmons are collective oscillations of conduction electrons generated by the interaction of light with metal nanoparticles (NPs) that are smaller than the incident wavelength. Metallic nanoparticles possess unique optical, mechanical, electrical and chemical properties and the most active ones for catalysis are those with defined edges, pointed corners and rough surfaces. The generation of surface plasmons by irradiation of nanoparticles with a wavelength matching the resonance (=absorption maximum) leads to a huge enhancement of the local electromagnetic field. Consequently, Raman signals of molecules, which are in close vicinity to the nanoparticles, experience a strong enhancement being the basis of surface-enhanced Raman scattering (SERS) and tip-enhanced Raman scattering (TERS). In this way the sensitivity of Raman spectroscopy is drastically increased and only concentration $<< 10^{-1}$ M is needed to obtain chemical information of a material. In contrast to SERS, which does not allow for an analysis with high spatial resolution, TERS can resolve nanometre and sub-nanometre features. TERS is the combination of Raman spectroscopy with scanning probe microscopy (SPM). In TERS, sample molecules are not directly adsorbed on the gold or silver nanoparticles but they are fixed on an inert substrate and scanned with a nanoparticle coated AFM tip. In such a configuration the enhancement of vibrational modes is confined to molecules directly beneath the tip apex providing a much higher spatial resolution compared to SERS. Both SERS and TERS are also very efficient techniques tools to investigate plasmon driven chemical reactions.

A chemical reaction is defined by the breakage / formation of bonds yielding one or more products. In many cases this process requires an external physical trigger like e. g. heat. Reactions can be carried out under mild conditions if an appropriate catalyst for the reaction system can be found. Typically, a catalyst decreases the activation barrier that has to be overcome to initiate a chemical reaction. In this context, plasmon driven chemical reactions have recently attracted attention from different scientific and engineering communities. Current results in this field are promising for the development of a new platform for chemical syntheses. Different catalytic reactions have been investigated involving surface plasmons but a detailed study of some simple reactions like protonation, deprotonation or dissociation has not been reported.

The first plasmon induced catalysis reaction was reported in 2010. A monolayer of p-aminothiophenol (p-ATP) on a SERS substrate was dimerized to 4,4-dimercaptoazobenzene (DMAB) when irradiated with 532 nm [4, 5]. Later in 2011, it was demonstrated that p-

nitrothiophenol (p-NTP) likewise reacts to DMAB when activated by surface plasmons [6, 7]. Such plasmon catalyzed reactions can also be carried out under TERS conditions under vacuum conditions as well as in an ambient [8, 9]. These studies reveal that plasmonic nanostructure opens a way to concentrate and transfer the energy of visible light to adsorbed molecules, hence, offering a route to control the reaction selectivity and to accelerate the reaction rate.

These results motivate the investigation of further chemical reactions and specifically the influence of environmental conditions. In particular, the effect of different excitation wavelengths, temperatures and sample concentrations is of interest. Another appealing aspect in this context is the comparison of TERS and SERS: does the confined field at the tip apex give the activation energy an extra boost? Previous studies have demonstrated that TERS and SERS do not only differ by the spatial resolution but also in peak position and full-width-half-maximum. A part of the following work is focused on the direct comparison of these techniques to gain a deeper understanding of the underlying mechanisms.

The information about the excited and ground state modes of a molecule can be accessed by selecting the laser wavelength close (resonance) and far away (off-resonance) from any electronic transition, respectively. Despite the very small Raman signal intensity if the selected wavelength is far away from any electronic transition it still provides specific information about ground state molecules. A direct comparison of the spectra from these two techniques on the same molecule can yield further insight into the molecular system. Furthermore, a combination of SERS/TERS and resonant molecular excitation increases the detection limit and the information at single molecule level should be accessible.

2.2 From Microscopy to Nanoscopy

In 1873 Ernst Abbe, a German physicist discovered that the spatial resolution of an optical instruments is limited by the wavelength of the light. This discovery revealed that the resolution of a microscope is not limited by the instrument's quality alone but by the wavelength of the light [10]. This means an optical microscope cannot resolve two objects which are located closer than

$$d = \frac{\lambda}{2 \cdot NA}$$

where λ is the wavelength of the incident light, NA is the numerical aperture of the imaging system and d is the resolution. Using modern optics in air, one can achieve a NA ≈ 1.0 and thus the Abbe limit is roughly half the wavelength of light used to image the sample. To increase the resolution, light with shorter wavelengths (X-ray, UV or gamma rays) can be used but these

sources are expensive and can destroy the sample. An immersion oil system can be used to increase the NA≈1.6.

2.2.1 Electron Microscopy

Electron microscopes were developed to overcome the limitations of light microscopes. An electron microscope uses a beam of electrons to image the sample. In the 1920s an analogy between light and electrons was discovered that accelerated electrons in the vacuum behave similar to light [11]. It was also found that electric and magnetic fields can be used to focus the electron beam similar to focusing a light beam using a glass lens.

In 1923, Louis de Broglie [12], a French physicist, discovered that electrons behave like a particle as well as a wave and found a direct relation between the wavelength of a massive particles and its velocity as

$$\lambda = \frac{h}{mv}$$

where λ is the de Broglie wavelength, h is Plank's constant, m is the mass and v is the velocity of a massive particle. The faster the electron travels, the shorter is the de Broglie wavelength and the higher is the spatial resolution. Since the size of electrons is very small and easily deflected by gaseous molecules, it is necessary to operate electron microscopes under vacuum. Despite the very high lateral resolution (in x and y-direction) electron microscopes do generally not provide height information. Depending on the transmission or scattering of electrons from the sample, transmission electron microscope (TEM) and scanning electron microscope (SEM) were developed.

Transmission Electron Microscope (TEM)

The first transmission electron microscope was developed my Max Knoll and Ernst Ruska in 1931 [13]. In TEM an electron gun generates a beam of electrons, which is accelerated by applying a voltage and focused using multiple electromagnetic lenses. The focused beam of electrons interacts with the ultra-thin sample while transmitted. Some parts of the sample allow the passing through of all incident electrons while others absorb some or all electrons. Thus, depending on how the electron beam is affected by the sample, an image on a fluorescent screen or charged coupled device (CCD) camera is formed.

TEM enables an imaging at a significantly higher resolution than light microscopes due to the small de Broglie wavelength of electrons, which renders it an excellent tool in nanotechnology,

material science, medical and biological research. Despite the very high resolution of TEM technique, it has a number of drawbacks like extensive sample preparation, which makes it relatively time consuming and the restriction to transparent and, hence, thin samples (typically below 200 nm). Furthermore, there is a high probability of sample damage by the electron beam, particularly for biological samples.

Scanning Electron Microscope (SEM)

The scanning electron microscope was invented in 1937 by Manfred von Ardenne to characterize the surface of a sample using an electron beam [14, 15]. In SEM the electron beam generated from an electron gun is accelerated and focused using electromagnetic lenses before it interacts with a conductive sample or a metal coated surface (for non-conductive samples). The interaction of high energy electrons with a solid sample generates secondary electrons, which are used for imaging of the surface topography. As a result, SEM can achieve a spatial resolution better than 1 nm.

SEM is a very important tool in a variety of fields that require the characterization of solid materials like geology, forensic and crystallography. Compared to TEM this technique only needs minimum sample preparation but has many drawbacks like e.g. the restriction to solid samples. To overcome the drawbacks of electron microscopy, scanning probe microscopy (SPM) was developed.

2.2.2 Scanning Probe Microscopy

The scanning probe microscopy (SPM) technique images surface structures with atomic resolution without damaging the sample. There are basically two main types of SPM microscopes: scanning tunnelling microscope (STM) and atomic force microscope (AFM). In STM and AFM an image is recorded by mechanically moving a tip (radius about 10 nm) as a sensor close to the surface in lines across the sample. Depending on the instrument, either the sample or the tip can be moved. Compared to electron microscopes, SPM can be also performed under ambient conditions and provides height information with very high resolution.

Scanning Tunneling Microscope (STM)

The development of scanning tunneling microscope (STM) by Gerd Binnig and Heinrich Rohrer in 1981 [16, 17] has revolutionized surface science as it provides the ability to investigate

conductive samples on the atomic-scale. STM can provide topographic image with sub-nanometer lateral resolution and thus became an important tool for surface characterization. STM uses a sharp conducting tip with a bias voltage between tip and sample. Electrons start to tunnel for typical tip-sample separation below 1 nanometer. The tunneling current varies exponentially with tip-sample distance is the origin of a remarkable sensitivity of this technique. However, an inherent restriction of STM technique is the requirement of a conducting sample.

Atomic Force Microscope (AFM)

To overcome the limitations of STM, Gerd Binnig and co-workers developed the atomic force microscope in 1986 [18]. A standard AFM uses laser beam deflection from the cantilever to image the sample topography. In this technique, the interaction forces between the sample and the tip (radius about 10 nm) is monitored by deflection of the laser beam from the back side of cantilever. When the tip is brought close to the surface, tip-sample interaction forces lead to a deflection of the cantilever which is detected on a 4-quadrant position sensitive detector as shown in figure 1. The signal on the photodiode is used as a feedback signal to adjust the cantilever position (along z-direction) while the tip is scanned across the sample in x and y-direction to image the topography. There are also other ways to detect the cantilever deflection, e.g. a tuning fork cantilever, made of piezoelectric material where the electrical signal is generated by the mechanical deformation of the cantilever[19, 20].

There are different forces which contribute to the deflection of the AFM cantilever during tip-sample interactions. The most crucial are van-der-Waals forces. There are also short-range chemical forces, which depend on the distance between tip and surface and the chemical nature of both. The interaction potential between the tip and the sample can be described by a simple Lennard-Jones potential model [21], which approximates the interaction between a pair of neutral atoms or molecules by the following equation

$$V = \frac{A}{r^{12}} - \frac{B}{r^{6}}$$

where A, B are constants and r^{-6} is the attractive long-range term, describing attractions at larger distances. r^{-12} is the repulsive term describing the short-range Pauli repulsion due to overlapping of electron orbitals. Figure 2 shows the tip-sample interaction force depending on their separation. Depending on the operating region of the AFM either repulsive or attractive force, operating modes can be roughly defined as static and dynamic.

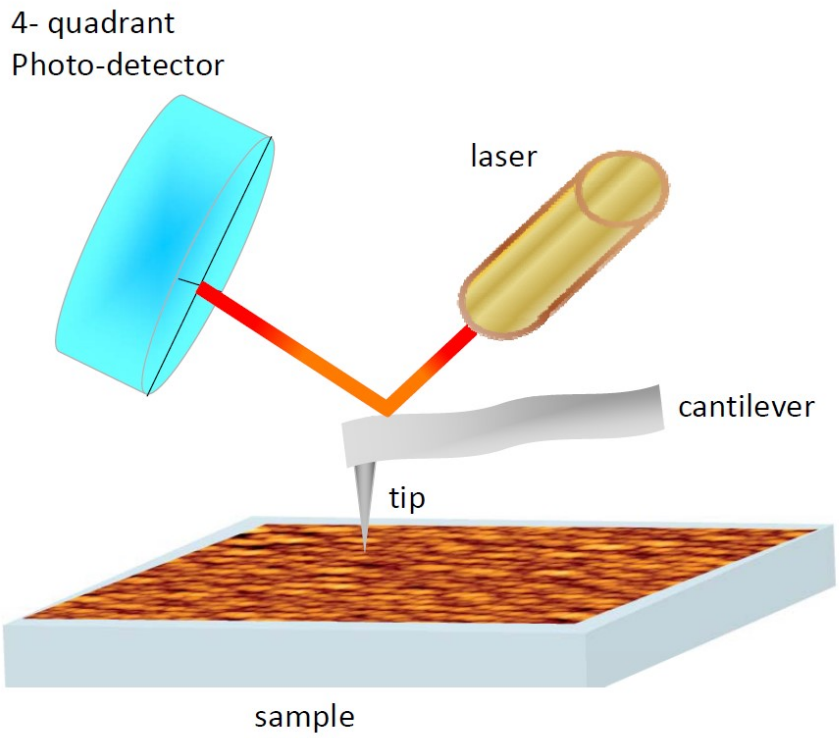

Figure 1: A sketch of the basic components of an AFM. The tip-sample interaction forces lead to a change in the deflection of the laser beam from the cantilever. The deflected laser beam from the back side of the cantilever is monitored on a 4-quadrant position sensitive detector.

Static or Contact mode: In this mode, an AFM tip has a soft physical contact with the sample and is operated in the repulsive region. In the contact mode a soft cantilever with stiffness lower than the measured surface is used and the contact force causes a bending of the cantilever. In the repulsive force region as shown in figure 2 (purple highlighted), the slope of the force is large thus the cantilever bends rather than forcing the tip atoms closer to the sample atoms. A constant cantilever deflection is maintained by selecting a setpoint where the force between the tip and the sample remains constant. The bending of the cantilever is detected using the reflected laser spot from cantilever on a photo diode. The sample under the tip is scanned in x and y-direction and the features on the sample surface changes the cantilever deflection and thus the laser spot position on the detector. This position change information is sent to a feedback loop. The feedback loop moves the sample in z-direction to restore the spot to its original position. The height image formed by an AFM is a plot of distances moved along x and y-direction and corrections made along z-direction. The high scanning speed and high (atomic) resolution images obtained in this mode makes it attractive [22, 23]. It is generally observed that in contact mode, the tip/sample quality degrades over time as the tip is always in contact with the hard/soft sample so soft cantilever with spring constant between 0.001 to 10 N/m are used.

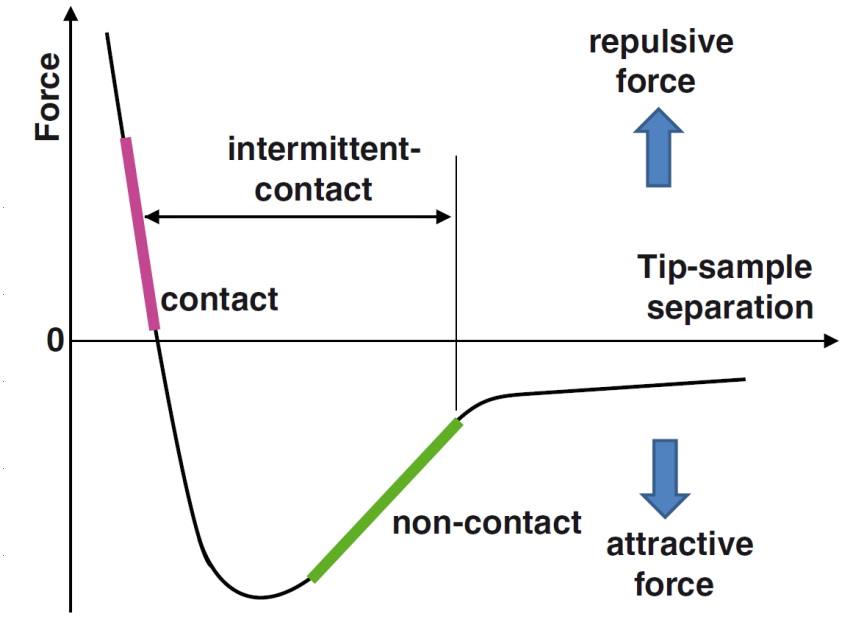

Figure 2: Force-distance curve between tip and sample which are approximated by a Lennard-Jones potential. In contact mode (purple), the tip is always in contact while in noncontact mode (green), it does not make any contact with the sample surface. The intermittent contact is located between the contact and the non-contact mode, here the tip oscillates at or near its resonance frequency and can make a very gentle contact with the surface during each oscillation.

Dynamic mode: Due to the problem of tip/sample degradation during the contact mode, an AFM can also be operated with a vibrating cantilever the so-called dynamic mode. There are two major techniques of dynamic AFM modes: the non-contact and the tapping/intermittent contact mode. A non-contact mode is normally used in the vacuum where the interaction forces between the tip and the sample is extracted by directly measuring the change in resonance frequency using frequency modulation technique [24, 25]. In this mode, a tip-sample separation with oscillation amplitude of the tip below 10 nm is used and an AFM is operated in the attractive force region (green in figure 2). In addition, cantilevers should be stiffer than those used in contact mode since soft cantilever can be pulled into contact with the surface. The stiff cantilever and small interaction force between the tip and the sample makes it difficult to measure the non-contact signal at ambient conditions. Thus, vacuum environment is preferred to achieve higher sensitivity which allows the measurement of much weaker forces. In this technique a change in the resonance frequency of the cantilever due to tip-sample interaction is measured using a phase-locked loop feedback.

The intermittent contact mode force regime is located between non-contact and contact mode in figure 2 and is used at ambient conditions. Here, a change of the oscillation amplitude is measured at a particular frequency using amplitude modulation technique [18, 26]. In the dynamic mode a stiff cantilever with a spring constant between 10 and 100N/m oscillates near its resonance frequency (typically 100-400 KHz).

In this work, all the experiments were performed in the tapping mode. In this mode, the cantilever oscillates with large oscillation amplitudes up to few tens of nanometers. If the selected frequency is smaller than the resonance frequency as shown in figure 3**,** this leads to a repulsive imaging regime [27, 28]. In this regime, the resonance frequency of the cantilever increases and the amplitude decrease as the tip is brought close to the surface and thus may hit or "tap" the sample. The decrease of the oscillation amplitude is used as a feedback signal by selecting a setpoint about 50% of the amplitude of the free oscillation for AFM imaging while during TERS experiments a setpoint of about 80% is used. Decreasing the amplitude setpoint increases the tip-sample interaction forces and thus the AFM tip taps harder on the surface. Typically, stiff cantilevers are used to avoid the sticking of the tip to the intrinsic water layer under ambient conditions. The advantage of this mode compared to the contact mode is the reduced applied force on the sample, thus can be used to image soft biological samples. Under ambient conditions normally amplitude modulation technique is used and a lock-in-amplifier provides the feedback control.

A lock-in amplifier [29] is used to extract amplitude and phase information from the measured position sensitive photodiode signal, the phase information can be used to identify different materials due to different stiffness and adhesion properties. The measured photodiode response (r) of an oscillating cantilever with a sinusoidal function $A\cos(\omega t)$, its higher harmonics and noise can be written as

$$r(t) = A\cos(\omega t - \varphi) + \text{higher harmonics+noise} \qquad (1)$$

where A is the oscillation amplitude, ω is the oscillation frequency, φ is the phase and t is the time. To extract the amplitude and phase information from the measured photodiode response, equation (1) is multiplied with $\cos(\omega t)$ as

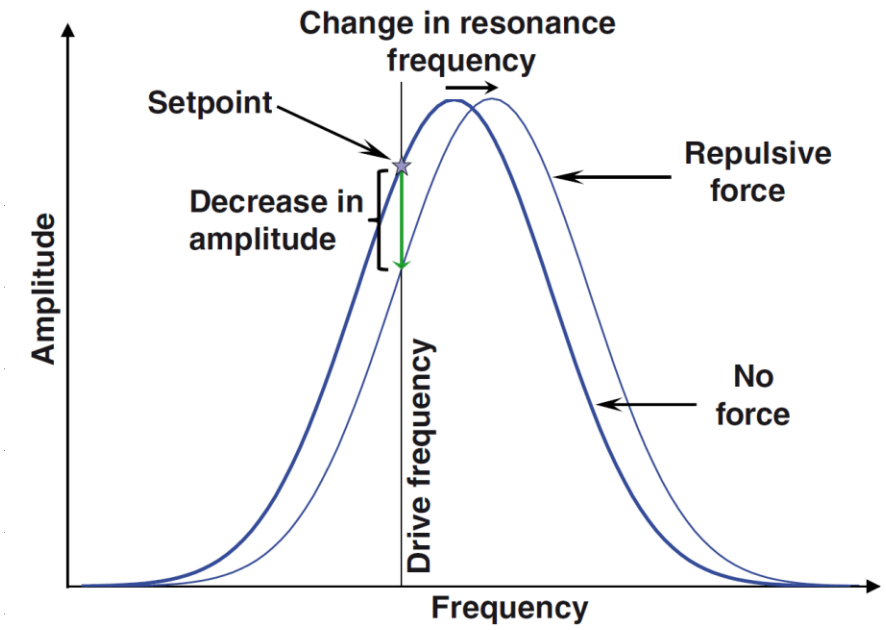

Figure 3: Operating region of the intermittent contact mode AFM. The free oscillation of the tip is shown in dark blue (No force) and the tip oscillation influenced by the sample is shown in light blue (Repulsive force). The setpoint is selected on the left side of the maximum and the decrease of the amplitude is used as a feedback signal.

$$r(t)\cos(\omega t) = A\left[\cos(\omega t)\cos(\varphi) + \sin(\omega t)\sin(\varphi)\right]\cos(\omega t) + \cos(\omega t) + \text{higher harmonics+noise}$$

$$= A\{\cos^2(\omega t)\cos(\varphi) + \cos(\omega t)\sin(\omega t)\sin(\varphi)\} + \cos(\omega t) + \text{ higher harmonics+noise}$$

$$= \frac{A}{2}\left[\{1+\cos 2(\omega t)\}\cos(\varphi) + \sin(2\omega t)\sin(\varphi)\right] + \cos(\omega t) + \text{ higher harmonics+noise}$$

$$= \frac{A}{2}\cos(\varphi) + \frac{A}{2}\cos(2\omega t)\cos(\varphi) + \frac{A}{2}\sin(2\omega t)\sin(\varphi) + \cos(\omega t) + \text{ higher harmonics} + \text{noise} \qquad (2)$$

Similarly multiplying equation (1) with $\sin(\omega t)$ gives

$$r(t)\sin(\omega t) = \frac{A}{2}\sin(\varphi) + \frac{A}{2}\sin(2\omega t)\cos(\varphi) + \frac{A}{2}\cos(2\omega t)\sin(\varphi) + \cos(\omega t) + \text{ higher harmonics} + \text{noise} \qquad (3)$$

To filter out the non-zero frequency components and noise from equation (2) and (3), these equations are integrated over the time, called lock in time (t_{lock}). The obtained signals are

$$S_x = \frac{2}{T_{lock}} \int_0^{t_{lock}} r(t)\cos(\omega t)dt = A\cos(\varphi)$$

$$S_y = \frac{2}{T_{lock}} \int_0^{t_{lock}} r(t)\sin(\omega t)dt = A\sin(\varphi)$$

From these signals (S_x and S_y) one can directly calculate the amplitude and phase as

$$A = \sqrt{S_x{}^2 + S_y{}^2} \qquad \text{and} \qquad \varphi = \tan^{-1}(S_y / S_x)$$

The time constant of lock-in amplifier should be large to effectively remove the noise and other frequencies.

2.3 Raman Spectroscopy

The Raman effect was discovered in 1928 by the Indian physicist, C. V. Raman [30]. This pioneering discovery made him the Nobel Prize winner of Physics in 1930. Raman spectroscopy is an excellent tool for chemical analysis, which allows the identification of the vibrational states of molecules, hence it can be used to assign molecular fingerprints and molecular structures [31-36]. In Raman spectroscopy, the laser interacts with sample molecules and its deformation due to electric field strength induces a dipole with the dipole moment P

$$P = \alpha E$$

where α is the molecular polarizability and E is the electric field strength. The oscillating electric field can be written as

$$E = E_0 \cos(2\pi\nu_0 t)$$

where E_0 is the vibrational amplitude, t is the time and ν_0 is the frequency of the laser oscillation. The physical displacement dq of the atoms about their equilibrium position due to a particular vibrational mode may be expressed as

$$dq = q\cos(2\pi\nu_m t)$$

where q is the maximum displacement and ν_m is the frequency of the mode. For small displacements, the polarizability may be approximated by a Taylor series expansion as

$$\alpha = \alpha_0 + q\left(\frac{\partial \alpha}{\partial t}\right)_{q=0} + \text{----------}$$

where α_0 is the polarizability of molecular mode at equilibrium position and q is the displacement of atoms. The selection rule for a Raman-active vibration states that there should be a change in the polarizability ($\partial\alpha/\partial t \neq 0$). Substituting the time dependence of E and q, the dipole moment can be written as

$$P = \alpha E = \left(\alpha_0 + q\cos(2\pi\nu_m t)\left(\frac{\partial \alpha}{\partial t}\right)_{q=0}\right)E_0\cos(2\pi\nu_0 t)$$

$$= \alpha_0 E_0\cos(2\pi\nu_0 t) + q_0 E_0\cos(2\pi\nu_0 t)\cos(2\pi\nu_m t)\left(\frac{\partial \alpha}{\partial t}\right)_{q=0}$$

$$= \alpha_0 E_0\cos(2\pi\nu_0 t) + \frac{q_0 E_0}{2}\left(\frac{\partial \alpha}{\partial t}\right)_{q=0}\left[\cos\left(2\pi(\nu_0 - \nu_m)t\right) + \cos\left(2\pi(\nu_0 + \nu_m)t\right)\right]$$

The first term in the equation corresponds to the Rayleigh scattering with no change in frequency while the term with a red-shifted frequency ($\nu_0 - \nu_m$) is called Stokes scattering and the term with blue-shifted frequency ($\nu_0 + \nu_m$) is called anti-Stokes scattering as shown in figure 4.

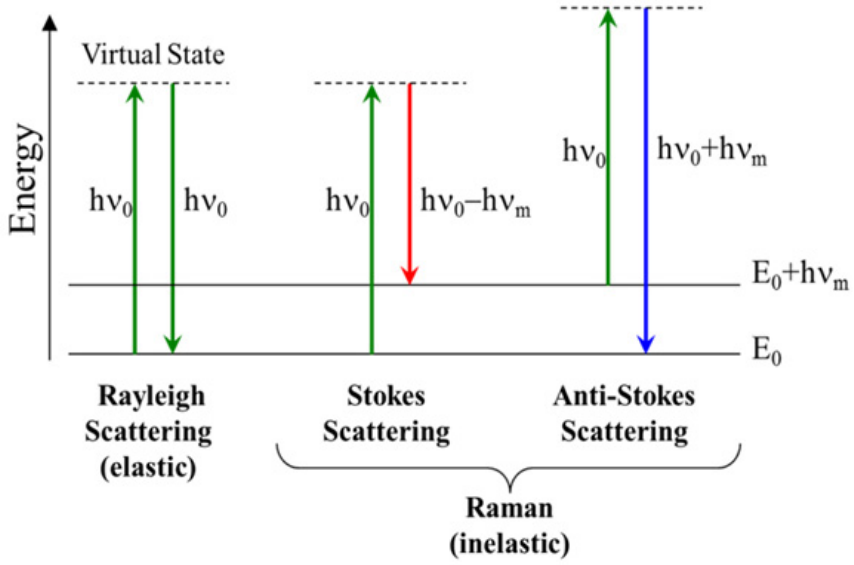

Figure 4: Schematic diagram of energy transitions in Rayleigh and Raman scattering.

The Raman effect is very weak since only one out of 10^7 photons is Raman scattered. The Stokes Raman signal is many orders of magnitude weaker than the Rayleigh signal so it is very important to filter out the Rayleigh signal using a notch filter or a long pass filter before it enters the spectrometer. The Raman shift ($\tilde{\nu}$) between incident and scattered photon is numerically calculated in wavenumbers (cm^{-1}) using the relation

$$\tilde{\nu} = \frac{1}{\lambda_{incident}} - \frac{1}{\lambda_{scattered}}$$

where $\lambda_{incident}$and $\lambda_{scattered}$ are the incident and scattered wavelengths, respectively. The intensity of Raman scattered light (I_s) is proportional to the product of incident photons intensity (I_0) and Raman differential scattering cross-section (σ_{Raman}).

$$I_s \propto I_0 \sigma_{Raman}$$

The Raman differential scattering cross-section varies with the fourth power of the excitation wavelength as

$$\sigma_{Raman} \propto \left(\frac{1}{\lambda_{incident}} - \frac{1}{\lambda_{scattered}} \right)^4$$

Thus, ideally a high intensity laser with shorter wavelength should be used to increase the intensity of the scattered Raman signal. However, if a laser in the ultraviolet (UV) region is used, fluorescence can dominate where absorbed photons undergo internal conversion, and are subsequently re-emitted at longer wavelengths. The fluorescence signal may interfere with the Raman scattered signal. Furthermore, higher laser intensities cannot be applied to biological samples as it can cause degradation. Thus, Raman experiments are normally performed with continuous wave (CW) lasers in the visible region either with 532 or 632 nm.

2.4 Surface Enhanced Raman Spectroscopy

Surface Enhanced Raman Spectroscopy (SERS) was accidently discovered in 1974 [37] when researchers were trying to use rough metal electrodes with a large surface area to study Raman spectroscopy. In 1977, two different groups have realized that not the surface itself but the rough nanostructure of the metal surface is the key to enhance a Raman signal [38, 39]. In SERS, molecules are adsorbed on a rough metal surface (normally silver and gold) with nanoscale roughness, which enhances the intensity of a Raman signal by many orders of magnitudes and thus overcome the low sensitivity of conventional Raman spectroscopy.

Noteworthy, that the specificity of Raman spectroscopy is maintained. SERS spectra can differ from conventional Raman spectra mainly due to two effects: 1) Specific orientation of molecules on the surface which changes the surface selection rules and 2) wavelength dependent plasmon resonances which depend on the shape and size of the nanoparticles. The wavelength dependence can lead to an amplification of different spectral regions of the spectrum. Hence, it might be possible that modes that are visible in conventional Raman spectrum disappear and new bands are visible in SERS spectra. There are two mechanisms contributing to the signal enhancement in SERS: 1) Electromagnetic enhancement and 2) chemical enhancement. The total enhancement of the SERS signal is the product of both mechanisms [40-43].

The electromagnetic enhancement mechanism provides a large part of the overall enhancement and for SERS an enhancement as high as 10^{14} is reported [44]. In SERS, a collection of nanoparticles is excited by the incident laser radiation. The dipole oscillation of individual nanoparticle couples generating normal mode oscillations. The collective excitation covers a wide range of frequencies from visible to near infrared depending on the nanoparticles shape, size and metal. Figure 5 shows the schematic enhancement mechanism of the incident electromagnetic field induced by the collective oscillation of conduction band electrons which amplifies the scattered Raman signal. The excitation is not uniform over the whole surface but forms spatially localized areas called "*hot spot"* [45-47]. The size of a "*hot spot"* can be very small (some nanometres) and its position depends on wavelength and polarization of incident field and geometry of nanoparticles.

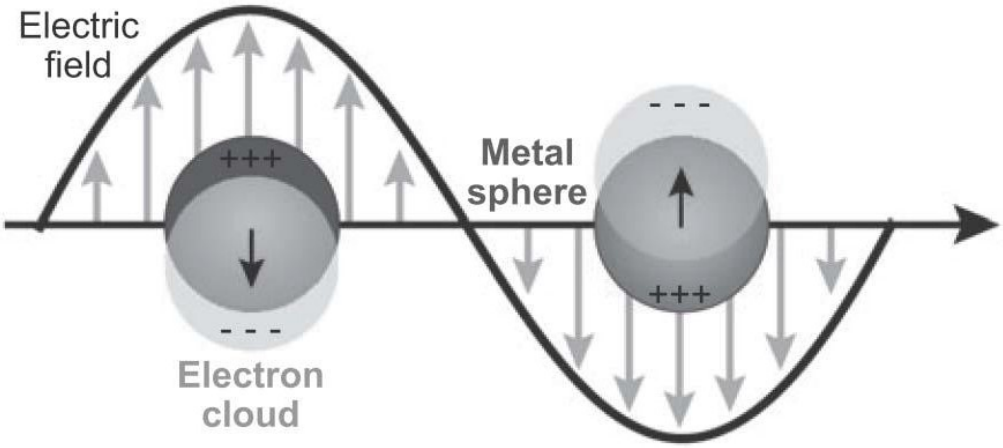

Figure 5: Collective oscillation of free electrons in metal nanoparticles which enhances the incident electromagnetic field.

As mentioned above, the electromagnetic enhancement is not the only enhancement mechanism in SERS. Otherwise there should be the same strong signal enhancement for all molecules which are brought in close vicinity to the nanostructures. Experimentally some molecules like methanol do not show any SERS enhancement while its normal Raman spectrum is significant [44, 48]. These observations indicate that an additional enhancement mechanism must exist which depends on the chemical behavior of the molecule and is called “chemical enhancement”. This effect is the origin of different changes observed in the SERS spectrum like band position shift, fluctuation in the relative band intensities etc.

2.5 Tip-Enhanced Raman Spectroscopy

A major development of the SERS technique to investigate nanoscale features is tip-enhanced Raman spectroscopy (TERS), which was proposed in 1985 by Wessel [49] and experimentally realized by Stöckle et. al. in 2000 [50]. Other groups followed promptly [51, 52]. The physical mechanism behind TERS is the same as in SERS. The technical difference is the usage of a special scanning probe tip instead of rough metal electrodes, films or colloids. This nanoparticle coated (gold or silver) tip acts as a plasmonic antenna. Incident radiation induces the collective oscillation of conduction band electrons, so called localized surface plasmons (LSP) which produce a highly enhanced electromagnetic field near the tip apex. This tip with an apex of radius about 10 nm allows not only a large Raman signal but also a nanometer spatial resolution. In the laboratory TERS is realized by mounting a scanning probe microscopy (SPM) on a Raman microscope. Two distinct SPM techniques namely, atomic force microscopy (AFM) and scanning tunneling microscopy (STM) are used to exploit the TERS effect [8, 53-57]. There are mainly three types of TERS configurations experimentally realized.

Bottom illumination: In this configuration, a SPM placed on top of an inverted microscope is illuminated from below and the laser beam is focused using a high numerical aperture (1.2-1.6). The generated Raman signal is collected through the same objective in back-reflection. This configuration eliminates the laser beam shadowing of the cantilever. The major drawback in this case is that only transparent samples can be measured. The first AFM based TERS setup [50] was based on bottom illumination configuration. Generally, an oil immersion objective is used to increase the illumination/collection efficiency and to ensure a high signal-to-noise ratio. This geometry is mostly used to investigate biological samples. Figure 6 shows schematically a bottom illuminated TERS setup as it was used in this work.

Side illumination: In this configuration, a SPM tip is illuminated from the side after focusing the laser beam through a long working distance objective with lower numerical aperture (< 0.6). The Raman signal can be collected through the same objective from the side. In this configuration opaque samples become accessible. In case of STM-TERS, generally the side

illumination configuration is preferred, since the required conductive substrate is not transparent [56, 58].

Top illumination: In this configuration, a SPM tip is illuminated by focusing the laser beam from top using a higher numerical aperture (~ 0.7) objective compared to the side illumination setup. The scattered light is collected through the same objective from the top. This configuration can also be used to measure opaque samples. In this configuration the tip is located between objective and laser focus and hence the cantilever will block (shadowing) a part of the light either for excitation and signal detection [59, 60].

The preparation of active and long lasting tips is a very important step in TERS, since shape, size and material of the tip determines the field enhancement and the spatial resolution [54, 61-64]. The generation of strong plasmonic resonances in noble metals (silver and gold) nanoparticles in the visible region renders them a suitable material for TERS tips. Metal coated TERS tips are commonly prepared by evaporation [50] or solid metal tips are prepared by electrochemical etching of a thin metal wire [58]. STM-TERS uses both gold and silver tips, depending on the excitation wavelength. In AFM-TERS silver coated tips are preferably used, even though these tips are easily oxidized in air but have better optical properties than gold tips. The optimum plasmonic enhancement of silver nanoparticles is at shorter wavelengths compared to gold, this provides an additional benefit of stronger Raman intensities as it depends strongly on the incident wavelength and is proportional to λ^{-4}.

TERS has been used to measure a variety of samples such as biological, chemical as well as semiconductors [53, 65-67]. Experiments on a single strand RNA have demonstrate the ability of TERS to distinguish nucleobases in the spectra and are promising with respect to single molecular sequencing [68]. The simultaneous acquisition of topography and TERS spectra is used to study the basic properties of carbon-nanotubes (CNT) [60, 69, 70]. TERS is also used to detect different plasmon induced catalytic reaction like dimerization, dissociation, decarboxylation [8, 9, 71, 72] and also for single molecule detection [73-75]. Recently TERS technique has revealed a much higher spatial resolution in sub-nanometre [54, 61, 62].

Performing a TERS experiment is straightforward but there are different challenges associated with the experimental implementation and interpretation of the measured spectra. The reproducibility of TERS experiments is a major concern and requires stable experimental parameters (e.g. temperature) but also the quality of the tip plays a major role and needs to be carefully controlled. Different techniques are used to achieve this task [76-81], however, a precise control of the tip shape remains difficult and renders the comparison of TERS experiments performed on different setups not straightforward. The physical background of the high signal-enhancement mechanism and the (sub-) nm spatial resolution is not fully understood, yet. Recent results reporting 0.5 nm spatial resolution by imaging a single molecule [61, 62] have sparked

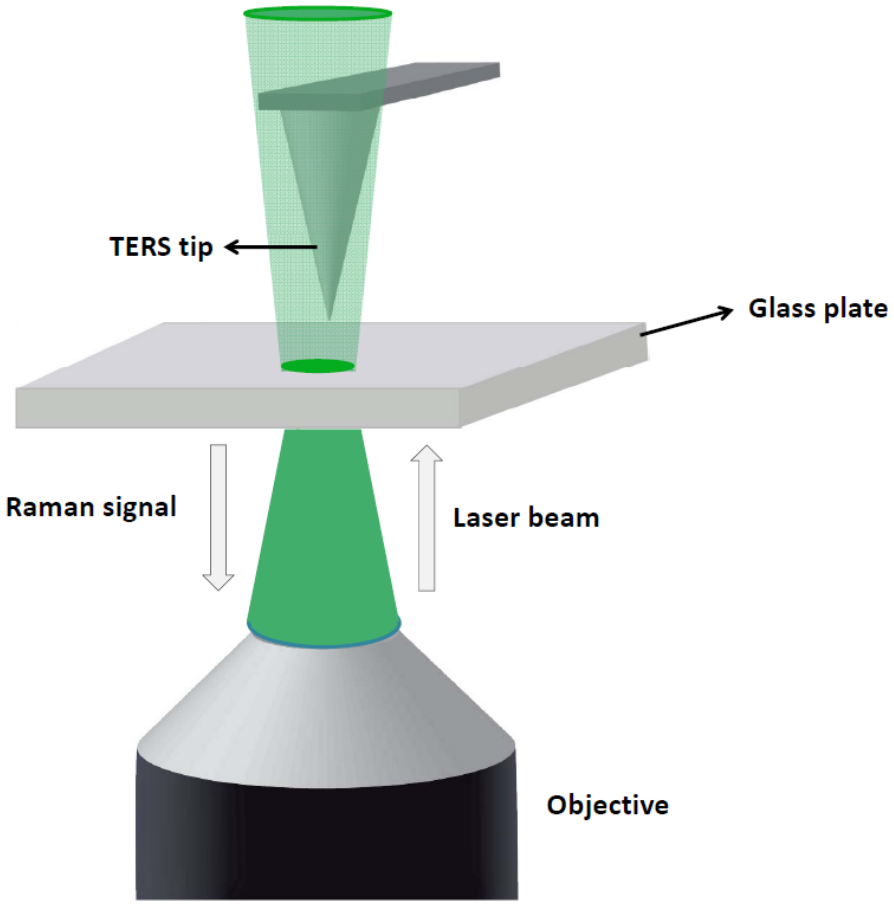

Figure 6: Schematic diagram of a bottom illuminated tip-enhanced Raman scattering setup. A high numerical aperture objective enables a high signal collection with high efficiency.

the debate on the contribution of the electric field enhancement in gap-mode experiments. It must not be neglected that a chemical mechanism can also contribute to the very high signal enhancement. Since this part has not been investigated thoroughly in this respect, further studies are necessary.

2.6 Development of a new multicolor TERS setup

The selection of the incident radiation wavelength plays an important role in vibrational spectroscopy like Raman and is since long a subject of great scientific interest. If the excitation wavelength was close to an allowed electronic transition of the studied molecule it can lead to a huge enhancement of the Raman signal. This phenomenon is called resonance Raman scattering and information of excited state modes can be collected. This effect increases the scattered intensity of standard Raman spectroscopy by a factor up to 10^6 and hence decreases the detection limit. As a reminder, a normal Raman scattering is observed if the excitation wavelength was far away from any electronic transition., Although the signal intensity in standard Raman spectra is very weak it provides specific information regarding the modes in the ground state [82]. Comparing the spectra from these two techniques can be used to gain a deeper understanding of the molecule under investigation.

As described in the previous chapters in SERS/TERS the matching of the laser wavelength with the plasmonic resonance is used to probe molecules with a signal enhancement at the same order as resonance Raman scattering. The combination of both specific types of Raman spectroscopy can lead to an extra enhancement of the Raman signal [83-85]. In that way the detection limit could be further increased and specifically deployed in single molecule detection [73, 86-88].

For this purpose, a multicolour tip-enhanced Raman scattering (TERS) setup was developed during this thesis. The schematic setup is shown in figure 7. The light from five different continuous wave (CW) lasers (405 nm, 457 nm, 532 nm, 632 nm and 660 nm) is available for the tip and sample excitation. The laser lines are divided in two groups according to their beam diameters. Three lasers with smaller beam diameter: 1) 457 nm, diameter = 0.7 mm, 2) 660 nm, diameter = 0.7 mm and 3) 632.8 nm, diameter = 0.72 mm) are grouped together while two other lasers: 1) 405 nm, diameter = 1mm and 2) 532 nm, diameter = 1mm are grouped together.

Individual laser radiation was guided to the microscope objective using a set of periscopes and telescopes. Periscopes were used to adjust the height of laser beams and telescopes were used to adjust the laser beam diameter required to fill the microscope objective. To adjust the beam diameters of both groups, a 1.5x telescope (fixed) was used after the smaller diameter lasers. After that, the beam diameter of all lasers were close to 1mm. To fill the objectives with different entrance pupil diameters, an individual or a combination of two or three telescopes (removable) could be used. Different irises were used to retain the laser alignment.

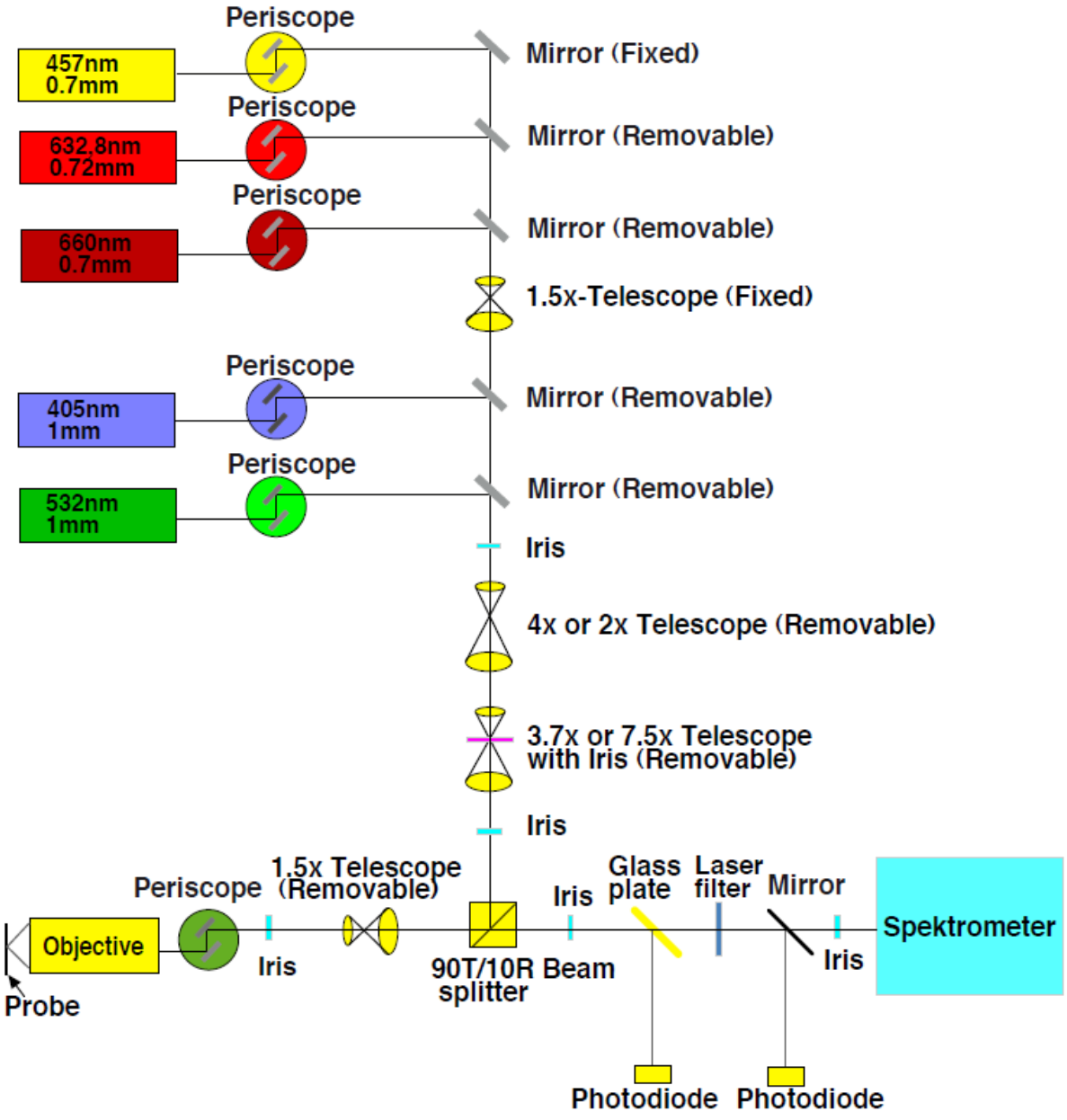

Figure 7: Schematic diagram of a new multicolour TERS setup.

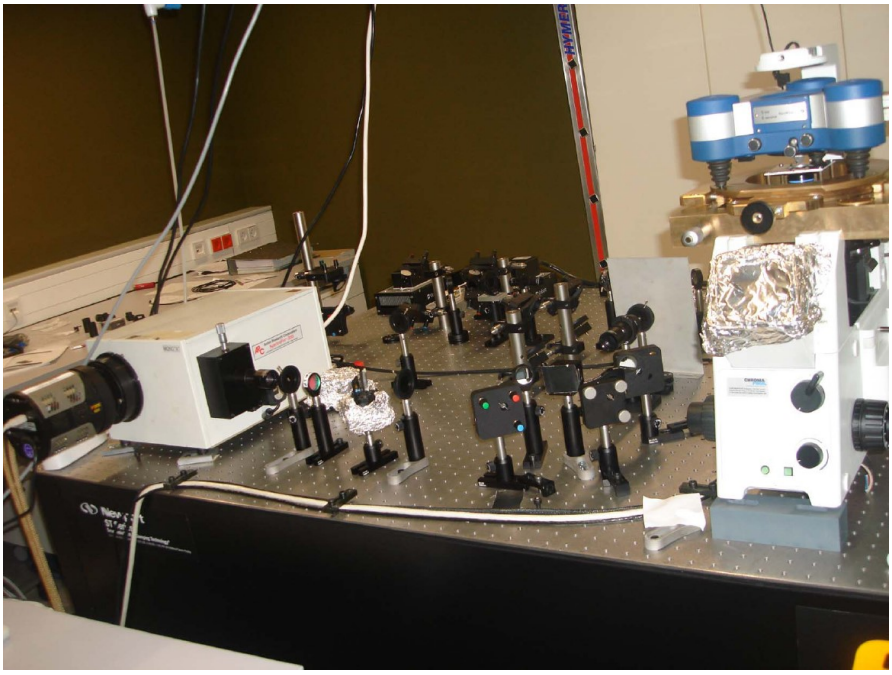

Figure 8: Lab picture of multicolour TERS setup.

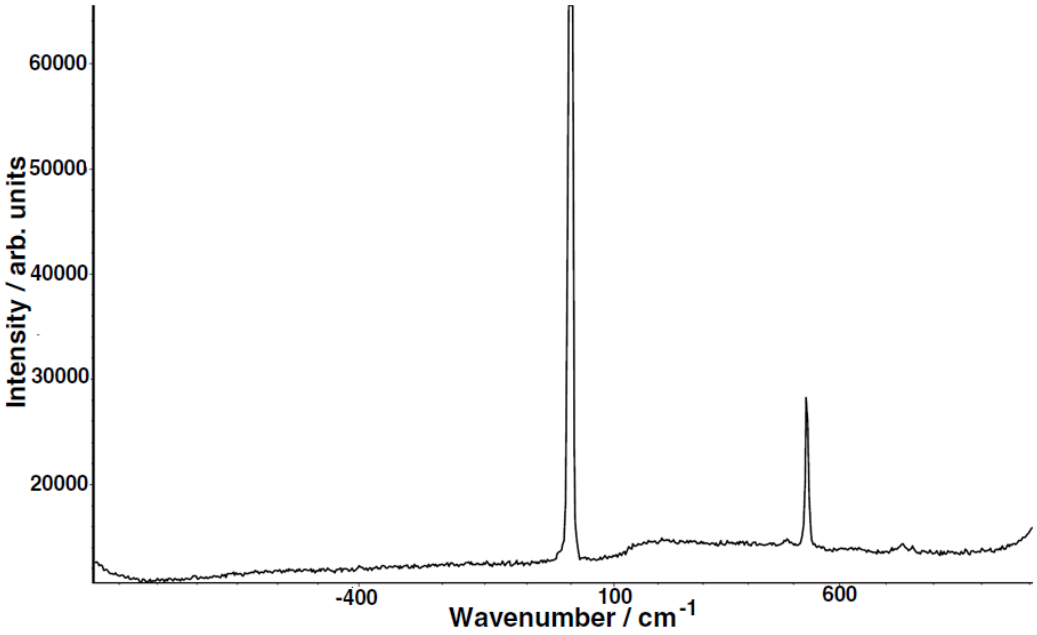

Figure 9: Raman spectrum of silicon using newly developed setup.

An important part of this setup is the double prism based beam splitter. In a general TERS setup, individual laser wavelength requires a separate dichroic mirror but here instead of a dichroic mirror, a double prism based beam splitter was used which allows working with all the wavelengths. A beam splitter having 10% reflection is used to transmit a large Raman signal and to avoid the sample burning due to high laser power. The light from the beam splitter is guided towards the objective which focuses the laser beam and the focussed laser beam generates the TERS signal after interacting with the AFM (Nanowizard II, JPK Instruments) silver coated tip. The generated Raman signal passes through the beam splitter and finally guided toward the spectrometer (SpectraPro-300i, Roper Scientific) and CCD camera (PIXIS-400, Princeton Instruments). A lab picture of the multicolour TERS setup is shown in figure 8. The Raman spectrum of the silicon using this setup is shown in figure 9 showing an intense Rayleigh peak and another peak with less intensity from silicon at 521cm^{-1}.

3 Research Summary

Plasmon induced catalytic reactions have been investigated on different molecular system in recent years [8, 9, 71, 72, 89-95]. However, a detailed study of simple reactions like protonation, deprotonation and dissociation was missing. The present work is focused on the investigation of these plasmonic reactions using small molecules like 4-mercaptopyridine, 2-mercaptopyridine and 4-nitrothiophenol with SERS and TERS. In addition, spectroscopic differences between these two techniques are demonstrated using thiophenol. Furthermore, comparison of resonance and off-resonance Raman scattering is expected to provide a deeper insight of molecule properties. In resonance Raman, the excitation wavelength should be close to an allowed electronic transition while in the case of off-resonance Raman an excitation wavelength far away from any electronic transition should be selected and thus a" multicolour TERS setup" was developed.

In the following the parts of the thesis are summarized in short.

1. Differences between SERS and TERS spectra

Large variations in the peak position in TERS and single molecule SERS [96-98] have been frequently observed by different groups. In this thesis a systematic study was performed to understand the fluctuations in the peak position as well as in the full-width-half-maximum (FWHM) in SERS and TERS spectra. The observations revealed that the number of molecules under investigation and charge transfer properties were responsible for the variations [99].

2. Plasmon induced protonation reaction

The plasmon induced protonation of 4-mercaptopyridine (4-MPY) was studied under ambient conditions. The proton source could not be explicitly determined but was either from atmospheric hydrogen (H_2) or water (H_2O) according to the experiments performed under argon. Although the H_2 content in the atmosphere is very low the collision frequency of these molecules on the investigated area "is potentially" large enough and could not be excluded as a possible proton source. In TERS experiments under ambient condition an instantaneous reaction was observed compared to SERS [100].

3. Plasmon induced deprotonation reaction

In this work it was demonstrated that 2-mercaptopyridine (2-MPY) could not be protonated under surface plasmon conditions. On the other hand, if the molecule was protonated in acidic solution (low pH) the protonated species could be deprotonated under plasmonic excitation. It was also found that the reaction rate was accelerated under TERS conditions [101].

4. Plasmon induced dissociation reaction

From previous studies it is known that p-nitrothiophenol (p-NTP) dimerizes when a self-assembled monolayer on gold is plasmonically excited with 532 nm [8, 9]. In the present work, a concentration dependent study of p-NTP was performed and it turned out that at a very low concentration (10^{-9} M) the distance between two neighbouring p-NTP molecules was large enough to prevent dimerization. At such low concentrations the dissociation of p-NTP to thiophenol (TP) was observed. The plasmonic hotspot was generated using gold nanoparticle dimers for substrates [102].

5. Setting up a multicolor TERS instrument

To understand the optical properties of a molecule the information regarding its ground and excitation states are of significant interest. Resonance and off-resonance Raman can provide such information. For resonant excitation, incident wavelength very close to an allowed electronic transition must be chosen while for off-resonance excitation wavelength was far away from any electronic transition is used. Applying these two techniques on a single molecule can provide useful information. For this purpose, a new multicolour TERS setup has been developed, where one can change the incident radiation from violet (405 nm) to red (660 nm). A single double prism based beam splitter makes this system unique compared to other TERS setup where each laser line needs an individual dichroic mirror.

3.1 Plasmonic differences at the micro- and nanoscale

Large peak position variations in TERS and single molecule SERS experiments have been observed in different studies [96-98]. So far no study is published comparing and explaining such variations. A systematic study has been performed in this work to understand the variations not only in the peak position but also in the FWHM by comparing the respective SERS and TERS spectra of thiophenol (TP).

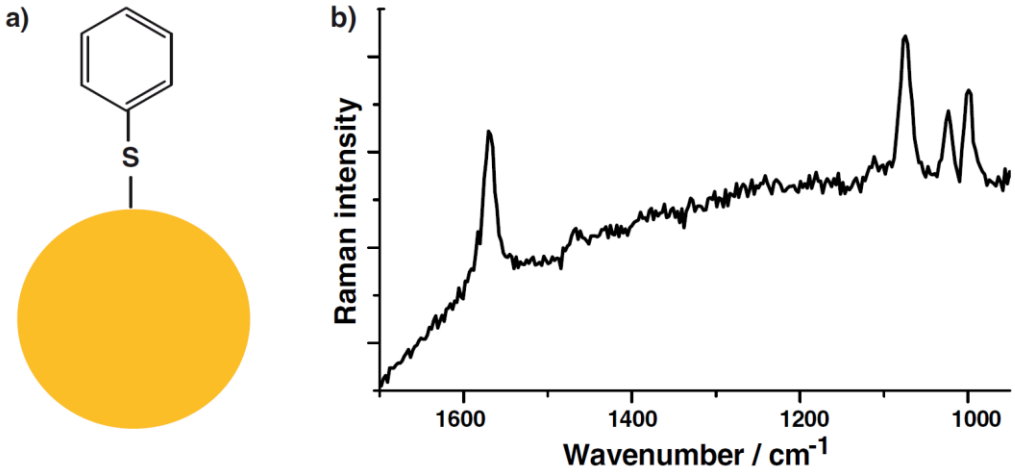

Figure 10: a) Schematic immobilization of thiophenol (TP) on gold, b) SERS spectrum of TP on a gold nanoparticle using laser excitation =532 nm, laser power =510 µW and an integration time of 10 s.

For the SERS experiments, gold nanoparticles were synthesized according to the literature [103, 104] and TP was adsorbed on the SERS substrate. For the TERS experiments, a self-assembled monolayer of TP was prepared on a gold nanoplate substrate.

Figure 10 (a) shows the schematic of TP immobilized on gold nanoparticles and the corresponding SERS spectrum is shown in figure 10 (b). Three marker bands were observed at 999 cm^{-1} (ring breathing mode), 1075 cm^{-1} (C–C in-plane bending) and 1569 cm^{-1} (C–C stretching). Two different bands (999 and 1075 cm^{-1}) were analyzed by fitted with a Lorentzian function to provide information on band positions and FWHM.

To study the position dependent behaviour 200 SERS and TERS spectra were measured with an acquisition time of 10 s. A large variation in peak position 6-9 cm^{-1} of TERS spectra, while in SERS only less than 2 cm^{-1} variation was observed. This large variation in TERS was postulated to originate from a domain formation of TP on the gold nanoparticles. As the tip moved to the next position it interacted with a different domain, where the molecules had the same orientation relative to one another, however, it differed from the previous location of the TERS tip but in SERS this effect was averaged out due to the large number of domain in the laser focus. To extract the information regarding the number of molecule in TERS and SERS we analyzed the FWHM of the above-mentioned peaks. In SERS, the FWHM was always larger compared to TERS, indicating a larger number of probed molecules in the SERS. In SERS all the molecule in the laser focus (about 10^7) contributed to the overall FWHM while in TERS only very few molecules (about 100 or less) under the TERS tip contributed to the FWHM.

To further corroborate the above-mentioned explanation, time dependent measurements were done and 200 SERS and TERS spectra were measured with an acquisition time of 10 s. Effectively, these measurements showed the same results and were found to contradict the above explained domain theory, as the tip and sample position were fixed during the time dependent measurements. Apparently, the chemical interactions between tip and sample were the dominant reason for the observed large shift in peak position in TERS. Furthermore, time dependent measurements show a larger FWHM of SERS compared to TERS spectra which further supports the explanation that in TERS very less number of molecules were excited.

To study the effect of different metals, we also performed SERS on a silver island film as shown in figure 11. We observed three discrepancies 1) there was an absolute band shift of different bands e.g. the ring breathing mode was observed at 995cm^{-1} when TP was adsorbed on silver and at 999cm^{-1} when TP was adsorbed on gold. These absolute shifts were due to a different binding of TP on the two metal surfaces [105]. 2) A much smaller peak position variation compared to gold nanoparticle SERS was due to an averaging effect as the density of nanoparticles in the silver island film was higher and so was the number of molecules in the laser focus. 3) The FWHM was even higher compared to SERS on gold nanoparticles, which again indicated a larger number of molecules in the laser focus.

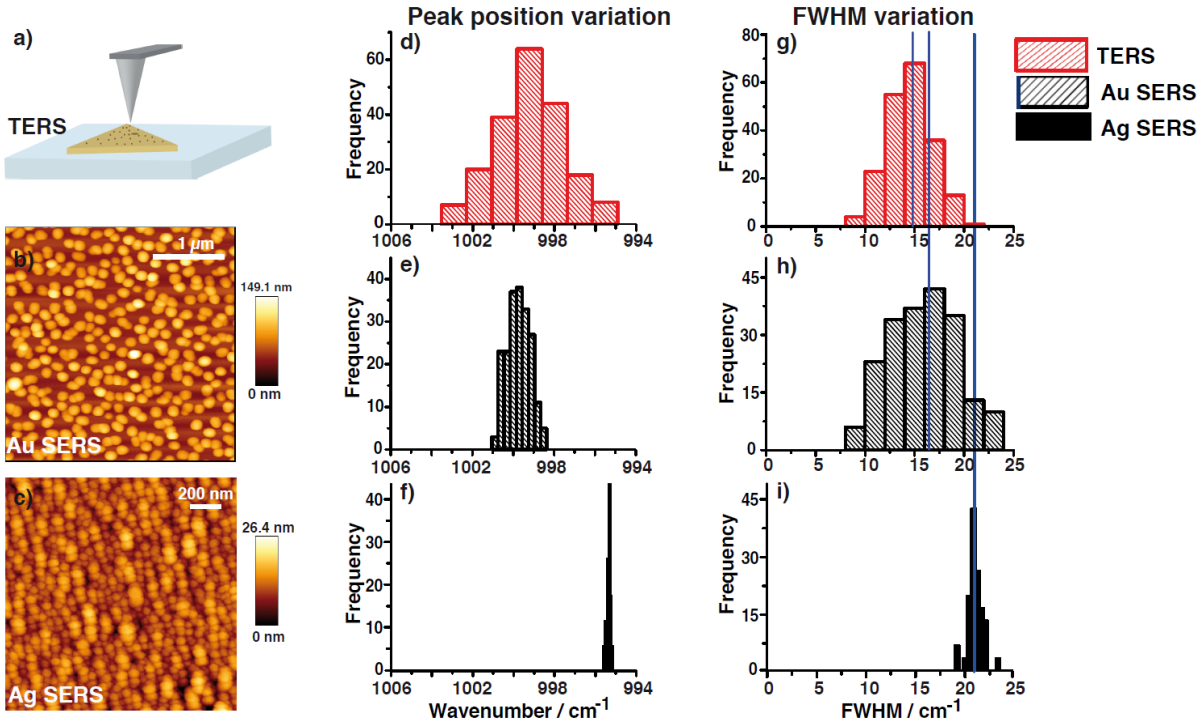

Figure 11: a) scheme of the TERS configuration, b) AFM topography of gold nanoparticles and c) AFM topography of a silver island film. Peak position d), e), f) and FWHM g), h), i) variation of thiophenol in TERS, gold nanoparticles SERS and a silver island SERS, respectively.

The presented results clearly reveal that SERS and TERS spectra should not be compared readily but band position shifts must always be considered when assigning vibrational modes.

3.2 Plasmon induced protonation

Protonation is a fundamental chemical reaction. Protonation is an essential step in many biological and chemical processes and can change different electronic, thermodynamic and optical properties of molecules [106-109]. Thus, it is essential to understand the protonation behaviour of a molecule in particular when the protonation is observed under novel conditions.

Here a plasmon induced protonation reaction is examined for the first time with SERS and TERS. For this purpose, the small organic thiol, 4-mercaptopyridine (4-MPY) was used (shown in figure 12). It is well known that functional thiol groups can generate a self-assembled monolayer (SAM) on a metal surface after abstracting a hydrogen atom in favor of a new metal-sulphur bond [110-112].

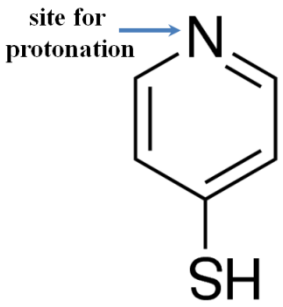

Figure 12: 4-mercaptopyridine (4-MPY) used for a plasmon induced protonation.

For all experiments in this work, SERS active silver island films were prepared by the evaporation of silver on cleaned glass plates [113]. For TERS experiments smooth gold nanoplates were synthesized and deposited on cleaned glass substrate [114]. In the TERS measurement silver coated non-contact TERS tips from NT-MDT and Budget Sensors were used.

To obtain a monolayer of 4-MPY for the SERS experiment, a drop (5µl) of 5 mM 4-MPY ethanolic solution was dropped on a silver island film, incubated for 5 minutes and washed with ethanol to remove any physically adsorbed molecules. To obtain a SAM for a TERS experiment, gold nanoplates immobilized on a glass plate were immersed in a 5 mM 4-MPY ethanolic

solution for 22 hours and then washed with ethanol. Figure 13 a) shows the SERS spectra of unprotonated species of 4-MPY at the beginning of the reaction (t = 0s) where the different peaks could be assigned: 1006 cm^{-1} (ring breathing), 1092 cm^{-1} (ring breathing/C–S), 1211 cm^{-1} (β(CH)/δ(NH)), 1575 cm^{-1} (ring stretching mode with unprotonated nitrogen (UP)). Spectra were measured with 532 nm laser excitation at 125 µw power with an acquisition time of 1s.

Over the time, the intensity of ring stretching mode of the unprotonated molecule at 1575 cm^{-1} (UP) decreased and finally almost vanished. At the same time the intensity of the ring stretching mode of the protonated molecule at 1608 cm^{-1} (PN) increased and finally dominated. This observation clearly indicated the conversion of unprotonated molecules to protonated molecules under the influence of surface plasmons as shown in figure 13 b). These results raise the question about the proton source. To find an answer the same experiments were performed under inert gas atmosphere (argon) and, no reaction was observed. Most likely, in the experiment under argon, 4-MPY could not come in direct contact with atmospheric H_2 or H_2O. These observations led us to the conclusion that the proton source was either atmospheric H_2 or H_2O. Although the H_2 content in the atmosphere is quiet low, the collision frequency *F* per unit area can be calculated as follows:

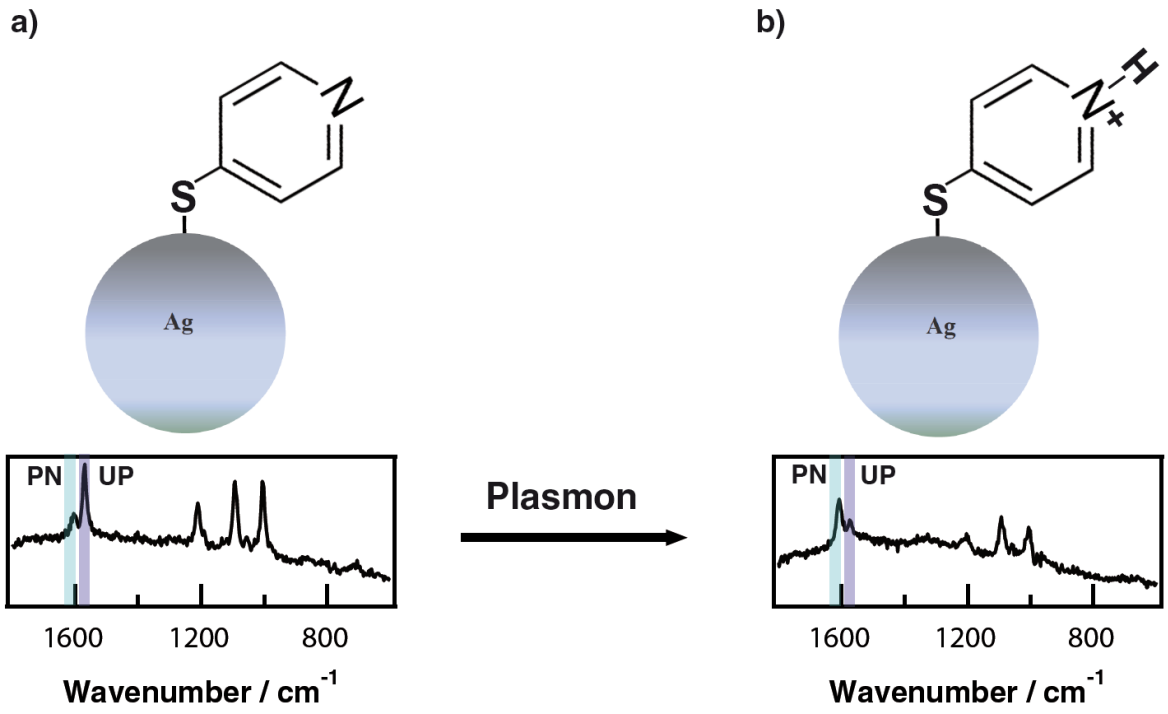

Figure 13: SERS spectra of 4-MPY, a) in the beginning of the reaction (t = 0 s) showing only signals of the unprotonated species, b) after t = 2800 s showing mainly signals of the protonated species. Experimental parameters: laser excitation = 532 nm, laser power = 125 µW and integration time = 1 s.

$$F = \frac{\rho \times V_{avg}}{4}$$

where ρ is molecular density and V_{avg} is mean velocity at room temperature. Assuming a hydrogen content in the atmosphere of about 5.5×10^{-5} % and approximating the hydrogen pressure (P) as 5.5×10^{-5} bar , the molecular density can be calculated as

$$\rho = \frac{P \times N_A}{R \times T} = 1.33 \times 10^{21} m^{-3}$$

where N_A is Avogadro's number (6.022×10^{23} mol^{-1}), R is the gas constant (8.3145 J/ mol.K) and T is room the temperature (298K). The mean velocity V_{avg} of hydrogen with a molar mass (M) of 2×10^{-3} kg/mol is

$$V_{avg} = \left[\frac{8RT}{\pi M} \right]^{1/2} = 1.776 \times 10^{3} m/s$$

.

Thus, the collision frequency per unit area is 5.93×10^{23} $m^{-2}s^{-1}$. In the TERS measurements the number of hits on the tip with a radius (r = 10 nm.) is $F \times \pi \times r^2 = 1.86 \times 10^{8} s^{-1}$. Hence, under the present experimental conditions we cannot simply rule out atmospheric H_2 as a possible proton source. Similarly, using the vapor pressure of water at room temperature (p = 2.98×10^{-2} bar), the collision frequency on the tip is 3.37×10^{10} s^{-1} . Previous studies from different groups have already demonstrated that surface plasmons can dissociate H_2 and H_2O [90, 115, 116]. These observation shows that the proton source was either atmospheric H_2 or H_2O.

In addition, measurements under atmospheric conditions also showed a gradual band intensity decrease. This was most likely due to the oxidation of silver island film under ambient conditions. Since the protonation rate was faster than the oxidation of the silver island film, these two processes were independent.

It was also observed that the protonation could be controlled either by changing the laser power or the incident wavelength. Below a certain laser power or far away from the plasmonic resonance maximum, a protonation could not be initiated. Laser power dependent studies further revealed that the reaction rate increased linearly with an increasing incident laser power. The threshold value below which no protonation reaction can be initiated depended on the wavelength of the light used. For the protonation of 4-MPY the threshold power for the 532 nm laser was about 25 μW.

To rule out any temperature induced effects due to the highly focussed laser beam, a temperature dependent study under atmospheric conditions was performed. For this purpose, an incident power just below the threshold value was used and the sample temperature was increased up to 60^{O} C as shown in figure 14. No signature of protonation was observed, which confirmed that the observed protonation reaction was not induced by the temperature but by surface plasmons.

In TERS measurements under ambient conditions, a very fast protonation compared to SERS was observed which could be explained by the following experimental differences

1) TERS measurements were performed in a gap-mode configuration generating an additional field confinement that resulted in an increased protonation rate.

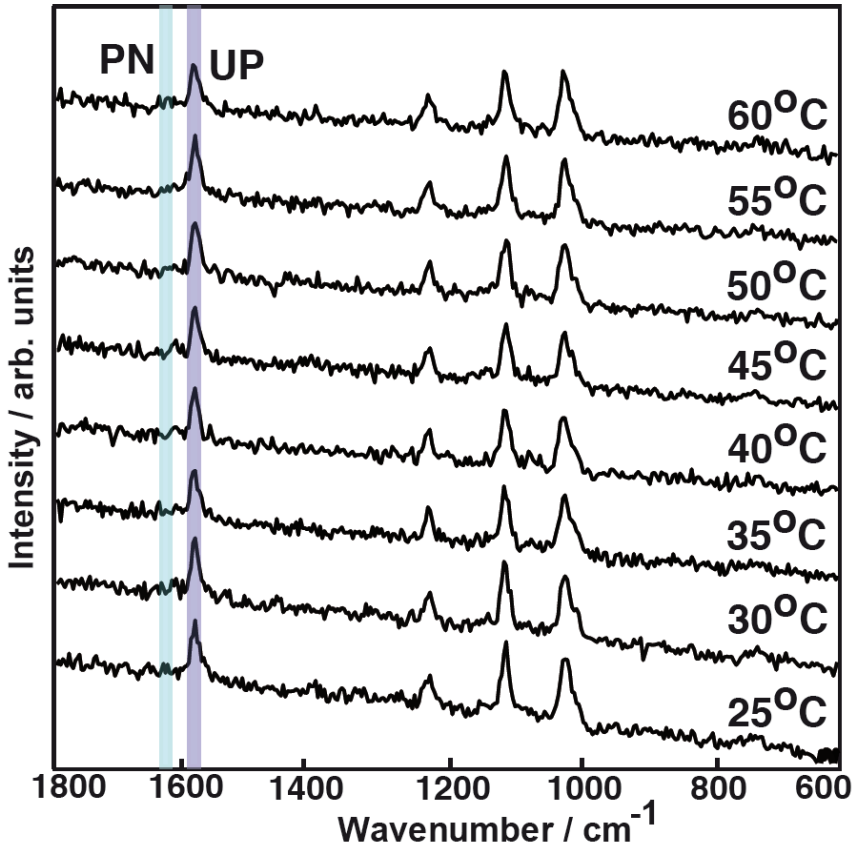

Figure 14: Temperature dependent SERS spectra of 4-MPY. The experimental parameters are: laser excitation = 532 nm, laser power = 20 μW and integration time =1 s. PN= protonated molecule, UP= unprotonated molecule.

2) The combination of two different metals in TERS (gold substrate, silver tip) could lead to an efficient electron transfer from the metals to the molecule which further increased the protonation rate.

TERS experiments were normally performed with higher power of about 650 µW to achieve a high signal to noise ratio compared to SERS where about 150 µW is used. To examine if the increased laser power in TERS is the source of faster protonation in TERS, we also performed SERS under atmospheric conditions with 650 µW but it still takes more than 500s for the complete protonation. These results clearly show that the faster protonation reaction under TERS condition is not due to higher laser power.

3.3 Plasmon induced deprotonation

Deprotonation is defined as the removal of a proton (H^+) from a molecule. Similar to protonation, deprotonation also alters properties of a molecule. In this study 2-mercaptopyridine (2-MPY), was protonated (2-MPY^+-H) as shown in figure 15, using a low pH (1.3) solution prior the SERS and TERS experiment, respectively. Plasmon induced deprotonation of the protonated species under SERS and TERS conditions were observed using 532 nm laser excitation.

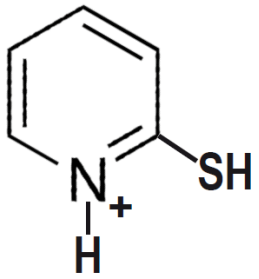

Figure 15: Protonated 2-mercaptopyridine (2-MPY^+-H) used for plasmon induced deprotonation.

To measure the SERS spectra of 2-MPY, a sample was prepared by dropping 5 µl of a 1mM ethanolic solution of 2-MPY on a silver island film, followed by drying and washing with ethanol to remove physically adsorbed molecules on the surface and to achieve a monolayer. Figure 16 a) shows the SERS spectra of 2-MPY after 600 s continuous laser irradiation. One can clearly see the unprotonated peak at 1574 cm^{-1} (UP) but no signature of the protonated species

around 1610 cm^{-1} (PN) was observed. Compared to 4-MPY no protonation of this molecule under surface plasmons occurred, which can be explained by the position of the sulfur atom in the ring. During the covalent Ag-S bond formation in the immobilization step, the nitrogen atom in 2-MPY comes very close to the metal surface causing an additional interaction between the Ag surface and the nitrogen in the ring and prohibits the protonation of 2-MPY.

As no protonation of 2-MPY under surface plasmons was observed, a protonated species of 2-MPY (2-MPY^{+}-H) was prepared by dissolving the molecule in a low pH (1.3) solution. The sample for SERS measurements was prepared as describe for 4-MPY. Figure 16 b) shows the SERS spectra of 2-MPY^{+}-H. At the time point t = 0 s one can clearly see the signal for the protonated species at 1610 cm^{-1}. This peak disappeared after 600 s of continuous laser irradiation as shown in figure 16 c), which pointed to a successful abstraction of the proton. To further proof the effect of surface plasmons, a low incident laser power (20 µW) was used but no deprotonation over time was observed which indicated that the intensity of surface plasmon was too low to initiate this reaction.

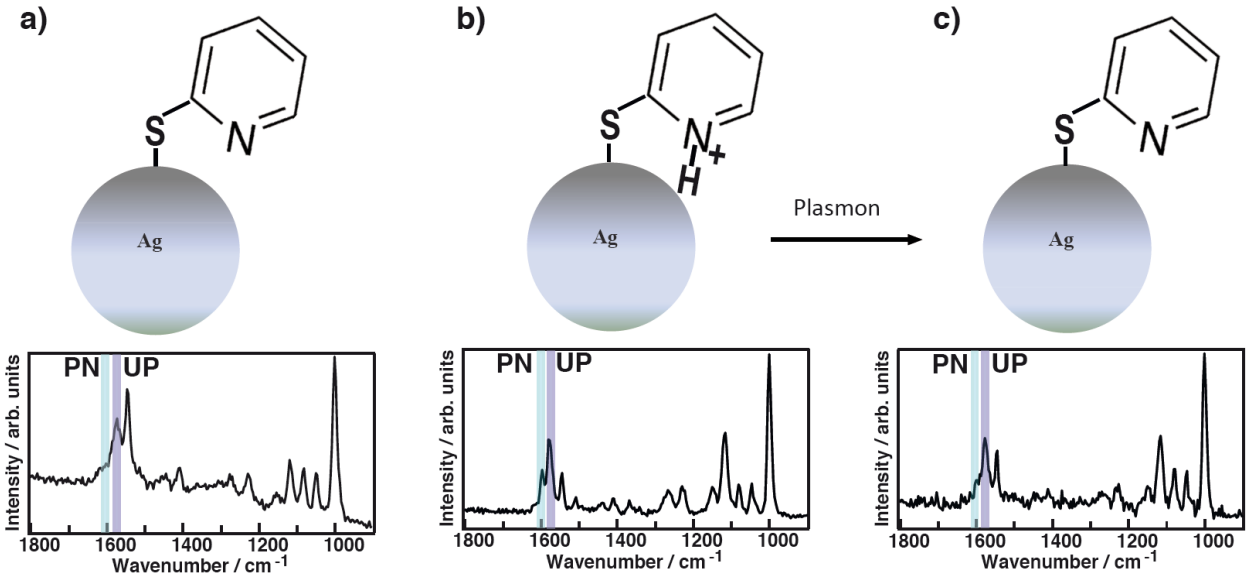

Figure 16: SERS spectra of, a) 2MPY after 600 s, b) 2-MPY^{+}-H at time t=0 and c) 2-MPY^{+}-H after 600s of laser irradiation. The experimental parameters are: laser excitation =532 nm, laser power =180 µW and integration time =1 s.

We also investigated the power dependent reaction rate by monitoring the band intensities of the protonated and unprotonated 2-MPY. For this, the incident power was increased by five times and at the same time the acquisition time was decreased by the same value. No variation in the peak intensity was observed which demonstrated a linear behaviour of the reaction rate.

Furthermore, to exclude the effect of sample heating in the laser focus, a temperature dependent study was performed. Similar to the protonation experiments of 4-MPY, the temperature of the sample was increased up to 60^{O} C at a low laser power where no deprotonation reaction takes (20 µW). Figure 17 shows the temperature dependent spectra but no change in the intensity of the band of the protonated molecule was observed. The temperature at 20 µW was assumed to be below 60^{O} C and thus either the reaction was temperature insensitive or a higher temperature is required for the deprotonation. Thus, under the present experimental conditions the deprotonation was not initiated by the temperature but the surface plasmons at the nanoparticles in the laser focus.

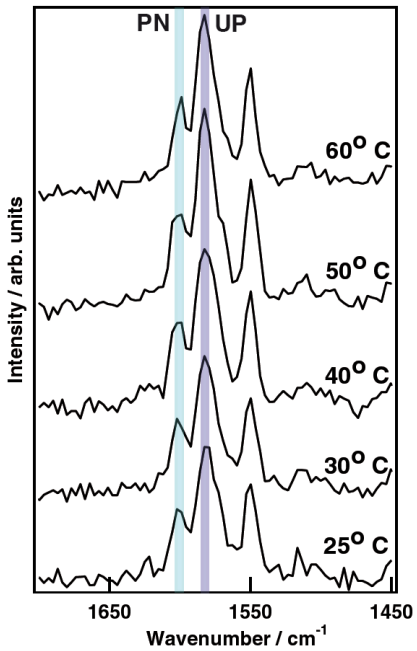

Figure 17: Temperature dependent SERS of 2-MPY^{+}-H at a laser power of 18 µW.

The sample for the TERS measurement was prepared as described for 4-MPY. TERS of 2-MPY did not show any protonation reaction while deprotonation of 2-MPY^{+}-H was faster compared to SERS. Most likely it was again the large field confinement. In the gap between gold substrate and silver tip that accelerated the reaction.

3.4 Plasmonic dissociation at single molecule level

The dissociation of a molecule is a process of splitting or breaking bond yielding at least two separate molecules. The breaking of molecular bonds is fundamental in chemical synthesis and an important task for chemists and physicists in general. The present work shows how surface plasmons allow the sensitive control of surface-adsorbed molecular dissociation.

A well known example for an intermolecular plasmon assisted reaction is the dimerization of p-nitrothiophenol (p-NTP) to 4,4-dimercaptoazobenzene (DMAB) which has been earlier demonstrated in our lab using SERS and TERS [8]. For a dimerization the distance between two reactants is a crucial parameter. If the concentration of a p-NTP solution is low enough to prevent the formation of a self-assembled monolayer during the adsorption process, the distance of p-NTP molecules should become too large for an intermolecular reaction and no reaction should occur. Then, any detected SERS signal could be related to a single or only to a few isolated and non-interacting separated molecules. To proof this consideration experimentally, a concentration dependent study was performed. In a first step, three different concentrations of aqueous p-NTP solutions (10^{-7}, 10^{-8} and 10^{-9} M) were mixed with a colloidal gold nanoparticle dimer [117] containing solution.

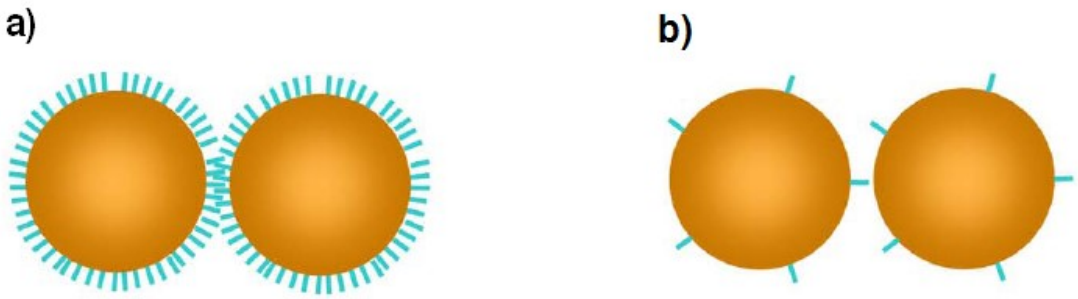

Figure 18: Control strategy: a) very high (10^{-2} M) and b) very low (10^{-9} M) concentration of p-NTP on gold dimer. At high concentrations neighbouring molecules can interact and dimerize in SERS, while at very low concentrations the distance between neighbours is too large for a dimerization.

Figure 18 shows schematically the concentration dependent coverage of p-NTP on a gold dimer where two molecules are very close to each other (a) and can easily dimerize, while in (b) the distance between the two molecules is too large for a dimerization.

The SERS spectra of the measurements with different concentrations of p-NTP (10^{-7}, 10^{-8} and 10^{-9} M) are shown in figure 19 a), b) and c) respectively. Figure 19 a) and b) show the dimerization of p-NTP which is characterized by disappearance of the Raman band at 1332 cm^{-1} (ν_{NO_2}), and the appearance of new Raman bands around 1140 cm^{-1} (β_{C-H}), 1387 cm^{-1} ($\nu_{NN}+\nu_{CN}+\nu_{NC}$) and 1432 cm^{-1} ($\nu_{NN}+\nu_{CN}+\beta_{C-H}$). These results demonstrate that with a 10^{-7} and 10^{-8} M concentration the gold surface is still densely covered with p-NTP molecules enabling a dimerization.

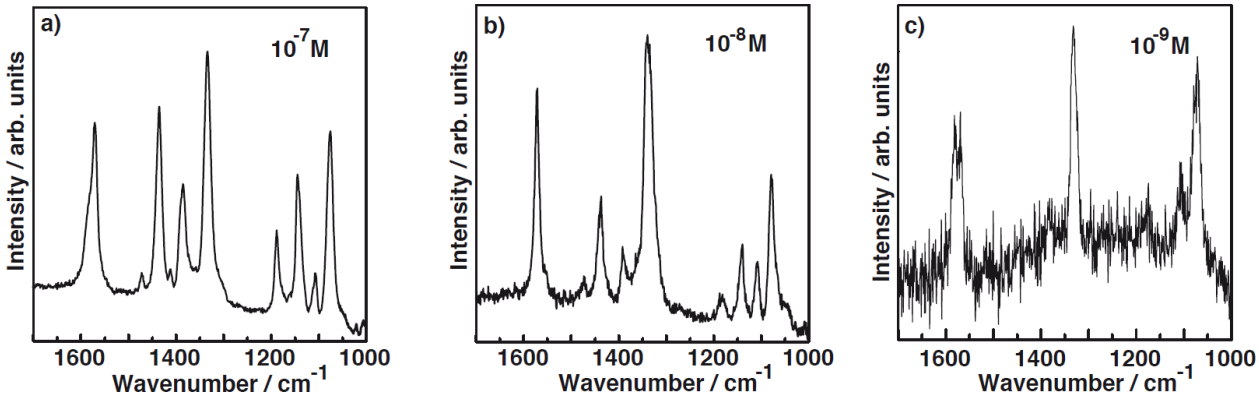

Figure 19: Concentration dependent spectra of p-NTP at a) 10^{-7} M, time t = 0 s and power = 30 µW, b) 10^{-8} M, time t = 0 s and power = 300 µW and c) 10^{-9} M, time t = 0 s and power = 3 mW.

Figure 19 c) shows the SERS spectrum of p-NTP at a 10^{-9} M solution. Here, no dimerization of p-NTP to DMAB was observed as the peaks, which characterize the dimerization, are not visible and shows that at a concentration below 10^{-9} M, dimerization can be inhibited. It was concluded that the distance between p-NTP molecules in the plasmonic hot-spot of the GD was too large to allow intermolecular reactions under these conditions. This finding is in accordance with the estimated molecular coverage (n) of p-NTP on a single gold dimer that was estimated as

$$n = \frac{c_M}{c_{GD}} = \frac{c_M M_{GD} N_A V}{M_{Au}}$$

where c_M and c_{GD} are the molarity of p-NTP and GD nanoparticles, M_{Au} and M_{GD} refer to the mass of Au and one single GD nanoparticle, respectively, N_A is Avogadro's constant and V is the volume of GDs solution in the preparation process. From the molecular coverage the average distance between two p-NTP molecules can be calculated as

$$d = R\sqrt{\frac{8\pi}{n}}$$

where R is the radius of the gold nanoparticle and n molecular coverage on a single nanoparticle GD. The calculated average distance between two p-NTP molecules at 10^{-9} M is 32 nm, which is large enough to prevent the dimerization.

Time dependent spectra of p-NTP were measured at the concentration of 10^{-9} M. Figure 20 a) shows the spectrum at t = 0s which corresponds to p-NTP but after a while of continuous irradiation a change in the spectra was observed. Finally, after 30 min a completely new spectrum as shown in figure 20 b) was detected, which remained stable. This spectrum agreed with that of TP. Obviously, the nitro group was split off and replaced by a hydrogen atom, most

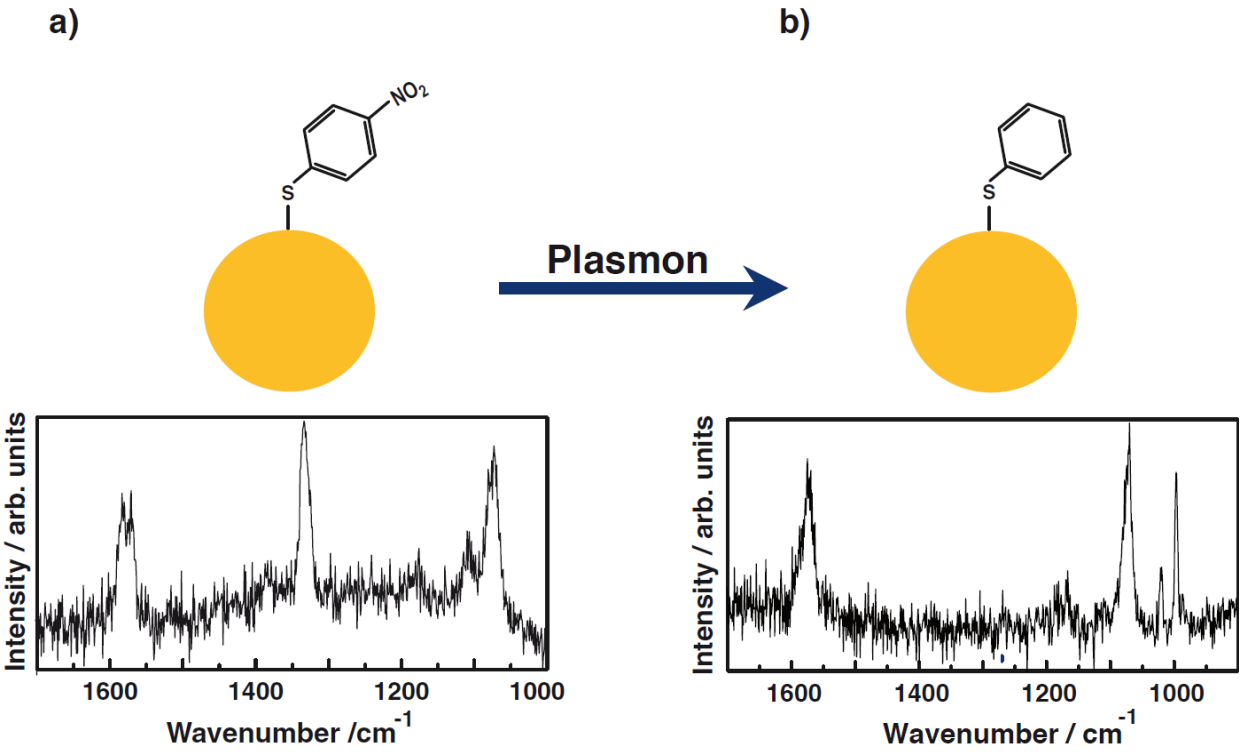

Figure 20: Spectrum of p-NTP at 10^{-9} M concentration with 3 mW laser power using 633 nm laser at a) t = 0s and b) after t = 30 min. The latter can be assigned to thiophenol.

probably the hydrogen derived from the surrounding water layer that was ubiquitously present under ambient conditions.

In conclusion, the work shows the dissociation of p-NTP near the single molecule level. From the spectra a dissociation of p-NTP to TP was concluded at low concentration where the distance between p-NTP molecules adsorbed on single isolated gold dimers became too large for a dimerization.

3.5 References

[1] C. L. A. Lamont, J. Wilkes, Attenuation Length of Electrons in Self-Assembled Monolayers of n-Alkanethiols on Gold. *Langmuir* **15**, 2037-2042 (1999).

[2] M. J. Tarlov, J. G. Newman, Static Secondary Ion Mass-Spectrometry of Self-Assembled Alkanethiol Monolayers on Gold. *Langmuir* **8**, 1398-1405 (1992).

[3] M. J. Schoenfisch, J. E. Pemberton, Air stability of alkanethiol selfassembled monolayers on silver and gold surfaces. *J. Am. Chem. Soc.* **120**, 4502-4513 (1998).

[4] Y. Fang, Y. Li, H. Xu, M. Sun, Ascertaining p,p′-Dimercaptoazobenzene Produced from p-Aminothiophenol by Selective Catalytic Coupling Reaction on Silver Nanoparticles. *Langmuir* **26**, 7737–7746 (2010).

[5] Y. Huang, H. Zhu, G. Liu, D. Wu, B. Ren, Z. Tian, When the Signal Is Not from the Original Molecule To Be Detected: Chemical Transformation of para-Aminothiophenol on Ag during the SERS Measurement. *J. Am. Chem. Soc.* **132**, 9244–9246 (2010).

[6] B. Dong, Y. Fang, L. Xia, H. Xu, M. Sun, Is 4-nitrobenzenethiol converted to p,p′-dimercaptoazobenzene or 4-aminothiophenol by surface photochemistry reaction? *J. Raman Spectrosc.* **42**, 1205–1206 (2011).

[7] B. Dong, Y. Fang, X. Chen, H. Xu, M. Sun, Substrate-, Wavelength-, and Time-Dependent Plasmon-Assisted Surface Catalysis Reaction of 4-Nitrobenzenethiol Dimerizing to p,p′-Dimercaptoazobenzene on Au, Ag, and Cu Films. *Langmuir* **27**, 10677–10682 (2011).

[8] E. M. von Schrojenstein Lantman, T. Deckert-Gaudig, A. J. G. Mank, V. Deckert, B. M. Weckhuysen, Catalytic processes monitored at the nanoscale with tip-enhanced Raman spectroscopy. *Nat. Nanotechnol.* **7**, 583-586 (2012).

[9] M. Sun, Z. Zhang, H. Zheng, H. Xu, In-situ plasmon-driven chemical reactions revealed by high vacuum tip-enhanced Raman spectroscopy. *Scientific Reports* **2**, 647 (2012).

[10] E. Abbe, Beitrage zur Theorie des Mikroskops und der mikroskopischen Wahrnehmung. *Arch. Mikrosk. Anat. Entwichlungsmech.* **9**, 413–418 (1873).

[11] M. Busch, On the mode of action of the concentrating coil in the Braun tube. *Arch. Elektrotechnik* **18**, (March 1927, Jena, Physikalisches Institut).

[12] L. de Broglie, Waves and quanta. *Nature* **112**, 450 (1923).

[13] E. Ruska, M. Knoll, The magnetic concentrating coil for fast electron beams. *Z. Techn. Physik* **12**, 389-400 (1931).

[14] M. von Ardenne, The scanning electron microscope. Theoretical foundamentals. *Z. Phys.* **109**, 553-572 (1938).

[15] M. von Ardenne, The scanning electron microscope. Practical implementation. *Z. Tech. Phys.* **19**, 407-416 (1938).

[16] G. Binnig, H. Rohrer, C. Gerber, E. Weibel, Tunneling through a controllable vacuum gap. *Appl. Phys. Lett.* **40**, 178–180 (1982).

[17] G. Binnig, H. Rohrer, C. Gerber, E. Weibel, Surface studies by scanning tunneling microscopy. *Phys. Rev. Lett.* **49**, 57–61 (1982).

[18] G. Binnig, C. F. Quate, C. Gerber, Atomic Force Microscope. *Phys. Rev. Lett.* **56**, 930–933 (1986).

[19] K. Karrai, R. D. Grober, Piezoelectric tip-sample distance control for near field optical microscopes. *Appl. Phys. Lett.* **66**, 1842-1844 (1995).
[20] F. J. Giessibl, High-speed force sensor for force microscopy and profilometry utilizing a quartz tuning fork. *Appl. Phys. Lett.* **73**, 3956-3958 (1989).
[21] J. E. Lennard-Jones, On the Determination of Molecular Fields. *Proc. R. Soc. Lond. A* **106**, 463–477 (1924).
[22] C. M. Mate, G. M. McClelland, R. Erlandsson, S. Chiang, Atomic-Scale Friction of a Tungsten Tip on a Graphite Surface. *Phys. Rev. Lett.* **59**, 1942-1946 (1987).
[23] H. Butt, B. Cappella, M. Kappl, Force measurements with the atomic force microscope: Technique, interpretation and applications. *Surf. Sci. Rep.* **59**, 1–152 (2005).
[24] T. R. Albrecht, P. Grütter, D. Horne, D. Rugar, Frequency modulation detection using high-Q cantilevers for enhanced force microscope sensitivity. *J. Appl. Phys.* **69**, 668-673 (1991).
[25] F. J. Giessibl, Advances in atomic force microscopy. *Rev. Mod. Phys.* **75**, 949-983 (2003).
[26] M. Lee, W. Jhe, General Theory of Amplitude-Modulation Atomic Force Microscopy. *Phys. Rev. Lett.* **97**, 036104 (2006).
[27] R. W. Stark, G. Schitter, A. Stemmer, Tuning the interaction forces in tapping mode atomic force microscopy. *Phys. Rev. B* **68**, 085401 (2003).
[28] J. P. Spatz, S. Sheiko, M. Möller, R. G. Winkler, P. Reineker, O. Martin, Forces affecting the substrate in resonant tapping force microscopy. *Nanotechnology* **6**, 40-44 (1995).
[29] S. Kotler, N. Akerman, Y. Glickman, A. Keselman, R. Ozeri, Single-ion quantum lock-in amplifier. *Nature* **473**, 61–65 (2011).
[30] C. V. Raman, A new radiation. *Indian J. Phys.* **2**, 387–398 (1928).
[31] R. S. Das, Y. K. Agrawal, Raman spectroscopy: Recent advancements, techniques and applications. *Vib. Spectrosc.* **57**, 163–176 (2011).
[32] A. Rygula, K. Majzner, K. M. Marzec, A. Kaczor, M. Pilarczyka, M. Baranskaa, Raman spectroscopy of proteins: a review. *J. Raman Spectrosc.* **44**, 1061–1076 (2013).
[33] A. C. Ferrari, D. M. Basko, Raman spectroscopy as a versatile tool for studying the properties of graphene. *Nat. Nanotechnol.* **8**, 235–246 (2013).
[34] A. K. Yadav, P. Singh, A review of the structures of oxide glasses by Raman spectroscopy. *RSC Adv.* **5**, 67583-67609 (2015).
[35] J. Huaizhou, L. Qipeng, C. Xingdan, D. Haiquan, G. Hongzhi, J. Shangzhong, The use of Raman spectroscopy in food processes: A review. *Appl. Spectrosc. Rev.* **51**, 12-22 (2016).
[36] H. Byrne, M. Keating, Raman Spectroscopy in Nanomedicine: Current Status and Future Perspectives. *Nanomedicine* **8**, 1335-1351 (2013).
[37] M. Fleischmann, P. J. Hendra, A. McQuillan, A. Raman Spectra of Pyridine Adsorbed at a Silver Electrode. *Chem. Phys. Lett.* **26**, 163–166 (1974).
[38] D. L. Jeanmaire, R. P. van Duyne, Surface Raman spectroelectrochemistry: Part I. Heterocyclic, aromatic, and aliphatic amines adsorbed on the anodized silver electrode. *J. Electroanal. Chem. Interfacial Electrochem.* **84**, 1–20 (1977).
[39] M. G. Albrecht, J. A. Creighton, Anomalously Intense Raman Spectra of Pyridine at a Silver Electrode. *J. Am. Chem. Soc.* **99**, 5215–5217 (1977).

[40] M. Moskovits, Surface-enhanced Raman Spectroscopy: A Brief Retrospective. *J. Raman Spectrosc.* **36**, 485–496 (2005).
[41] J. P. Camden, J. A. Dieringer, Y. Wang, D. J. Masiello, L. D. Marks, G. C. Schatz, R. P. Van Duyne, Probing the Structure of Single-Molecule Surface-Enhanced Raman Scattering Hot Spots. *J. Am. Chem. Soc.* **130**, 12616–12617 (2008).
[42] A. Campion, J. Ivanecky, C. Child, M. Foster, On the Mechanism of Chemical Enhancement in Surface-Enhanced Raman Scattering. *J. Am. Chem. Soc.* **117**, 11807–11808 (1995).
[43] A. Otto, I. Mrozek, H. Grabhorn, W. Akemann, Surface-Enhanced Raman Scattering. *J. Phys. Condens. Matter* **4**, 1143 (1992).
[44] K. Kneipp, Y. Wang, H. Kneipp, L. T. Perelman, I. Itzkan, R. R. Dasari, M. S. Feld, Single Molecule Detection Using Surface-Enhanced Raman Scattering (SERS). *Phys. Rev. Lett.* **78**, 1667-1670 (1997).
[45] S. L. Kleinman, R. R. Frontiera, A. Henry, J. A. Dieringer, R. P. Van Duyne, Creating, characterizing, and controlling chemistry with SERS hot spots. *Phys. Chem. Chem. Phys.* **15**, 21–36 (2013).
[46] M. J. Banholzer, J. E. Millstone, L. Qin, C. A. Mirkin, Rationally Designed Nanostructures for Surface-Enhanced Raman Spectroscopy. *Chem. Soc. Rev.* **37**, 885–897 (2008).
[47] D. Radziuk, H. Moehwald, Prospects for plasmonic hot spots in single molecule SERS towards the chemical imaging of live cells *Phys. Chem. Chem. Phys.,* **17**, 21072-21093 (2015).
[48] K. Kneipp, H. Kneipp, V. B. Kartha, R. Manoharan, G. Deinum, I. Itzkan, R. R. Dasari, M. S. Feld, Detection and identification of a single DNA base molecule using surface-enhanced Raman scattering (SERS). *Phys. Rev. E* **57**, R6281 (1998).
[49] J. Wessel, Surface-enhanced optical microscopy. *J. Opt. Soc. Am. B* **2**, 1538-1541 (1985).
[50] R. M. Stöckle, Y. D. Suh, V. Deckert, R. Zenobi, Nanoscale chemical analysis by tip-enhanced Raman spectroscopy. *Chem. Phys. Lett.* **318**, 131-136 (2000).
[51] N. Hayazawa, Y. Inouye, Z. Sekkat, S. Kawata, Metallized tip amplification of near-field Raman scattering. *Opt. Comm.* **183**, 333–336 (2000).
[52] M. S. Anderson, Locally enhanced Raman spectroscopy with an atomic force microscope. *Appl. Phys. Lett.* **76**, 3130-3132 (2000).
[53] T. Schmid, L. Opilik, C. Blum, R. Zenobi, Nanoscale Chemical Imaging Using Tip-Enhanced Raman Spectroscopy: A Critical Review. *Angew. Chem. Int. Ed.* **52**, 5940 – 5954 (2013).
[54] C. Chen, N. Hayazawa, S. Kawata, A 1.7 nm resolution chemical analysis of carbon nanotubes by tip-enhanced Raman imaging in the ambient. *Nat. Commun.* **5**, 3312 (2014).
[55] L. Meng, Z. Yang, J. Chen, M. Sun, Effect of Electric Field Gradient on Sub-nanometer Spatial Resolution of Tip-enhanced Raman Spectroscopy. *Sci. Rep.* **5**, 9240 (2015).
[56] B. Pettinger, P. Schambach, C. J. Villagómez, N. Scott, Tip-Enhanced Raman Spectroscopy: Near-Fields Acting on a Few Molecules. *Annu. Rev. Phys. Chem.* **63**, 379-399 (2012).
[57] C. Zhang, B. Chen, Z. Li, Optical Origin of Subnanometer Resolution in Tip-Enhanced Raman Mapping. *J. Phys. Chem. C* **119**, 11858−11871 (2015).

[58] B. Pettinger, B. Ren, G. Picardi, R. Schuster, G. Ertl, Nanoscale probing of adsorbed species by tip-enhanced Raman spectroscopy. *Phys. Rev. Lett.* **92**, 096101 (2004).
[59] J. Stadler, T. Schmid, R. Zenobi, Nanoscale Chemical Imaging Using Top-Illumination Tip-Enhanced Raman Spectroscopy. *Nano Lett.* **10**, 4514–4520 (2010).
[60] K. L. A. Chan, S. G. Kazarian, Tip-enhanced Raman mapping with top-illumination AFM. *Nanotechnology* **22**, 175701 (2011).
[61] R. Zhang, Y. Zhang, Z. C. Dong, S. Jiang, C. Zhang, L. G. Chen, L. Zhang, L. Y., J. Aizpurua, Y. Luo, J. L. Yang, J. G. Hou, Chemical mapping of a single molecule by plasmon-enhanced Raman scattering. *Nature* **498**, 82–86 (2013).
[62] S. Jiang, Y. Zhang, R. Zhang, C. Hu, M. Liao, Y. Luo, J. Yang, Z. Dong, J. G. Hou, Distinguishing adjacent molecules on a surface using plasmon-enhanced Raman scattering. *Nat. Nanotechnol.* **10**, 865 (2015).
[63] T. Yano, P. Verma, Y. Saito, T. Ichimura, S. Kawata, Pressure-assisted tip-enhanced Raman imaging at a resolution of a few nanometres. *Nat. Photonics* **3**, 473-477 (2009).
[64] T. Deckert-Gaudig, E. Kämmer, V. Deckert, Tracking of nanoscale structural variations on a single amyloid fibril with tip-enhanced Raman scattering. *J. Biophoton.* **5**, 215–219 (2012).
[65] N. Kumar, S. Mignuzzi, W. Su, D. Roy, Tip-enhanced Raman spectroscopy: principles and applications. *EPJ Tech. Instrum.* **2**, 9 (2015).
[66] L. Langelüddecke, P. Singh, V. Deckert, Exploring the Nanoscale: Fifteen Years of Tip-Enhanced Raman Spectroscopy. *Appl. Spectrosc.* **69**, 1357-1371 (2015).
[67] Z. Zhang, T. Deckert-Gaudig, V. Deckert, Label-free monitoring of plasmonic catalysis at the nanoscale. *Analyst* **140**, 4325-4335 (2015).
[68] E. Bailo, V. Deckert, Tip-enhanced Raman spectroscopy of single RNA strands: Towards a novel direct-sequencing method. *Angew. Chem. Int. Ed.* **47**, 1658-1661 (2008).
[69] N. Peica, C. Thomsen, J. Maultzsch, Tip-enhanced Raman scattering along a single wall carbon nanotubes bundle. *Phys. Status Solidi B* **247**, 2818–2822 (2010).
[70] L. G. Cancado, A. Hartschuh, L. Novotny, Tip-enhanced Raman spectroscopy of carbon nanotubes. *J. Raman Spectrosc.* **40**, 1420–1426 (2009).
[71] M. Sun, Z. Zhang, Z. H. Kim, H. Zheng, H. Xu, Plasmonic Scissors for Molecular Design. *Chem. Eur. J.* **19**, 14958 – 14962 (2013).
[72] Y. Zong, Q. Guo, M. Xu, Y. Yuan, R. Gua, J. Yao, Plasmon-induced decarboxylation of mercaptobenzoic acid on nanoparticle film monitored by surface-enhanced Raman spectroscopy. *RSC Adv.* **4**, 31810-31816 (2014).
[73] M. D. Sonntag , J. M. Klingsporn, L. K. Garibay, J. M. Roberts, J. A. Dieringer, T. Seideman, K. A. Scheidt, L. Jensen, G. C. Schatz, R. P. Van Duyne, Single-Molecule Tip-Enhanced Raman Spectroscopy. *J. Phys. Chem. C* **116**, 478-483 (2012).
[74] Z. Liu, S. Ding, Z. Chen, X. Wang, J. Tian, J. R. Anema, X. Zhou, D. Wu, B. Mao, X. Xu, B. Ren, Z. Tian, Revealing the molecular structure of single-molecule junctions in different conductance states by fishing-mode tip-enhanced Raman spectroscopy. *Nat. Commun.* **2**, 305 (2011).
[75] S. Duan, G. Tian, Y. Ji, J. Shao, Z. Dong, Y. Luo, Theoretical Modeling of Plasmon-Enhanced Raman Images of a Single Molecule with Subnanometer Resolution. *J. Am. Chem. Soc.* **137**, 9515−9518 (2015).

[76] M. Fleischer, A. Weber-Bargioni, M. V. P. Altoe, A. M. Schwartzberg, P. J. Schuck, S. Cabrini, D. P. Kern, Gold Nanocone Near-Field Scanning Optical Microscopy Probes. *ACS. Nano.* **5**, 2570–2579 (2011).

[77] M. Lopes, T. Toury, M. L. Chapelle, F. Bonaccorso, P. G. Gucciardi, Fast and reliable fabrication of gold tips with sub-50 nm radius of curvature for tip-enhanced Raman spectroscopy. *Rev. Sci. Instrum.* **84**, 073702 (2013).

[78] C. Leiterer, T. Deckert-Gaudig, P. Singh, J. Wirth, V. Deckert, W. Fritzsche, Dielectrophoretic positioning of single nanoparticles on atomic force microscope tips for tip-enhanced Raman spectroscopy. *Electrophoresis* **36**, 1142-1148 (2015).

[79] L. Yang, T. Huang, Z. Zeng, M. Li, X. Wang, F. Yang, B. Ren, Rational fabrication of a gold-coated AFM TERS tip by pulsed electrodeposition. *Nanoscale* **7**, 18225-18231 (2015).

[80] T. Umakoshi, T. Yano, Y. Saito, P. Verma, Fabrication of Near-Field Plasmonic Tip by Photoreduction for Strong Enhancement in Tip-Enhanced Raman Spectroscopy. *Appl. Phys. Expr.* **5**, 052001 (2012).

[81] L. Meng, T. Huang, X. Wang, S. Chen, Z. Yang, B. Ren, Gold-coated AFM tips for tip-enhanced Raman spectroscopy: theoretical calculation and experimental demonstration. *Opt. Express* **23**, 13804-13813 (2015).

[82] J. Conyard, K. Addison, I. A. Heisler, A. Cnossen, W. R. Browne, B. L. Feringa, S. R. Meech, Ultrafast dynamics in the power stroke of a molecular rotary motor. *Nat. Chem.* **4**, 547-551 (2012).

[83] E. Sheremet, A. G. Milekhin, R. D. Rodriguez, T. Weiss, M. Nesterov, E. E. Rodyakina, O. D. Gordan, L. L. Sveshnikova, T. A. Duda, V. A. Gridchin, V. M. Dzhagan, M. Hietscholdf, D. R. T. Zahn, Surface- and tip-enhanced resonant Raman scattering from CdSe nanocrystals. *Phys.Chem.Chem.Phys.* **17**, 21198--21203 (2015).

[84] G. McNay, D. Eustace, W. E. Smith, K. Faulds, D. Graham, Surface-Enhanced Raman Scattering (SERS) and Surface-Enhanced Resonance Raman Scattering (SERRS): A Review of Applications. *Appl. Spectrosc.* **65**, 825-837 (2011).

[85] H. Kim, K. M. Kosuda, R. P. Van Duyne, P. C. Stair, Resonance Raman and surface- and tip-enhanced Raman spectroscopy methods to study solid catalysts and heterogeneous catalytic reactions. *Chem. Soc. Rev.* **39**, 4820–4844 (2010).

[86] S. L. Kleinman, E. Ringe, N. Valley, K. L. Wustholz, E. Phillips, K. A. Scheidt, G. C. Schatz, R. P. Van Duyne, Single-Molecule Surface-Enhanced Raman Spectroscopy of Crystal Violet Isotopologues: Theory and Experiment. *J. Am. Chem. Soc.* **133**, 4115–4122 (2011).

[87] A. B. Zrimsek, A. Henry, R. P. Van Duyne, Single Molecule Surface-Enhanced Raman Spectroscopy without Nanogaps. *J. Phys. Chem. Lett.* **4**, 3206–3210 (2013).

[88] T. Itoh, Y. S. Yamamoto, H. Tamaru, V. Biju, S. Wakida, Y. Ozaki, Single-molecular surface-enhanced resonance Raman scattering as a quantitative probe of local electromagnetic field: The case of strong coupling between plasmonic and excitonic resonance. *Phys. Rev. B* **89**, 195436 (2014).

[89] B. Dong, Y. Fang, X. Chen, H. Xu, M. Sun, Substrate-, Wavelength-, and Time-Dependent Plasmon-Assisted Surface Catalysis Reaction of 4-Nitrobenzenethiol Dimerizing to p, p'-Dimercaptoazobenzene on Au, Ag, and Cu Films. *Langmuir* **27**, 10677-10682 (2011).

[90] S. Mukherjee, F. Libisch, N. Large, O. Neumann, L. V. Brown, J. Cheng, J. B. Lassiter, E. A. Carter, P. Nordlander, N. J. Halas, Hot Electrons Do the Impossible: Plasmon-Induced Dissociation of H2 on Au. *Nano Lett.* **13**, 240−247 (2013).
[91] M. Sun, Y. Huang, L. Xia, X. Chen, H. Xu, The pH-Controlled Plasmon-Assisted Surface Photocatalysis Reaction of 4-Aminothiophenol to p,p′-Dimercaptoazobenzene on Au, Ag, and Cu Colloids. *J. Phys. Chem. C* **115**, 9629–9636 (2011).
[92] P. Xu, L. Kang, N. H. Mack, K. S. Schanze, X. Han, H. Wang, Mechanistic understanding of surface plasmon assisted catalysis on a single particle: cyclic redox of 4-aminothiophenol. *Sci. Rep.* **3**, 2997 (2013).
[93] Z. Zhang, T. Deckert-Gaudig, V. Deckert, Label-free monitoring of plasmonic catalysis at the nanoscale. *Analyst* **40**, 4325-4335 (2015).
[94] W. Xie, B. Walkenfort, S. Schlücker, Label-Free SERS Monitoring of Chemical Reactions Catalyzed by Small Gold Nanoparticles Using 3D Plasmonic Superstructures. *J. Am. Chem. Soc.* **135**, 1657−1660 (2013).
[95] L. Cui, P. Wang, Y. Fang, Y. Li, M. Sun, A plasmon-driven selective surface catalytic reaction revealed by surface-enhanced Raman scattering in an electrochemical environment. *Sci. Rep.* **5**, 11920 (2015).
[96] S. Nie, S. R. Emory, Probing Single Molecules and Single Nanoparticles by Surface-Enhanced Raman Scattering. *Science* **275**, 1102-1106 (1997).
[97] T. Ichimura, H. Watanabe, Y. Morita, P. Verma, S. Kawata, Y. Inouye, Temporal fluctuation of tip-enhanced Raman spectra of adenine molecules. *J. Phys. Chem. C* **111**, 9460-9464 (2007).
[98] T. Vosgröne, A. J. Meixner, Surface- and Resonance-Enhanced Micro-Raman Spectroscopy of Xanthene Dyes: From the Ensemble to Single Molecules. *ChemPhysChem* **6**, 154–163 (2005).
[99] P. Singh, T. Deckert-Gaudig, H. Schneidewind, K. Kirsch, E. M. van Schrojenstein Lantman, B. M. Weckhuysen, V. Deckert, Differences in single and aggregated nanoparticle plasmon spectroscopy. *Phys. Chem. Chem. Phys.* **17**, 2991-2995 (2015).
[100] P. Singh, V. Deckert, Local protonation control using plasmonic activation. *Chem. Commun.* **50**, 11204-11207 (2014).
[101] P. Singh, T. Deckert-Gaudig, Z. Zhang, V. Deckert, Plasmon induced deprotonation of 2-mercaptopyridine. *Analyst*, Submitted.
[102] Z. Zhang, T. Deckert-Gaudig, P. Singh, V. Deckert, Single molecule level plasmonic catalysis: a dilution study of p-nitrothiophenol on gold dimers. *Chem. Commun.* **51**, 3069-3072 (2015).
[103] J. Turkevich, P. C. Stevenson, J. Hillier, A study of the nucleation and growth processes in the synthesis of colloidal gold *Discuss. Faraday Soc.* **11**, 55-75 (1951).
[104] G. Frens, Controlled Nucleation for the Regulation of the Particle Size in Monodisperse Gold Suspensions. *Nature* **241**, 20–22 (1973).
[105] J. C. Love, L. A. Estroff, J. K. Kriebel, R. G. Nuzzo, G. M. Whitesides, Self-Assembled Monolayers of Thiolates on Metals as a Form of Nanotechnology. *Chem. Rev.* **105**, 1103-1169 (2005).
[106] S. S. Mallajosyula, S. K. Pati, Effect of Protonation on the Electronic Properties of DNA Base Pairs: Applications for Molecular Electronics. *J. Phys. Chem. B,* **111**, 11614-11618 (2007).

[107] P. Wu, H. Hara, Y. Kawamoto, N. Sugimoto, Effect of cytosine protonation and cation on thermodynamic properties of parallel DNA triplex family. *Nucleic Acids Res Suppl.* **1**, 39-40. (2001).
[108] S. Kappaun, S. Horner, A. Kelterer, K. Waich, F. Grasse, M. Graf, L. Romaner, F. Niedermair, K. Müllen, A. C. Grimsdale, R. Saf, E. J. W. List, E. Zojer, C. Slugovc, The Effect of Protonation on the Optical Properties of Conjugated Fluorene–Pyridine Copolymers. *Macromol. Chem. Phys.* **209**, 2122–2134 (2008).
[109] K. Chingin, R. M. Balabin, V. Frankevich, H. Chen, K. Barylyuk, R. Nieckarz, A. Fedorova, R. Zenobi, Optical properties of protonated Rhodamine 19 isomers in solution and in the gas phase. *Phys. Chem. Chem. Phys.* **12**, 14121-14127 (2010).
[110] H. Häkkinen, The gold–sulfur interface at the nanoscale. *Nat. Chem.* **4**, 443-455 (2012).
[111] C. D. Bain, H. A. Biebuyck, G. M. Whitesides, Comparison of Self -Assembled Monolayers on Gold: Coadsorption of Thiols and Disulfides1. *Langmuir* **5**, 723-727 (1989).
[112] L. Strong, G. M. Whitesides, Structures of self-assembled monolayer films of organosulfur compounds adsorbed on gold single crystals: electron diffraction studies. *Langmuir* **4**, 546–558 (1988).
[113] R. Stöckle, V. Deckert, C. Fokas, R. Zenobi, Controlled formation of isolated silver islands for surface-enhanced Raman scattering. *Appl. Spectrosc.* **54**, 1577–1583 (2000).
[114] T. Deckert-Gaudig, V. Deckert, Ultraflat transparent gold nanoplates - ideal substrates for tip-enhanced Raman scattering experiments. *Small* **5**, 432-436 (2009).
[115] J. Lee, S. Mubeen, X. Ji, G. D. Stucky, M. Moskovits, Plasmonic Photoanodes for Solar Water Splitting with Visible Light. *Nano Lett.* **12**, 5014–5019 (2012).
[116] D. B. Ingram, S. Linic, Water Splitting on Composite Plasmonic-Metal/Semiconductor Photoelectrodes: Evidence for Selective Plasmon-Induced Formation of Charge Carriers near the Semiconductor Surface. *J. Am. Chem. Soc.* **133**, 5202–5205 (2011).
[117] Z. L. Zhang, P. F. Yang, H. X. Xu, H. R. Zheng, Surface enhanced fluorescence and Raman scattering by gold nanoparticle dimers and trimers. *J. Appl. Phys.* **113**, 033102 (2013).

4 Publications

4.1 Differences in single and aggregated nanoparticle plasmon spectroscopy

Author contributions

Differences in single and aggregated nanoparticle plasmon spectroscopy, Phys.Chem.Chem.Phys., 17, 2991-2995, 2015 https://doi.org/10.1039/C4CP04850D							
	Pushkar Singh	Tanja Deckert-Gaudig	Henrik Schneidewind	Konstantin Kirsch	Evelien. M. van Schrojenstein Lantman	Bert M. Weckhuysen	Volker Deckert
Conceptual research design	X						X
Planning of research activities	X	X	X	X			X
Data collection	X						
Data analyses and interpretation	X	X					X
Manuscript writing	X	X			X	X	X
Suggested publication equivalence value	1.0						

Reprinted with kind permission from the Royal Society of Chemistry.

[PS1] Pushkar Singh, Tanja Deckert-Gaudig, Henrik Schneidewind, Konstantin Kirsch, Evelien. M. van Schrojenstein Lantman, Bert M. Weckhuysen and Volker Deckert, "Differences in single and aggregated nanoparticle plasmon spectroscopy" Phys.Chem.Chem.Phys., 17, 2991-2995, 2015

PCCP

COMMUNICATION

View Article Online
View Journal | View Issue

Differences in single and aggregated nanoparticle plasmon spectroscopy

Cite this: *Phys. Chem. Chem. Phys.*, 2015, **17**, 2991

Received 23rd October 2014,
Accepted 9th December 2014

DOI: 10.1039/c4cp04850d

www.rsc.org/pccp

Pushkar Singh,[a] Tanja Deckert-Gaudig,[a] Henrik Schneidewind,[a] Konstantin Kirsch,[a] Evelien M. van Schrojenstein Lantman,[b] Bert M. Weckhuysen*[b] and Volker Deckert*[ac]

Vibrational spectroscopy usually provides structural information averaged over many molecules. We report a larger peak position variation and reproducibly smaller FWHM of TERS spectra compared to SERS spectra indicating that the number of molecules excited in a TERS experiment is extremely low. Thus, orientational averaging effects are suppressed and micro ensembles are investigated. This is shown for a thiophenol molecule adsorbed on Au nanoplates and nanoparticles.

Tip-enhanced Raman scattering (TERS) allows investigating molecular information on the nanometer scale. This technique is a combination of scanning probe microscopy (SPM) and Raman spectroscopy, which is applied in different branches of nano-sciences enabling high spatial resolution and high sensitivity simultaneously. A metal-coated atomic force microscope tip produces localized surface plasmon resonance (LSPR) when illuminated with an appropriate wavelength of light. This leads to a Raman signal enhancement of several orders of magnitude. Additionally, due to the confinement of the electromagnetic field at the tip apex, a spatial resolution in the nanometer range can be achieved.[1–4]

Recent experiments indicate that even single molecules can be detected using TERS.[5–8] Thus it is an excellent tool to get vibrational information down to a single molecule (SM) level as well as to perform fundamental research where high spatial resolution is required *e.g.* distinction of isotopes,[6] nano-scale pressure sensors,[9] identification of nano-oxidation sites in biological molecules,[10] separation of lipid and protein domains in a single cell,[11] the study of molecular catalytic reaction,[12] *etc.*

In many cases it seems to be sensible to compare the well-known surface-enhanced Raman scattering (SERS) spectra of a compound with the data obtained by a TERS experiment due to identical enhancement mechanisms in both types of experiments. However, variations in the peak position and full-width-half-maximum (FWHM) in many TERS and SERS experiments can hardly be ignored. In general, band position fluctuation and sometimes even the suppression of a band reflects a specific molecular environment. Thus, information regarding molecular orientation, adsorption site, bond strength and molecular environment can be extracted.[12,13]

In a typical SM-SERS experiment[13–17] a very low concentration of molecules ($<10^{-8}$ M) is used to ensure that on average less than one molecule is present in the large electromagnetic field of the laser focus. In such SM experiments large peak position fluctuations are observed.[18] TERS can be regarded as close to SM-SERS experiments where the signal-enhancing unit is reduced to a single nanoparticle. Consequently, only a few molecules experience the above mentioned signal enhancement. Considering this, vibrational spectra collected at the SM level using SERS and TERS should look alike and provide similar chemical information. On the other hand, one important difference between SERS and TERS experiments must be considered: as the tip can be positioned freely, the interaction between the molecule and the nanoparticle in TERS does not have to be thermodynamically or kinetically favored. In SERS, in contrast, molecules will preferentially bind to favored sites. This can lead to a broader variation in potential conformations in a TERS experiment.

TERS has already been applied to study the tip position and time dependent properties of DNA nucleobases by different groups.[19–22] Temporal variations in contact-mode TERS spectra of an adenine crystal show large peak position fluctuations.[19] This was attributed to changes in the molecular orientation with respect to the tip and chemical interaction of the tip with the sample. Recently, the position and time dependent TERS spectra of an adenine homopolymer were studied in a gap mode arrangement.[21] These studies demonstrate that characteristic bands are reproducibly detected but fluctuations in the peak position are always an issue and that sample orientation with respect to tip plays a vital role.

While band position fluctuations in TERS with resonantly excited molecules have already been studied by the van Duyne

[a] *Leibniz Institute of Photonic Technology, Albert-Einstein-Str. 9, 07745 Jena, Germany*
[b] *Inorganic Chemistry and Catalysis, Debye Institute for Nanomaterial Science, Utrecht University, Universiteitsweg 99, 3584 CG Utrecht, The Netherlands. E-mail: b.m.weckhuysen@uu.nl*
[c] *Institute of Physical Chemistry and Abbe Center of Photonics, Friedrich-Schiller University Jena, Helmholtzweg 4, 07743 Jena, Germany. E-mail: volker.deckert@ipht-jena.de*

group and the variations have been attributed to the variations in the excited state properties,[23,24] to our knowledge a direct comparison to non-resonant molecules and their corresponding SERS data regarding such fluctuations is missing. As aforementioned, SERS spectra are usually the closest reference data available and a better understanding of the reliability of SERS data for TERS spectra assignment is desirable. Here, TERS and SERS data of thiophenol were compared. Thiophenol was chosen to keep the system comparably simple and to control orientation and coverage of the molecule by specific adsorption *via* the thiol group to a single atomically flat gold nanoplate (TERS) and gold nanoparticles (SERS), respectively. From the results it was concluded that the main reason for peak fluctuations in TERS is the small number of molecules in the sampled area and their specific orientation.

The experimental TERS setup has been described in detail elsewhere.[20] In short, laser radiation is focused in transmission geometry on a silver coated AFM non-contact tip using an oil immersion microscope objective (40X, 1.35NA, Olympus). The AFM head (JPK AG, Germany) is mounted on an inverted microscope. The scattered TERS signal is collected using the same objective and passes through a dichroic mirror and notch filter before it enters the spectrometer (Action Advanced SP2750 A, SI GmbH, Germany). The same setup was used for the all SERS measurements. TERS and SERS spectra were recorded using 532 nm laser excitation and using 10 s acquisition time. The power on the sample was 830 μW (TERS) and 810 μW (SERS), respectively, in order to achieve a similar signal-to-noise ratio in the spectra.

Synthesis of gold nanoplates on chemically cleaned glass slides (concentration HNO_3/30% H_2O_2 (3 : 1) solution, 2 h) was performed according to a previously described method.[25] For the TERS experiments, a self-assembled monolayer of thiophenol was prepared by immersing the gold nanoplate substrate for 18 h in a 5×10^{-3} M ethanolic solution of thiophenol. Gold nanoparticles for SERS were synthesized and immobilized on glass slides according to ref. 26 and 27. 2 μL of 5×10^{-3} M ethanolic thiophenol solution was dropped on the substrate and dried before the measurement.

It is commonly known that thiophenol covalently binds *via* sulfur to gold surfaces, *i.e.* to nanoparticles in SERS and to nanoplates in TERS. Specifically in the latter case this was a crucial step to avoid undesired binding of the molecule to the Ag tip. This would cause a band shift as can be seen in experiments when SERS on Ag islands is compared to TERS. In our case such shifts were never observed, hence the Au-S bonds are stable under our conditions.

A topographic AFM image of the gold nanoplate used to assemble the thiophenol monolayer is shown in Fig. 1(a), a corresponding SERS substrate is shown in Fig. 1(b). For position and time dependent experiments 200 TERS and SERS spectra were recorded using 532 nm laser excitation and 10 s acquisition time. Typical TERS and SERS spectra are shown in Fig. 1(c) for TERS and (d) for SERS, respectively. The three thiophenol marker bands in SERS at 999 cm^{-1} (ring breathing mode), 1075 cm^{-1} (C–C in-plane bending) and 1569 cm^{-1} (C–C stretching) are

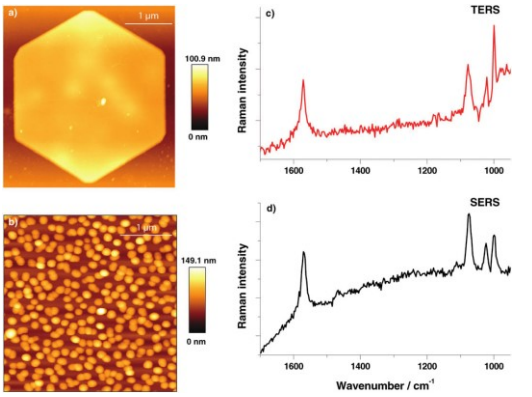

Fig. 1 AFM topography of (a) Au nanoplate for TERS and (b) gold nanoparticles for SERS. Typical thiophenol spectra on (c) gold nanoplate (10 s acquisition time – TERS). (d) Gold nanoparticles (10 s acquisition time – SERS).

clearly visible in all spectra. The C–C in plane bending mode at 1075 cm^{-1} having a1-type symmetry is known to show a peak position shift on different substrates[28] and therefore was excluded from analysis. Each peak was fitted with a Lorentzian function (Igor PRO 6.22A, Wavemetrics, USA) to provide information on the band position and FWHM.

TERS spectra were recorded at different locations (distance 10 nm between positions) on the gold nanoplates. Similarly, SERS spectra were also recorded at different positions on the gold nanoparticle substrate. Here the distance between locations was 150 nm. The band position variation for the two selected modes in TERS is shown in the histograms in Fig. 2(a) and (c). A relatively large band position fluctuation of about 6–9 cm^{-1} can be observed. The same bands in the SERS spectra show only

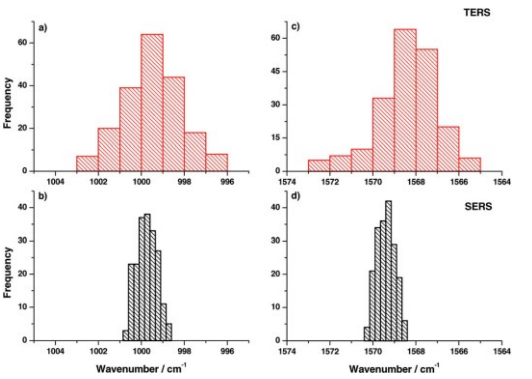

Fig. 2 (a, c) Position dependent distribution of the peak position for two selected thiophenol bands (ring breathing and C–C stretching mode) in the TERS experiment (on flat Au plates). (b, d) Corresponding histogram of the peak position for the same thiophenol bands in position dependent SERS (on gold nanoparticles) showing smaller variations in the peak position compared to TERS.

This journal is © the Owner Societies 2015

a small peak position fluctuation of about 2 cm^{-1}. Comparing the band position variation of the present TERS data with SM-SERS spectra by Nie and Emory[13] a similar fluctuation can be found. Actually, the current TERS measurement cannot be considered as the SM experiment, but the observed band position fluctuation already points to a very small number of molecules in the interaction region of the TERS tip. As a monolayer was probed this was an unexpected behavior. To explain this SM-like fluctuation in TERS spectra, two possible mechanisms are proposed:

(1) The electromagnetic enhancement of a tip with a radius of 10 nm is supposed to excite at least hundreds of molecules from the thiophenol monolayer. Thus, a SM-like behavior can be explained if all those molecules under investigation have the same orientation and neighborhood. As the tip moves to the next position it interacts with a different set of molecules, where again the molecules have the same orientation relative to one another, however it differs from the previous location of the TERS probe.

(2) A "single-molecule like" vibrational spectrum under TERS conditions can be expected if an additional chemical enhancement is taken into account. This can lead to a much higher spatial resolution since an interaction between the apex of the tip to the surface can only occur to a few if not only a single molecule being in direct neighborhood to the tip.[7] Such an effect could also lead to the observed variation in the peak position.

It is already known that the thiophenol monolayer on a gold surface forms ordered domains of about 15 nm diameter.[29–31] Reorientation of the molecules will cause a different response to the polarization of the exciting light.[32]

In a SERS measurement the orientation effect is averaged over many nanoparticles in the laser focus contributing to the overall signal. Hence, no fluctuation in the peak position was expected as experimentally observed and shown in Fig. 2(b) and (d).

In the next step, FWHM of the Raman bands in the respective experiments was analyzed in the same way. The FWHM was determined for every TERS and SERS spectrum and plotted in histograms as shown in Fig. 3. The vertical lines drawn in the histograms correspond to the average FWHM values. The comparison clearly illustrates that the average FWHM in TERS spectra is smaller than in the SERS spectra. In general, the FWHM of a Raman band is determined by several factors. If instrumental influences like slit width are neglected, the line width of a spectral band for gases and liquids is mostly influenced by vibrational relaxation and dephasing. Already for liquid mixtures the effect of the microscopic environment must be considered and the actual observed line width is a superposition of all possible micro-environments weighted to their respective probabilities.[33–35] As vibrational relaxation and dephasing usually take place in a range of up to hundreds of picoseconds and the mechanisms should be similar in TERS and SERS.[36] Thus, the main effect that leads to the observed changes can be attributed to the different roles of the micro-environments. In the SERS experiments more than ten nanoparticles and around 10^6 molecules

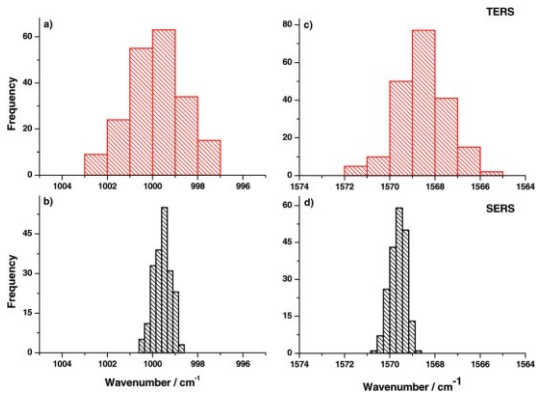

Fig. 4 (a, c) Peak position variation for the selected thiophenol bands (ring breathing and C–C stretching modes) in a TERS time trace (on flat Au plates). (b, d) Peak position histogram for the same thiophenol signals in a corresponding SERS (on gold nanoparticles) time trace, showing smaller peak shifts compared to TERS.

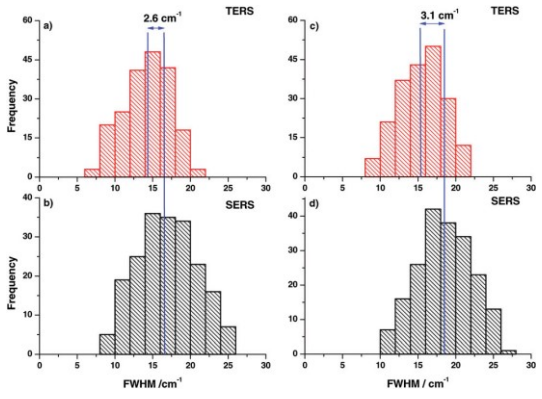

Fig. 3 (a, c) Histogram of position dependent FWHM variations of the thiophenol ring breathing and C–C stretching modes in TERS. (b, d) Corresponding histogram of position dependent SERS. The average FWHM in SERS is reproducibly larger compared to TERS.

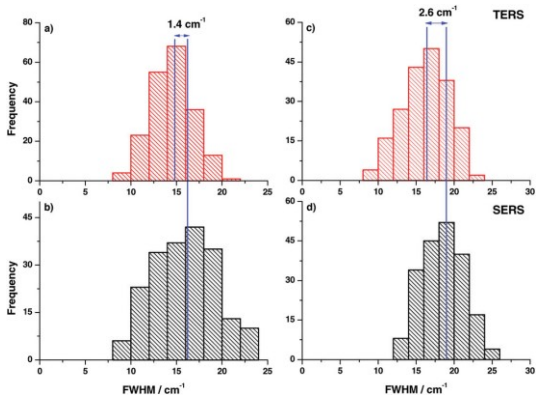

Fig. 5 (a, c) FWHM of the selected thiophenol bands (ring breathing and C–C stretching modes) for a TERS time trace. (b, d) FWHM of the same thiophenol bands for the corresponding SERS time trace on gold nanoparticles.

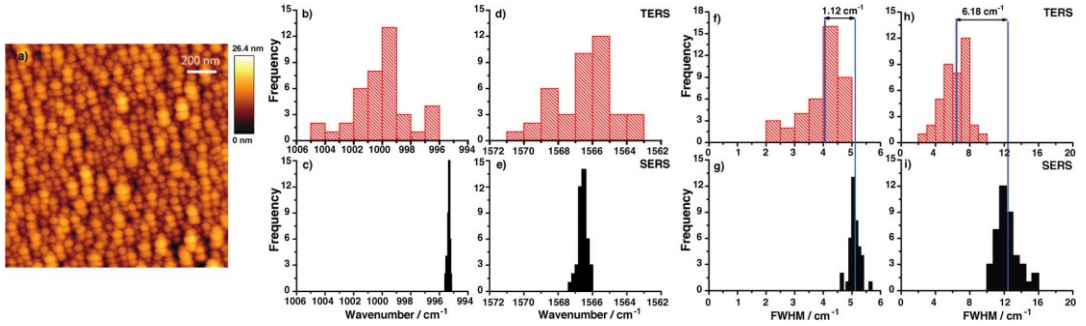

Fig. 6 (a) AFM topography of silver island film used to produce a thiophenol monolayer. (b, d) Histogram of peak position variation for the selected thiophenol bands (ring breathing and C–C stretching modes) in position dependent TERS (on flat Au plates) and (c, e) corresponding histogram for the same thiophenol bands in position dependent SERS (on silver island film). (f, h) Histogram of FWHM variation in position dependent TERS (on flat Au plates) and (g, i) corresponding histogram for the same thiophenol bands in position dependent SERS (on silver island film).

(assuming a laser spot size of 500 nm) contribute to the overall line width, while in a TERS experiment only one nanoparticle and at most only a few hundred molecules contribute to the overall line width. These observations are supported by the observation of concentration dependent line width variations in Raman band studies by different groups,[37,38] which is in line with our experiments as well.

In order to further support this hypothesis, measurements on a single location were done and the time dependent behavior of TERS and SERS spectra was studied. Hence, the sample position was fixed with respect to tip and laser focus and spectra were collected consecutively. The histograms of peak position variation of different bands in TERS experiments are shown in Fig. 4(a) and (c). The corresponding SERS results are shown in Fig. 4(b) and (d). Comparing peak position variations in time traces and the position dependent TERS measurements, similar variations were observed. Again this indicates that the observed area under a TERS tip is very small, otherwise a thermal drift (if any) would not change the peak position notably. Small changes in the monolayer position with respect to the tip are expected due to diffusion.[39] No correlation was observed in peak position variation in consecutive TERS time traces, which indicates that the dominant mechanism for large peak position variation is likely a chemical interaction between the tip and the sample that detects even small conformational changes of the probed molecule.

In addition, the FWHM variation in the time trace (Fig. 5) clearly demonstrates that the average FWHM in the SERS experiment is larger compared to TERS, indicating that more molecules are involved in SERS measurements yielding a larger FWHM. The difference in average FWHM varies from peak to peak, which indicates nonlinear coupling of modes from different molecules.

Different substrates (Au, Ag, *etc.*)[28,40] can also potentially influence the results. To check this effect we additionally performed SERS on silver island films by adding 2 μL of 5×10^{-3} M ethanolic thiophenol solution and drying it before the measurement. SERS spectra are recorded using 75 μW power of 532 nm laser excitation with 1s acquisition time. A comparison of the 40 spatially dependent SERS and TERS spectra is shown in Fig. 6. Fig. 6(a) shows the AFM topography of silver island film.[41,42] On the silver island film more than hundred nanoparticles with around 10^7 molecules contribute to the SERS signal. Fig. 6(b) and (d) and Fig. 6(c) and (e) give histograms of the peak position variation of the selected bands in TERS and corresponding SERS spectra on silver island film in position dependent measurements. An absolute band shift was observed, which was different for each marker band. The absolute band shift between TERS and SERS is caused by (1) a slightly different binding of thiophenol to the substrate (Au or Ag) and (2) tip-sample nanogap. The relative peak position variations are still comparable with the SERS experiment on Au nanoparticles. In Fig. 6(f) and (h) and Fig. 6(g) and (i) histograms of position dependent FWHM variations in TERS and corresponding SERS spectra on the silver island film are plotted showing higher FWHM in SERS compared to TERS. Again, nonlinear coupling of modes leads to asymmetric FWHM variation of the selected bands.

Conclusions

We have demonstrated the large peak position fluctuations in the TERS study (6–9 cm^{-1}) of the thiophenol monolayer, which indicate a single molecule like behavior and two possible mechanisms for such behavior were suggested. No correlation in peak position variation of consecutive TERS spectra in time dependent measurement was observed. Thus, the dominant mechanism for fluctuations in the peak position is the direct chemical interaction between the tip and the sample. TERS probes the small conformational molecular changes on such a small scale that the normally observed averaging is absent.

Bands in the TERS spectra of thiophenol exhibit a narrower line-width than the SERS spectra. These observations can also be related to the apparently smaller number of molecules excited in TERS compared to SERS experiments. While in TERS only molecules in closest vicinity to the single nanoparticle at the tip apex experience a signal enhancement, in SERS many hot spots and all the molecules in their vicinity contribute to the over-all signal. Additionally, differences in average values of FWHM in SERS and TERS spectra vary from peak to peak and

 This journal is © the Owner Societies 2015

can be explained by the nonlinear coupling of modes between different molecules which could be influenced by metal nanoparticles under investigation.

Both the peak position and FWHM comparisons of TERS and SERS spectra indicate that in TERS experiments a micro-ensemble of molecules is excited by the field at the tip apex in contrast to a macro-ensemble of investigated molecules in the SERS experiments. Thus, the results demonstrate that SERS databases can only be used with caution for TERS spectra assignment. In particular band position variations of 10 cm^{-1} and more in TERS can occur as only a few molecules are probed.

Acknowledgements

Support from the European Union and the state of Thuringia (FKZ: 2011 FE 9048; 2011 VF 0016) as well as through the Deutsche Forschungsgemeinschaft (FR 1348/19-1) is gratefully acknowledged. B.M.W. acknowledges financial support from an European Research Council (ERC) Advanced Grant (no. 321140). We would like to thank Matthias Thiele for the preparation of gold nanoparticle SERS substrates.

Notes and references

1 D. Cialla, T. Deckert-Gaudig, C. Budich, M. Laue, R. Möller, D. Naumann, V. Deckert and J. Popp, *J. Raman Spectrosc.*, 2009, **40**, 240–243.
2 T. Deckert-Gaudig and V. Deckert, *Phys. Chem. Chem. Phys.*, 2010, **12**, 12040–12049.
3 U. Neugebauer, P. Rösch, M. Schmitt, J. Popp, C. Julien, A. Rasmussen, C. Budich and V. Deckert, *ChemPhysChem*, 2006, **7**, 1428–1430.
4 B. Pettinger, P. Schambach, C. J. Villagómez and N. Scott, *Annu. Rev. Phys. Chem.*, 2012, **63**, 379–399.
5 C. C. Neacsu, J. Dreyer, N. Behr and M. B. Raschke, *Phys. Rev. B: Condens. Matter Mater. Phys.*, 2006, **73**, 193406.
6 M. D. Sonntag, J. M. Klingsporn, L. K. Garibay, J. M. Roberts, J. A. Dieringer, T. Seideman, K. A. Scheidt, L. Jensen, G. C. Schatz and R. P. Van Duyne, *J. Phys. Chem. C*, 2012, **116**, 478–483.
7 R. Zhang, Y. Zhang, Z. C. Dong, S. Jiang, C. Zhang, L. G. Chen, L. Zhang, Y. Liou, J. Aizpurua, Y. Luo, J. L. Yang and J. G. Hou, *Nature*, 2013, **498**, 82–86.
8 W. H. Zhang, B. S. Yeo, T. Schmid and R. Zenobi, *J. Phys. Chem. C*, 2007, **111**, 1733–1738.
9 T. Yano, P. Verma, Y. Saito, T. Ichimura and S. Kawata, *Nat. Photonics*, 2009, **3**, 473–477.
10 B. R. Wood, M. Asghari-Khiavi, E. Bailo, D. McNaughton and V. Deckert, *Nano Lett.*, 2012, **12**, 1555–1560.
11 M. Richter, M. Hedegaard, T. Deckert-Gaudig, P. Lampen and V. Deckert, *Small*, 2011, **7**, 209–214.
12 E. M. van Schrojenstein Lantman, T. Deckert-Gaudig, A. J. G. Mank, V. Deckert and B. M. Weckhuysen, *Nat. Nanotechnol.*, 2012, **7**, 583–586.
13 S. Nie and S. R. Emory, *Science*, 1997, **275**, 1102–1106.
14 J. A. Dieringer, K. L. Wustholz, D. J. Masiello, J. P. Camden, S. L. Kleinman, G. C. Schatz and R. P. Van Duyne, *J. Am. Chem. Soc.*, 2009, **131**, 849–854.
15 K. Kneipp, Y. Wang, H. Kneipp, L. T. Perelman, I. Itzkan, R. R. Dasari and M. S. Feld, *Phys. Rev. Lett.*, 1997, **78**, 1667–1670.
16 H. Liu, L. Zhang, X. Lang, Y. Yamaguchi, H. Iwasaki, Y. Inouye, Q. Xue and M. Chen, *Sci. Rep.*, 2011, **1**, 112.
17 P. G. Etchegoin and E. C. Le Ru, *Phys. Chem. Chem. Phys.*, 2008, **10**, 6079–6089.
18 T. Vosgröne and A. J. Meixner, *ChemPhysChem*, 2005, **6**, 154–163.
19 T. Ichimura, H. Watanabe, Y. Morita, P. Verma, S. Kawata and Y. Inouye, *J. Phys. Chem. C*, 2007, **111**, 9460–9464.
20 A. Rasmussen and V. Deckert, *J. Raman Spectrosc.*, 2006, **37**, 311–317.
21 R. Treffer, X. M. Lin, E. Bailo, T. Deckert-Gaudig and V. Deckert, *Beilstein J. Nanotechnol.*, 2011, **2**, 628–637.
22 D. Zhang, K. F. Domke and B. Pettinger, *ChemPhysChem*, 2010, **10**, 1662–1665.
23 M. D. Sonntag, D. Chulhai, T. Seideman, L. Jensen and R. P. Van Duyne, *J. Am. Chem. Soc.*, 2013, **135**, 17187–17192.
24 J. M. Klingsporn, N. Jiang, E. A. Pozzi, M. D. Sonntag, D. Chulhai, T. Seideman, L. Jensen, M. C. Hersam and R. P. Van Duyne, *J. Am. Chem. Soc.*, 2014, **136**, 3881–3887.
25 T. Deckert-Gaudig and V. Deckert, *Small*, 2009, **5**, 432–436.
26 J. Turkevich, P. C. Stevenson and J. Hillier, *Discuss. Faraday Soc.*, 1951, **11**, 55–75.
27 G. Frens, *Nature*, 1973, **241**, 20–22.
28 B. Ren, G. Picardi, G. Pettinger, R. Schuster and G. Ertl, *Angew. Chem., Int. Ed.*, 2005, **44**, 139–142.
29 A. Dhirani, R. W. Zehner, R. P. Hsung, P. Guyot-Sionnest and L. R. Sita, *J. Am. Chem. Soc.*, 1196, **118**, 3319–3320.
30 D. Käfer, A. Bashir and G. Witte, *J. Phys. Chem. C*, 2007, **111**, 10546–10551.
31 L. Wan, H. Terashima, H. Noda and M. Osawa, *J. Phys. Chem. B*, 2000, **104**, 3563–3569.
32 T. Deckert-Gaudig, E. Rauls and V. Deckert, *J. Phys. Chem. C*, 2010, **114**, 7412–7420.
33 F. Bondarev and A. I. Mardaeva, *Opt. Spektrosk.*, 1973, **35**, 286–288.
34 E. W. Knapp and S. F. Fischer, *J. Chem. Phys.*, 1981, **74**, 89–95.
35 E. W. Knapp and S. F. Fischer, *J. Chem. Phys.*, 1982, **76**, 4730–4735.
36 E. J. Heilweil, M. P. Casassa, R. R. Cavanagh and J. C. Stephenson, *Annu. Rev. Phys. Chem.*, 1989, **40**, 143–171.
37 S. Bratos and G. Tarjus, *Phys. Rev. A: At., Mol., Opt. Phys.*, 1985, **32**, 2431–2438.
38 A. K. Ojha, S. K. Srivastava, R. K. Singh and B. P. Asthana, *J. Phys. Chem. A*, 2006, **110**, 9849–9853.
39 K. F. Domke, D. Zhang and B. Pettinger, *J. Phys. Chem. C*, 2007, **111**, 8611.
40 K. T. Carron and L. G. Hurley, *J. Phys. Chem.*, 1991, **95**, 9979–9984.
41 R. Stöckle, V. Deckert, C. Fokas and R. Zenobi, *Appl. Spectrosc.*, 2000, **54**, 1577–1583.
42 R. Stöckle, V. Deckert, C. Fokas, D. Zeisel and R. Zenobi, *Vib. Spectrosc.*, 2000, **22**, 39–48.

This journal is © the Owner Societies 2015

4.2 Local protonation control using plasmonic activation

Author contributions

Local protonation control using plasmonic activation, Chem. Commun., 50, 11204 - 11207, 2014 https://doi.org/10.1039/C4CC04642K		
	Pushkar Singh	Volker Deckert
Conceptual research design	X	X
Planning of research activities	X	X
Data collection	X	
Data analyses and interpretation	X	X
Manuscript writing	X	X
Suggested publication equivalence value	1.0	

Reprinted with kind permission from the Royal Society of Chemistry.

[PS2] Pushkar Singh and Volker Deckert "Local protonation control using plasmonic activation" Chem. Commun., 50, 11204 -11207, 2014.

ChemComm

COMMUNICATION

View Article Online
View Journal | View Issue

Local protonation control using plasmonic activation†

Pushkar Singh[a] and Volker Deckert*[ab]

Cite this: *Chem. Commun.*, 2014, **50**, 11204

Received 18th June 2014,
Accepted 5th August 2014

DOI: 10.1039/c4cc04642k

www.rsc.org/chemcomm

Localized protonation of 4-mercaptopyridine (4-MPY), activated by light in the presence of silver nanoparticles is monitored under ambient conditions using surface-enhanced Raman scattering (SERS) and tip-enhanced Raman scattering (TERS). The reaction can be controlled by the excitation wavelength and the atmospheric conditions, thus, providing a tool for site-specific control of protonation.

Coupling of electromagnetic radiation under specific conditions to a metal–dielectric interface results in surface plasmons (SP), which play a key role in many areas like biosensors,[1,2] DNA sequencing,[3,4] plasmon microscope,[5–7] dissociation of H_2,[8] splitting of water[9–11] *etc.* Controlling chemical reactions by light-induced catalytic processes is a long-standing goal in physical chemistry. Recently, surface plasmon induced chemical reactions are gaining much attention. For instance, reduction reaction,[12,13] oxidation reaction[14,15] and pH dependence[16,17] have been reported. In this communication we will focus on the reaction of an immobilized pyridine compound as an example for a plasmon assisted protonation.

To our knowledge, this is the first experimental report discussing a protonation reaction induced by surface plasmons under ambient conditions (Scheme 1). The experiments were performed under ambient conditions and we hypothesize that the proton generation is based on the dissociation of atmospheric water. Dissociation of atmospheric hydrogen seems unlikely, however, cannot be entirely excluded at present. The hypothesis is confirmed by SERS experiments under inert atmosphere (argon) where no protonation signature was observed.

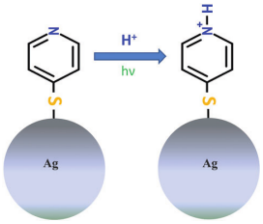

Scheme 1 Protonation of 4-MPY in the presence of metal nanoparticles and light.

In the present study 4-mercaptopyridine (4-MPY) was chosen as a model compound for plasmon induced protonation. The adsorption of 4-MPY on metal surfaces can occur *via* three potential sites (1) the sulphur function, (2) *via* lone pair electrons of the nitrogen and (3) *via* aromatic π-electrons of the ring. Previous studies on different metal surfaces (Ag, Au and Pt) strongly suggest the binding of 4-MPY through the S atom by cleavage of the S–H bond.[18–21] Furthermore, pH dependent surface enhanced Raman scattering (SERS) studies of 4-MPY show that at pH > 12 the unprotonated (UP) compound is observed. This is indicated by a single Raman peak at 1575 cm^{-1} (ring stretching mode with unprotonated nitrogen). Decreasing the pH < 1 results in a loss of this peak while, at 1608 cm^{-1} a new signal appears, that is assigned to ring stretching mode with a protonated nitrogen (PN).[18,20,22–24] Protonation on SERS substrates has been studied on various molecular systems[22,25–27] using different experimental techniques and all these studies show a pH dependency. Generally, the protonation is reversible and depending on the pH conditions, protonation and deprotonation can be observed.

For the detailed investigation of such surface dependent reactions, a site specific detection at single molecule level would be extremely valuable. Tip-enhanced Raman scattering (TERS) provides a tool to investigate structural information of surfaces with nanometre resolution using a plasmonic hot spot at a scanning probe tip to probe the sample interface. The electromagnetic field

[a] *Leibniz Institute of Photonic Technology, Albert-Einstein-Str. 9, 07745 Jena, Germany*
[b] *Institute of Physical Chemistry and Abbe Center of Photonics, Friedrich-Schiller University Jena, Helmholtzweg 4, 07743 Jena, Germany. E-mail: volker.deckert@ipht-jena.de*

† Electronic supplementary information (ESI) available: Experimental details, preparation of SERS substrate, synthesis of gold nanoplates. See DOI: 10.1039/c4cc04642k

This journal is © The Royal Society of Chemistry 2014

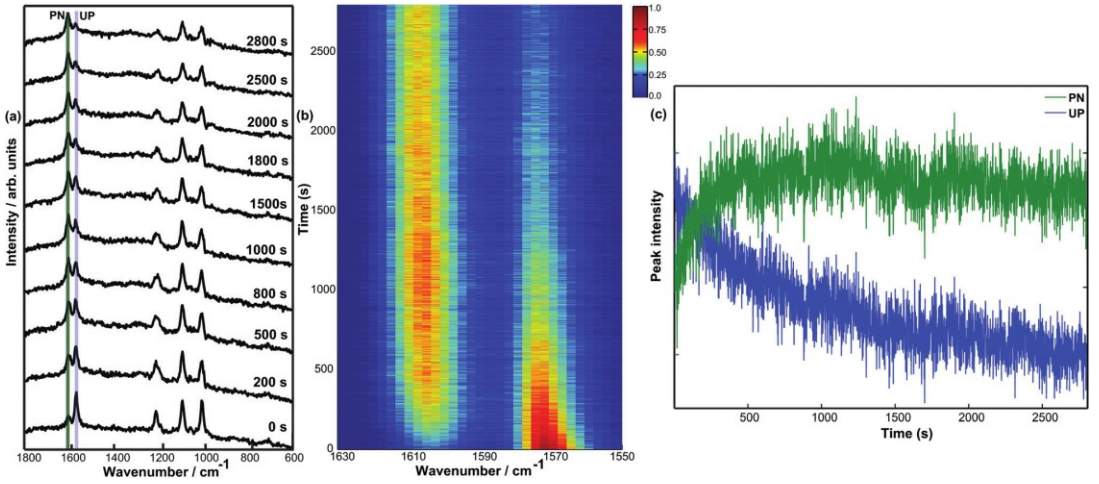

Fig. 1 (a) Selected time-dependent SERS spectra of 4-MPY under 532 nm/125 μW laser radiation, acquisition time of 1 s. (b) SERS intensity plot of the full series in a wavenumbers range from 1550–1630 cm^{-1}. (c) Integrated peak intensity of the protonated peak in green and unprotonated peak in blue. The bands are assigned as 1006 cm^{-1} (ring breathing), 1092 cm^{-1} (ring breathing/C–S), 1211 cm^{-1} (β(CH)/δ(NH)), 1575 cm^{-1} (ring stretching mode with unprotonated nitrogen (UP)) and 1608 cm^{-1} (ring stretching mode with protonated nitrogen (PN)).

enhancement at this hot spot leads to a Raman signal enhancement of several orders of magnitude and even single molecule sensitivity has been demonstrated.[28–32] Recently it has been shown that surface plasmon induced chemical reactions can be monitored using TERS under ambient conditions and also under ultrahigh vacuum conditions.[12,13] In the present study we use a combined SERS and TERS approach to investigate the protonation of 4-MPY.

Initially SERS spectra of 4-MPY adsorbed on silver island films using a laser wavelength of 532 nm at 125 μW were measured over several minutes. Fig. 1a shows 10 selected spectra measured at different time-points. Initially Raman band at 1575 cm^{-1} (indicating the unprotonated compound) with high intensity and a very small protonated band at 1608 cm^{-1} is visible. Gradually the Raman band at 1608 cm^{-1} increases indicating the protonation of 4-MPY. Thus a conversion from unprotonated to protonated 4-MPY is monitored. Fig. 1b clarifies this conversion in the form of a colour coded intensity plot. The results suggest that a proton source must be present, as no further reaction of the 4-MPY (*e.g.* decomposition) could be detected. Different hydrogen containing components in air could be responsible for the observations. As the dissociation of H_2[8] and H_2O[9–11] under surface plasmon conditions were already shown, this further strengthens our assumption of protonation of 4-MPY using surface plasmon under ambient conditions. Fig. 1c shows the intensity of unprotonated and protonated peak as time progresses. One can see that the intensity of the protonated peak increases initially and reaches to a maximum. We also noticed that the intensity of different peaks shown in Fig. 1a decrease as time progresses. This could be attributed to an oxidation of the silver island film during the measurement. This effect will not be discussed further as it will not affect the main conclusion of this work.

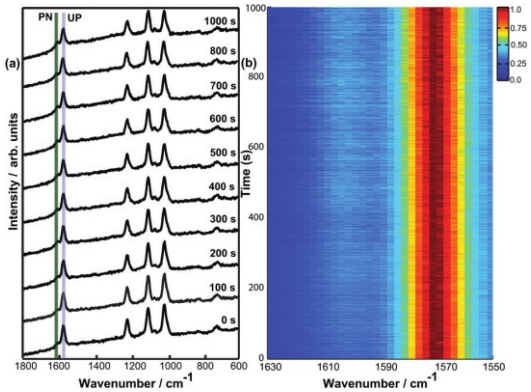

Fig. 2 (a) Time-dependent SERS spectra of 4-MPY under a continuous flow of argon during the experiment. Laser excitation at 532 nm/150 μW, integration time 1 s. (b) Colour coded intensity plot of same series in wavenumbers range from 1550–1630 cm^{-1}. No protonation is observed.

Considering H_2O or H_2 under ambient as a possible hydrogen sources required for the surface plasmon induced protonation reaction, we performed time dependent measurements under a continuous flow of argon. Fig. 2a shows the time development of 10 spectra at different times-points. The data clearly indicate that no protonation takes place. Fig. 2b shows all time dependent SERS spectra as a colour coded intensity plot.

It has been shown experimentally and theoretically that silver nanoparticles generate higher electromagnetic field enhancement under 532 nm radiation compared to 632 nm as the resonance wavelength of the silver nanoparticles (diameter 100 nm) used in the present study is very close to 532 nm.[33–35] Consequently, employing

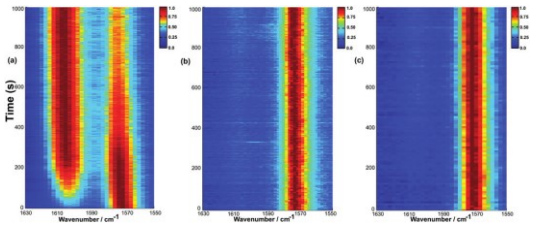

Fig. 3 (a) Colour coded SERS intensity plot of 4-MPY under 532 nm laser radiation with laser power of 50 μW with an integration time of 2 s, clearly show protonation as a function of time. (b) SERS intensity plot of 4-MPY under 632 nm/50 μW laser radiation, integration time 4 s; no protonation is observed (c) SERS intensity plot of 4-MPY under 532 nm/18 μW laser radiation, integration time of 10 s; under low power conditions no protonation is observed either.

the same incident laser power (50 μW) and 632 nm laser excitation (Fig. 3b) compared to 532 nm (Fig. 3a), no protonation could be detected, thus the intensity of the surface plasmon with 632 nm excitation is not sufficient to start the reaction. Low power (18 μW) of 532 nm laser excitation (see Fig. 3c) shows also no protonation signature. Thus a minimum intensity of surface plasmon is the decisive factor to initiate the protonation which can be controlled using either incident laser power or excitation wavelength.

The results of different excitation wavelengths at 50 μW further imply that the protonation reaction is not induced due to a temperature increase in the laser focus since under same laser power the temperature should be approximately the same. To further investigate the temperature dependence we performed temperature dependent experiments. A low incident power (12 μW @ 532 nm) was used such that no protonation could be observed at room temperature, increasing the temperature of the substrate up to 60 °C (data not shown), did not yield the protonation either.

In comparison to SERS where many nanoparticles are present in the laser focus and contribute to the overall Raman signal, in tip-enhanced Raman scattering (TERS) the signal is generated from a silver coated AFM tip of about 10 nm in radius and thus reducing the enhancing unit to a single nanoparticle. In a TERS experiment the silver coated AFM tip is positioned in the laser focus, thus only one specific plasmonic feature contributes to the signal. In order to warrant similar conditions a monolayer of 4-MPY was immobilized on a flat transparent gold nanoplate[36,37] (see ESI† for detail).

Fig. 4a shows 10 selected TERS spectra under ambient conditions and Fig. 4b shows the time-dependent TERS spectra plotted as a colour coded intensity plot. Interestingly under TERS conditions a much faster protonation of 4-MPY was observed compared to SERS. A control TERS measurement was also performed under inert atmosphere. Fig. 4c shows 10 selected spectra of TERS measurement under inert atmosphere at different timepoints and Fig. 4d shows the corresponding time dependent TERS spectra plotted as a colour coded intensity plot. The results nicely confirm the role of atmospheric conditions as seen in the SERS experiments. The difference between Au and Ag as the binding site has surprisingly little effect to the band positions of the protonated and unprotonated peaks.

With respect to the "instantaneous" protonation, previous theoretical and experimental studies showed that field confinement between two metal nanoparticles leads to an increased enhancement.[38,39] This effect also occurs in a particle-on-metal-surface geometry ("gap-mode") as in the case of the TERS experiment. Furthermore the tip-sample nanogap allows an efficient electron transfer from tip to sample.[40,41] These effects can explain a faster protonation under TERS conditions with very defined and optimized geometry, whereas under SERS conditions many sites with different efficiencies contribute to the overall signal changes. Hence, in the case of the SERS experiments a gradual protonation is observed. To exclude any power related aspects a SERS experiment also using 650 μW (data not shown) was done and a comparable behavior regarding an increase in the reaction rate was observed which also

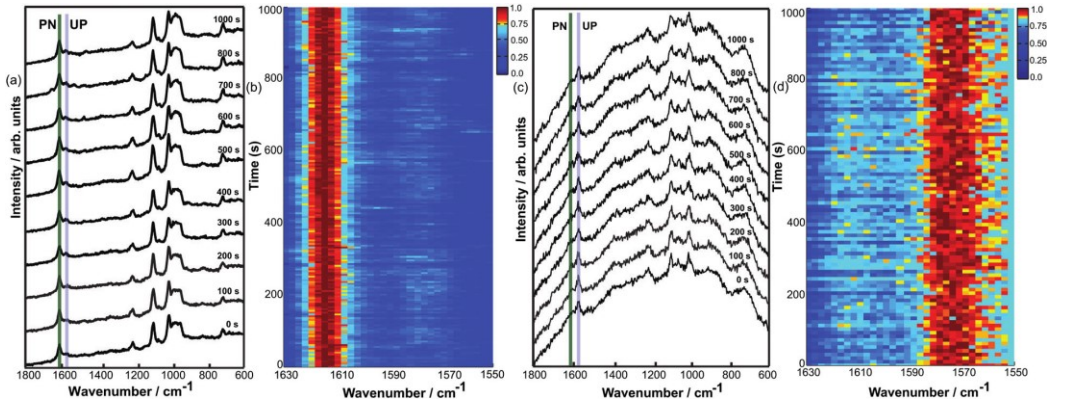

Fig. 4 (a) Time-dependent TERS spectra of 4-MPY under ambient conditions (excitation 532 nm/650 μW; integration time 5 s), (b) colour coded intensity plot of the data (a) wavenumbers range from 1550–1630 cm^{-1}, (c) time-dependent TERS spectra of 4-MPY under argon (excitation 532 nm/650 μW; integration time 10 s). (d) TERS intensity plot of the data in (c) wavenumbers range from 1550–1630 cm^{-1}.

 This journal is © The Royal Society of Chemistry 2014

agrees with recent power dependent SERS measurement on 4-MPY.[24] We also like to note a difference in the appearance of a broad peak around 980 cm^{-1} in TERS measurements. This peak is due to silicon tip and its nature changes from tip to tip. Since the TERS experiments with and without argon were performed with different tips, a direct comparison regarding the spectral background is difficult.

In conclusion, we report the experimental observation of protonation reaction under ambient condition using 4-MPY as a model system. While the actual mechanism of the protonation cannot be revealed with the presented experiments, it demonstrates the conditions under which the surface catalytic reaction can be controlled. The control experiment under a continuous flow of argon confirms that atmospheric H_2O (H_2 cannot be fully excluded yet) acts as a potential proton source required for the reaction. The study further demonstrates that the intensity of the surface plasmon is a key factor to initiate the protonation reaction. The TERS experiments not only confirm the findings of the SERS, but also demonstrate a site specific protonation catalyst that can be located at specific sites and synchronously act as a structurally specific sensor. Interestingly, despite the lower number of plasmonic particles in the case of TERS the protonation happen much faster compared to SERS. This can be attributed to large electromagnetic fields produced in the metal–metal nanogap between tip and substrate and an efficient electron transfer. Consequently, the observed reaction depends more on the specific nanoparticle activity rather than the number of particles. This opens interesting perspective for site specific protonation with nanometre control.

Financial Support from the European Union and the state of Thuringia (FKZ: 2011 FE 9048; 2011 VF 0016) as well as through the Deutsche Forschungsgemeinschaft (FR 1348/19-1) is gratefully acknowledged.

Notes and references

1 M. Piliarik, H. Šípová, P. Kvasnička, N. Galler, J. R. Krenn and J. Homola, *Opt. Express*, 2012, **20**, 672–680.
2 J. Zhao, X. Zhang, C. R. Yonzon, A. J. Haes and R. P. Van Duyne, *Nanomedicine*, 2006, **1**, 219–228.
3 K. Nakatani, S. Sando and I. Saito, *Nat. Biotechnol.*, 2001, **19**, 51–55.
4 R. Robelek, L. Niu, E. L. Schmid and W. Knoll, *Anal. Chem.*, 2004, **76**, 6160–6165.
5 B. Rothenhäusler and W. Knoll, *Nature*, 1988, **332**, 615–617.
6 M. G. Somekh, S. Liu, T. S. Velinov and C. W. See, *Appl. Opt.*, 2000, **39**, 6279–6287.
7 B. Gjonaj, J. Aulbach, P. M. Johnson, A. P. Mosk, L. Kuipers and A. Lagendijk, *Phys. Rev. Lett.*, 2013, **110**, 266804.
8 S. Mukherjee, F. Libisch, N. Large, O. Neumann, L. V. Brown, J. Cheng, J. B. Lassiter, E. A. Carter, P. Nordlander and N. J. Halas, *Nano Lett.*, 2013, **13**, 240–247.
9 D. B. Ingram and S. Linic, *J. Am. Chem. Soc.*, 2011, **133**, 5202–5205.
10 J. Lee, S. Mubeen, X. Ji, G. D. Stucky and M. Moskovits, *Nano Lett.*, 2012, **12**, 5014–5019.
11 C. G. Silva, R. Juárez, T. Marino, R. Molinari and H. García, *J. Am. Chem. Soc.*, 2011, **133**, 595–602.
12 E. M. v. Schrojenstein Lantman, T. Deckert-Gaudig, A. J. G. Mank, V. Deckert and B. M. Weckhuysen, *Nat. Nanotechnol.*, 2012, **7**, 583–586.
13 M. Sun, Z. Zhang, H. Zheng and H. Xu, *Sci. Rep.*, 2012, **2**, 647.
14 P. Christopher, H. Xin and S. Linic, *Nat. Chem.*, 2011, **3**, 467–472.
15 W. H. Hung, M. Aykol, D. Valley, W. Hou and S. B. Cronin, *Nano Lett.*, 2010, **10**, 1314–1318.
16 Y. Toh, P. Yu, X. Wen, J. Tang and T. Hsieh, *Nanoscale Res. Lett.*, 2013, **8**, 103.
17 M. Sun, Z. Zhang, Z. H. Kim, H. Zheng and H. Xu, *Chem. – Eur. J.*, 2013, **19**, 14958–14962.
18 J. Baldwin, N. Schühler, I. S. Butler and M. P. Andrews, *Langmuir*, 1996, **12**, 6389–6398.
19 M. A. Bryant, S. L. Joa and J. E. Pemberton, *Langmuir*, 1992, **8**, 753–756.
20 H. S. Jung, K. Kim and M. S. Kim, *J. Mol. Struct.*, 1997, **407**, 139–147.
21 T. Sueoka, J. Inukai and M. Ito, *J. Electron Spectrosc. Relat. Phenom.*, 1993, **64–65**, 363–370.
22 J. Hu, B. Zhao, W. Xu, B. Li and Y. Fan, *Spectrochim. Acta, Part A*, 2002, **58**, 2827–2834.
23 J. A. Baldwin, B. Vlčková, M. P. Andrews and I. S. Butler, *Langmuir*, 1997, **13**, 3744–3751.
24 X. S. Zheng, P. Hu, J. H. Zhong, C. Zong, X. Wang, B. J. Liu and B. Ren, *J. Phys. Chem. C*, 2014, **118**, 3750–3757.
25 J. Herranz, F. Jaouen, M. Lefevre, U. I. Kramm, E. Proietti, J. Dodelet, P. Bogdanoff, S. Fiechter, I. Abs-Wurmbach, P. Bertrand, T. M. Arruda and S. Mukerjee, *J. Phys. Chem. C*, 2011, **115**, 16087–16097.
26 H. T. Miles, F. B. Howard and J. Frazier, *Science*, 1963, **142**, 1458–1463.
27 D. B. Spry and M. D. Fayer, *J. Phys. Chem. B*, 2009, **113**, 10210–10221.
28 C. C. Neacsu, J. Dreyer, N. Behr and M. B. Raschke, *Phys. Rev. B: Condens. Matter Mater. Phys.*, 2006, **73**, 193406.
29 M. D. Sonntag, J. M. Klingsporn, L. K. Garibay, J. M. Roberts, J. A. Dieringer, T. Seideman, K. A. Scheidt, L. Jensen, G. C. Schatz and R. P. Van Duyne, *J. Phys. Chem. C*, 2012, **116**, 478–483.
30 R. Zhang, Y. Zhang, Z. C. Dong, S. Jiang, C. Zhang, L. G. Chen, L. Zhang, Y. Liao, J. Aizpurua, Y. Luo, J. L. Yang and J. G. Hou, *Nature*, 2013, **498**, 82–86.
31 E. Bailo and V. Deckert, *Angew. Chem., Int. Ed.*, 2008, **47**, 1658–1661.
32 T. Deckert-Gaudig, R. Böhme, E. Freier, A. Sebesta, T. Merkendorf, J. Popp, K. Gerwert and V. Deckert, *J. Biophotonics*, 2012, **5**, 582–591.
33 B. Dong, Y. Fang, X. Chen, H. Xu and M. Sun, *Langmuir*, 2011, **27**, 10677–10682.
34 L. Kang, P. Xu, B. Zhang, H. Tsai, X. Han and H. L. Wang, *Chem. Commun.*, 2013, **49**, 3389–3391.
35 R. Stöckle, V. Deckert, C. Fokas and R. Zenobi, *Appl. Spectrosc.*, 2000, **54**, 1577–1583.
36 T. Deckert-Gaudig, E. Bailoa and V. Deckert, *Phys. Chem. Chem. Phys.*, 2009, **11**, 7360–7362.
37 T. Deckert-Gaudig and V. Deckert, *Small*, 2009, **5**, 432–436.
38 M. Futamata, Y. Maruyama and M. Ishikawa, *J. Phys. Chem. B*, 2003, **107**, 7607–7617.
39 T. Yanoa, T. Ichimuraa, A. Taguchi, N. Hayazawaa, P. Vermaa, Y. Inouyea and S. Kawataa, *Appl. Phys. Lett.*, 2007, **91**, 121101.
40 K. J. Savage, M. M. Hawkeye, R. Esteban, A. G. Andrei, G. Borisov, J. Aizpurua and J. J. Baumberg, *Nature*, 2012, **491**, 574–577.
41 Z. Zhang, M. Sun, P. Ruan, H. Zheng and H. Xu, *Nanoscale*, 2013, **5**, 4151–4155.

This journal is © The Royal Society of Chemistry 2014

Supporting information

Local Protonation Control using Plasmonic Activation

Pushkar Singh[a] and Volker Deckert[a,b]

[a] *Leibniz Institute of Photonic Technology, Albert-Einstein-Str. 9, 07745 Jena, Germany.*

[b] *Institute of Physical Chemistry and Abbe Center of Photonics, Friedrich-Schiller University Jena, Helmholtzweg 4, 07743 Jena, Germany.*
Email: volker.deckert@ipht-jena.de

All SERS and TERS measurements are performed with an experimental setup described previously.[1] Laser radiation is focused using an oil immersion microscope objective (40X, 1.35NA, Olympus). The scattered signal is collected with the same objective and passes through a dichroic mirror and notch filter before it enters the spectrometer (Acton Advanced SP2750 A, SI GmbH, Germany). The control experiments under continuous flow of argon and temperature dependent studies are performed in a *Biocell* (JPK, Germany).

SERS active silver island film were prepared by evaporation of silver on cleaned glass plate according to the literature.[2] A drop of $5x10^{-3}$ M ethanolic solution of 4- MPY was put on SERS substrate and then dried and washed with ethanol to remove any unattached molecules on the surface.

For the TERS measurements the synthesis of gold nanoplates on cleaned glass substrate was performed according to a previously described method.[3] A self-assembled monolayer of 4-MPY was prepared by immersing the gold nanoplate substrate for 22 hours in a $5x10^{-3}$ M ethanolic solution and washed with ethanol before the measurement. For the TERS measurement silver coated non-contact AFM tips (ND-MDT, NSG10) were used. 20 nm of silver was evaporated onto the tips following Ref 2.

References:

1. A. Rasmussen and V. Deckert, *J. Raman Spectrosc.*, 2006, **37**, 311-317.
2. R. Stöckle, V. Deckert, C. Fokas and R. Zenobi, *Appl. Spectrosc.*, 2000, **54**, 1577–1583
3. T. Deckert-Gaudig and V. Deckert, *Small*, 2009, **5**, 432-436.

4.3 Plasmon induced deprotonation of 2-mercaptopyridine

Author contributions

Plasmon induced deprotonation of 2-mercaptopyridine, Analyst, submitted				
	Pushkar Singh	Tanja Deckert-Gaudig	Zhenglong Zhang	Volker Deckert
Conceptual research design	X			X
Planning of research activities	X	X	X	X
Data collection	X			
Data analyses and interpretation	X	X		X
Manuscript writing	X	X	X	X
Suggested publication equivalence value	1.0			

Reprinted with kind permission from the Royal Society of Chemistry.

[PS3] Pushkar Singh, Tanja Deckert-Gaudig, Zhenglong Zhang, and Volker Deckert, "Plasmon induced deprotonation of 2-mercaptopyridine" Analyst, submitted.

Plasmon induced deprotonation of 2-mercaptopyridine

Pushkar Singh,[a] Tanja Deckert-Gaudig,[a] Zhenglong Zhang,[a] and Volker Deckert [a, b,*]

[a] Leibniz Institute of Photonic Technology, Albert-Einstein-Str. 9, 07745 Jena, Germany.
[b] Institute of Physical Chemistry and Abbe Center of Photonics, Friedrich-Schiller University Jena, Helmholtzweg 4, 07743 Jena, Germany
Email: volker.deckert@ipht-jena.de

Surface plasmons can provide a novel route to induce and simultaneously monitor selective bond formation and breakage. Here pH-induced protonation, followed by plasmon-induced deprotonation of 2-mercaptopyridine was investigated using surface- and tip-enhanced Raman scattering (SERS and TERS). A large difference in the deprotonation rate between SERS and TERS is demonstrated and discussed with respect to hot-spot distribution.

The pathway of a chemical reaction can be controlled by varying the experimental conditions such as temperature, concentration, pH or, a recent development, by the application of laser induced surface plasmons. Plasmon induced catalysis is an emerging approach to induce chemical reactions and can for instance be applied to protonation and/or deprotonation reactions, which are observed in many homogeneously catalyzed reactions.[1-9] The background of this type of catalysis is the photo-induced plasmonic activity of metal nanostructures. In such experiments an increasing catalytic turn-over rate of different reactions like dimerization of p-nitrothiophenol,[10, 11] p-aminothiophenol,[12, 13] or the protonation of 4-mercaptopyridine[14] can be observed. Furthermore, the breaking of bonds by abstracting molecular hydrogen,[15] splitting of water,[16, 17] oxidation[18, 19] or the dissociation[20] of molecules can also be realized by surface plasmons. Such reactions would otherwise need extreme conditions like e.g. very high temperatures or short excitation wavelengths.[21-23]

Laser irradiation of metal nanoparticles at their plasmon resonance leads to an efficient generation of collective oscillations of free conduction band electrons at the surface of the nanoparticles. As a result, localized surface plasmon resonances are generated.[24, 25] In general, surface plasmons can locally enhance the electromagnetic field by many orders of magnitude. In combination with Raman spectroscopy, as realized in surface-enhanced Raman scattering (SERS) or tip-enhanced Raman scattering (TERS), such nanostructured surfaces yield a huge signal enhancement of the sample.[26, 27] For more details on both methods it is referred to ref. [28] and [29].

In this study, we experimentally demonstrate that surface plasmons can induce a deprotonation reaction. In our approach, the model system 2-mercaptopyridine (2-MPY) was protonated (2-MPY-H+) at low pH conditions prior to adsorption on the substrate. Subsequent deprotonation was achieved by exposing the pyridinium cation to surface plasmons.

In a previous study we reported that 4-mercaptopyridine (4-MPY) can be protonated under ambient conditions utilizing surface plasmons.[14] There, the protonation of 4-MPY immobilized on a silver island film under ambient conditions was tracked using SERS. The intensity increase of the ring stretching mode associated with the protonated nitrogen and the simultaneous intensity decrease of the ring stretching mode corresponding to the unprotonated nitrogen was observed. 2-MPY differs from 4-MPY only by the thiol group position with respect to the nitrogen in the pyridine ring. Nevertheless, the position of the nitrogen atom (para vs. ortho) is decisive for the different chemical behavior of 2-MPY and 4-MPY, as it will be demonstrated using SERS and TERS techniques.

In the SERS case, all molecules attached to a nanoparticle that are in the laser focus potentially can contribute to the signal while in TERS only molecules directly underneath the tip apex experience a signal enhancement. Furthermore, a previously detected faster reaction rate under TERS condition[14] needed to be further investigated.

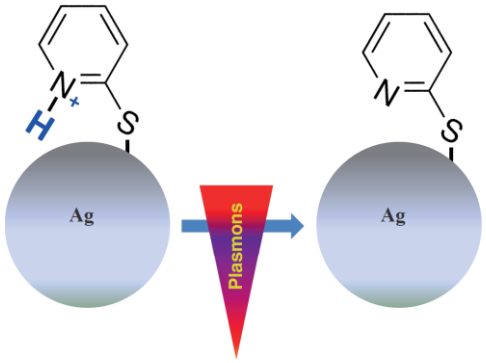

Scheme 1: Surface plasmon induced deprotonation of 2-MPY-H+ generated under low pH conditions.

The instrumental setup for the SERS and TERS used in this work has been described in detail previously.[30] A 10^{-3} M ethanolic solution of 2-MPY or a 10^{-3} M ethanol-water solution, either at pH 7 or pH 1.3, was used for SERS and TERS sample preparation. For SERS, 2µL of the solution was drop cast on a silver island film, dried, and washed with ethanol to remove any unbound molecules. In the TERS study gold nanoplates were immersed in the respective solution for 20 h and then washed with ethanol. Figure 1 shows SERS spectra (@532nm, P=180µW) of 2-MPY at different time-points. A gradual intensity decrease of all bands indicates a slow degradation (probably oxidation) of the silver island film, since the measurements were carried out under ambient conditions. This effect did not further interfere with the experiment and can be accounted for by normalization procedures. The main interest was the behavior of the band at 1574 cm^{-1}, a marker for the unprotonated pyridine ring (UP). The constant intensity of this peak over 600 s indicates that 2-MPY was stable and was not protonated under atmospheric SERS conditions. In case of a protonation, an additional

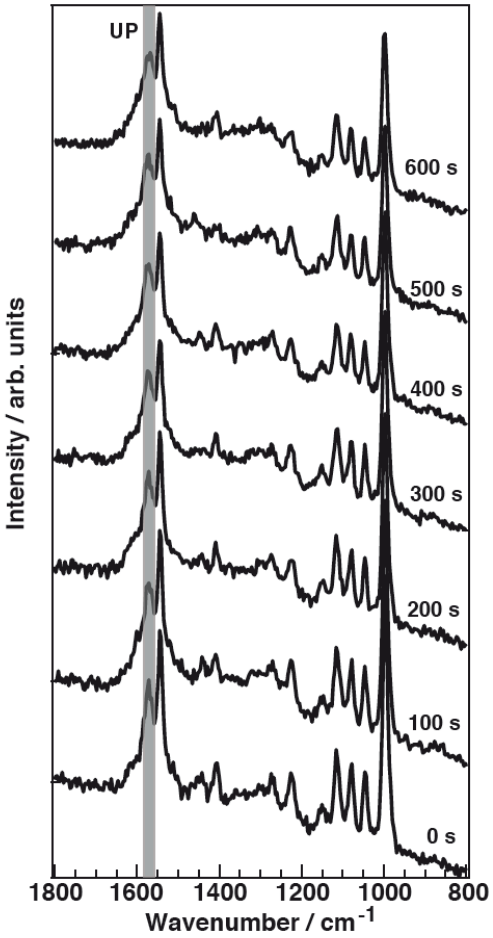

Figure 1: Selected time-dependent SERS spectra of 2-MPY adsorbed from ethanolic solution (pH 7) on a silver island film with 180µW@532nm, acquisition time: 2 s / spectrum. Band assignment: 1000 cm-1(ring breathing), 1048 cm^{-1} (β(C-H)), 1082 cm^{-1} (β(C-H)), 1116 cm^{-1} (ring breathing / ν(C-S)), 1546 cm^{-1} (ν(C=C)) and 1574 cm^{-1} (ring stretching mode with unprotonated nitrogen(UP)).[31-35] No band at 1605 cm^{-1} (indicator for protonated 2-MPY (PN)) was detected.

peak around 1605 cm^{-1}, a marker for the protonated pyridine ring (PN), would have been observed. Hence, in contrast to the previously studied 4-MPY, no protonation occurred for 2-MPY under similar surface plasmons conditions. Structurally, a different binding situation of 2-MPY on the silver nanoparticles can be considered for the different behavior. When the covalent Ag-S bond is formed during immobilization, the nitrogen atom of the tilted 2-MPY will be close to the metal surface resulting in additional Ag-N interactions. Such interactions clearly obstructs the access to the nitrogen atom. Even when the SERS experiment was repeated at a higher incident laser power (up to 1 mW), a protonation was never observed (data not shown here).

In a subsequent experiment 2-MPY was drop cast as indicated above, but this time from a pH 1.3 solution on a silver island film. The investigation under otherwise similar conditions as

before indicates that a new peak at 1605 cm^{-1} could be detected (see Fig. 2). The presence of this peak indicates that a protonated compound, 2-MPY-H+, exists right from the beginning. As time progressed the relative intensity of this peak decreased and after 500 s it finally disappeared, thus clearly indicating a complete reversal of the protonation.

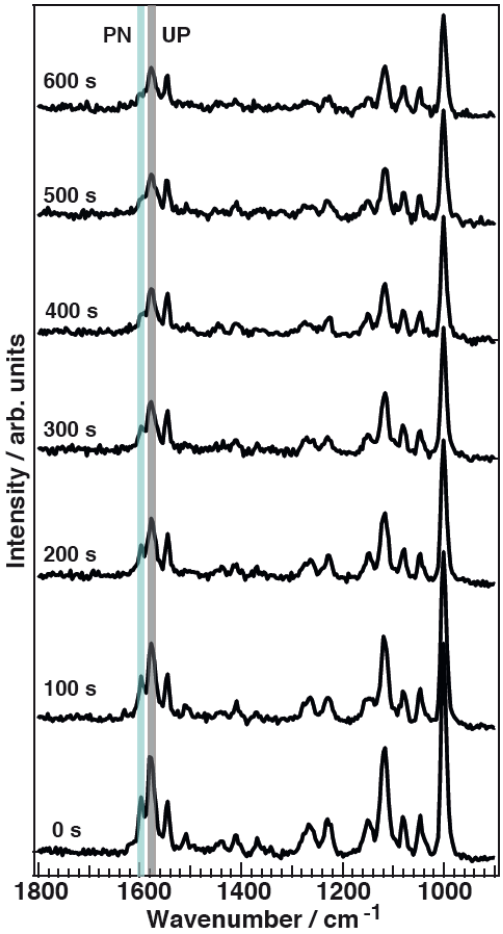

Figure 2: Selected time-dependent SERS spectra of 2-MPY-H+ on a silver island film adsorbed from pH 1.3 solution with 180µW@532nm; acquisition time 2 s / spectrum. The band at 1605 cm^{-1} (indicator for protonated 2-MPY) was detected under low pH which is deprotonated under surface plasmons.

Follow-up experiments addressed the laser power dependence of the deprotonation. Below 25µW no deprotonation was observed, but above this threshold the deprotonation rate increased linearly with increasing incident laser power. This observation indicates that either temperature in the laser focus, which correlates to the incident power, or the photon flux determines the reaction rate.

To exclude temperature effects due to sample heating in the laser focus, experiments were performed at various temperatures. Figure 3(a) shows the intensities of protonated and unprotonated bands as a function of temperature. No intensity change of these peaks was

observed. Here, the laser power was kept at 20µW, which was just below the minimum value to initiate a deprotonation at room temperature. Heating the sample up to 60°C did not change the 2-MPY-H+ spectra, pointing to the stability of the N+-H bond. Since the temperature in the focus at 20 µW was presumably below 60°C we concluded that the reaction is either temperature independent or higher temperatures are needed to abstract the proton. Consequently, under the present experimental conditions the rate of deprotonation is not determined by the temperature but by the surface plasmons generated in the laser focus. Figure 3(b) shows the relative protonated and unprotonated peak intensities measured at different incident laser powers (50, 100, 125 and 250 µW). To keep the radiant fluence constant, measurements were done at different time points (250, 125, 100 and 50s), respectively. No variations in the peak intensities of protonated and unprotonated species were observed which shows that the reaction rate depends only on the radiant fluence.

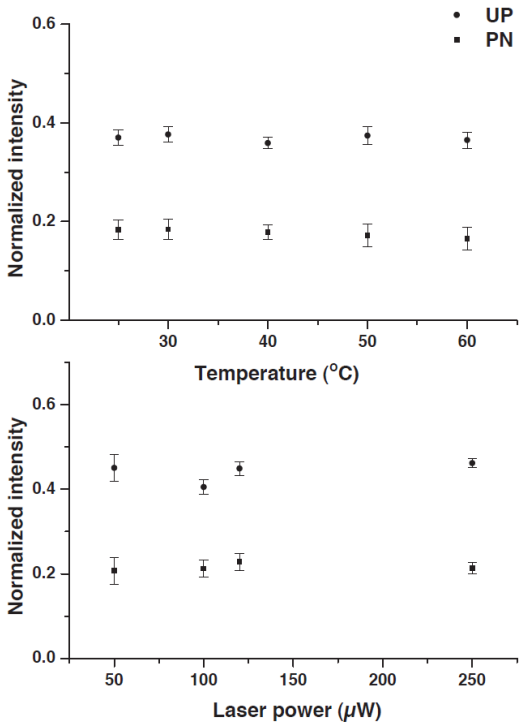

Figure 3: Normalized intensities of (a) protonated (PN) and unprotonated (UP) band measured during the temperature-dependent SERS of 2-MPY-H+ on a silver island film adsorbed from pH=1.3 solution. No variation in band intensities at different temperatures was observed. All spectra were measured with 20µW@532nm acquisition time 5 s / spectrum. (b) Variation in the intensity of PN and UP bands for 4 different incident powers (50, 100, 125 and 250µW) measured at different times (250, 125, 100 and 50 s), demonstrate that the reaction rate depends on the radiant fluence.

Finally, the protonation/deprotonation of 2-MPY was investigated with TERS to examine if a single silver particle is capable to initiate either both or neither reaction. Such a local

controllability essentially would allow confining the reaction to any selected position on the sample substrate. For the TERS measurements 2-MPY was immobilized on transparent gold nanoplates from either a pH 1.3 solution or directly from ethanolic solution. The gold surface was used to uniformly adsorb the thiol to the substrate and thus generating a gap-mode configuration.[29, 36] From the neat ethanol solution merely the unprotonated species was detected (see Figure 4a). Similarly, to the SERS experiments also for TERS no protonation signature was observed for more than 200 s at (excitation at 532nm and 620µW at sample, time-series data not shown). In contrast, the same sample preparation from the acidic medium yielded 2-MPY-H+ signals only for a short time (see Figure 4b) and complete deprotonation occurred already after 15 s (see Figure 4c). This faster reaction corresponds with previous protonation experiments and confirms the hypothesis that the gold-silver gap in TERS provides a uniform reaction center with a high turn-over rate. The average particle orientation / gap formation of the SERS substrate used here in contrast seems to yield much less efficient reaction sites.

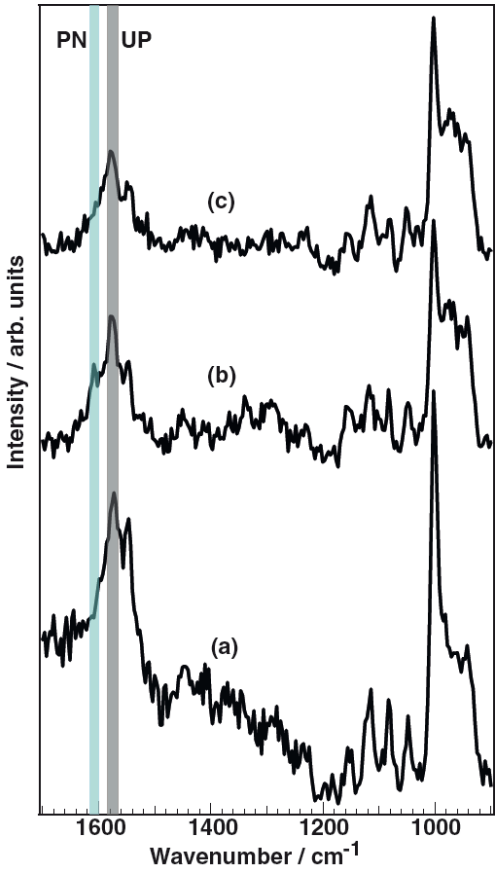

Figure 4: TERS spectra of (a) 2-MPY, (b) 2-MPY-H+ on an ultra-flat gold nanoplate adsorbed from pH 1.3 solution at time t=0 and (c) 2-MPY-H+ after 15 s of continuous irradiation, showing the complete deprotonation of the species. All spectra were measured at 620µW@532nm; acquisition time 5 s / spectrum.

The experiments clearly show the surface plasmon induced deprotonation of 2-MPY under SERS and TERS conditions. A comparison of reaction rate under SERS and TERS shows a faster reaction of 2-MPY under TERS which was also observed in our previous work.[14] Moreover, comparison of reaction rate for these two molecules under TERS shows a faster reaction for 4-MPY.

The difference in the reaction rate of these molecules under TERS conditions can be explained by a charge-transfer model where the electron transfer from the tip to the nitrogen atom of the pyridine ring determines the rate of chemical reaction. In the case of 4-MPY the nitrogen atom, which is far away from the gold substrate, faces the tip and presumably a direct electron transfer to the nitrogen facilitates the binding of a hydrogen proton. In case of 2-MPY, direct tip-nitrogen atom interactions are sterically hindered by the orientation of the pyridine ring on the gold surface and also due to increase in the distance between them, which leads to a slower reaction rate compared to 4-MPY.[37, 38] The faster reaction under TERS compared to SERS is attributed to the higher enhancement in the nanogap between two metals (Ag-tip and Au-substrate) and the effective charge transfer in the tip-sample geometry.[39-44]

In conclusion, we experimentally demonstrated that 2-MPY cannot be protonated in the presence of surface plasmons in SERS nor TERS due to strong substrate-nitrogen interactions. As expected 2-MPY can be protonated chemically under low pH conditions and this resulting pyridinium cation can be deprotonated in the presence of surface plasmons on a silver island film. To exclude photo thermal mechanisms by sample heating a temperature dependent study was performed. Increasing the sample temperature up to 60°C and keeping the laser power constant did not change the reaction rate, which indicates that the deprotonation reaction is temperature independent, at least under the specific reaction conditions. The faster reaction rate for the TERS experiments can be attributed to a large field confinement between metal-metal nanogap and charge transfer properties under experimental geometry. The higher laser power used in the TERS experiment (compared to SERS) increased the reaction rate, which is apparent in the linear increase of the reaction rate with radiant fluence. A plausible explanation of the slower plasmon induced reaction kinetics of 2-MPY compared to 4-MPY in TERS is due to change in charge-transfer properties. A faster reaction of 4-MPY can be understood as direct electron transfer from the tip to the nitrogen atom as they are in direct vicinity. In contrast, the position of the nitrogen atom in 2-MPY is far away from the tip, which prohibits a direct electron transfer and leads to slower reaction compared to 4-MPY.

Financial Support from the European Union and the state of Thuringia (FKZ: 2011 FE 9048; 2011 VF 0016) and COST Action MP1302 “Nanospectroscopy” as well as through the Deutsche Forschungsgemeinschaft (FR 1348/19-1) is gratefully acknowledged. P. Singh acknowledges financial supports from Thüringer Aufbaubank (grant number: 2011SE9048) and Z. Zhang from the Alexander von Humboldt foundation.

1. T. Nakamura, Y. Zhao, Y. Yamagata, Y. Hua and W. Yang, Nature, 2012, 487, 196–201.
2. M. D. Jeppesen, P. Westh and D. E. Otzen, FEBS Lett., 2010, 584, 780–784.
3. A. Bodi, J. Csontos, M. Kállay, S. Borkarc and B. Sztáray, Chem. Sci., 2014, 5, 3057-3063.
4. M. Breedon, M. C. Per, I. S. Cole and A. S. Barnard, J. Mater. Chem. A, 2014, 2, 16660–16668.
5. S. J. Cho, C. Cui, J. Y. Lee, J. K. Park, S. B. Suh, J. Park, B. H. Kim and K. S. Kim, J. Org. Chem., 1997, 62, 4068-4071.
6. E. S. Moon, C. W. Lee, J. K. Kim, S. C. Park and H. Kang, J Chem Phys, 2008, 128, 191101 (191101-191104).
7. G. A. Olah and M. Calin, J. Am. Chem. Soc., 1968, 90, 401–404.
8. Y. Song, D. Zou, Z. Xie, G. Zhang, Z. Li and C. Wang, Chem. Phys. Lett, 2013, 588, 155-159.
9. J. L. Castro, M. R. Lopez-Ramirez, J. F. Arenas, J. Juan Soto and J. C. Otero, Langmuir, 2012, 28, 8926−8932.
10. E. M. von Schrojenstein Lantman, T. Deckert-Gaudig, A. J. G. Mank, V. Deckert and B. M. Weckhuysen, Nat. Nanotechnol., 2012, 7, 583-586.
11. M. Sun, Z. Zhang, H. Zheng and H. Xu, Scientific Reports, 2012, 2, 647.
12. P. Xu, L. Kang, N. H. Mack, K. S. Schanze, X. Han and H. Wang, Sci. Rep., 2013, 3, 2997.
13. M. Sun, Y. Huang, L. Xia, X. Chen and H. Xu, J. Phys. Chem. C, 2011, 115, 9629–9636.
14. P. Singh and V. Deckert, Chem. Commun., 2014, 50, 11204-11207.
15. S. Mukherjee, F. Libisch, N. Large, O. Neumann, L. V. Brown, J. Cheng, J. B. Lassiter, E. A. Carter, P. Nordlander and N. J. Halas, Nano Lett., 2013, 13, 240−247.
16. D. B. Ingram and S. Linic, J. Am. Chem. Soc., 2011, 133, 5202–5205.
17. J. Lee, S. Mubeen, X. Ji, G. D. Stucky and M. Moskovits, Nano Lett., 2012, 12, 5014–5019.
18. W. H. Hung, M. Aykol, D. Valley, W. Hou and S. B. Cronin, Nano Lett., 2010, 10, 1314–1318.
19. P. Christopher, H. Xin and S. Linic, Nat. Chem., 2011, 3, 467-472.
20. Z. Zhang, T. Deckert-Gaudig, P. Singh and V. Deckert, Chem. Commun., 2015, 51, 3069--3072.
21. M. L. Hause, N. Herath, R. Zhu, M. C. Lin and A. G. Suits, Nat. Chem., 2011, 3, 932.
22. C. Rosado-Reyes and W. Tsang, J. Phys. Chem. A, 2013, 117, 10170.
23. Y. Li, J. Sun, H. Yin, K. Han and G. He, J Chem Phys, 2003, 118.
24. E. Hutter and J. H. Fendler, Adv. Mater., 2004, 16, 1685-1706.
25. P. K. Jain, X. Huang, I. H. El-Sayed and M. A. El-Sayed, Acc. Chem. Res., 2008, 41, 1578–1586.
26. D. L. Jeanmaire and R. P. Van Duyne, J. Electroanal. Chem, 1977, 84, 1-20.

27. R. M. Stockle, Y. D. Suh, V. Deckert and R. Zenobi, Chem. Phys. Lett., 2000, 318, 131-136.
28. M. F. Cardinal, E. V. Ende, R. A. Hackler, M. O. McAnally, P. C. Stair, G. C. Schatz and R. P. Van Duyne, Chem Soc Rev, 2017, 46, 3886-3903.
29. T. Deckert-Gaudig, A. Taguchi, S. Kawata and V. Deckert, Chem Soc Rev, 2017, 46, 4077-4110.
30. A. Rasmussen and V. Deckert, J. Raman Spectrosc., 2006, 37, 311-317.
31. J. A. Baldwin, B. Vlčková, M. P. Andrews and I. S. Butler, Langmuir, 1997, 13, 3744–3751.
32. W. Zhang, T. Schmid, B. S. Yeo and R. Zenobi, Isr. J. Chem., 2007, 47, 177–184.
33. Y. S. Pang, H. J. Hwang and M. S. Kim, J. Mol. Struct., 1998, 441, 63-76.
34. M. Takahashi, M. Fujita and M. Ito, Surf. Sci., 1985, 158, 307–313.
35. W. H. Do, C. J. Lee, D. Y. Kim and M. J. Jung, J. Ind. Eng. Chem., 2012, 18, 2141–2146.
36. T. Deckert-Gaudig and V. Deckert, Small, 2009, 5, 432-436.
37. F. C. Grozema, Y. A. Berlin, L. D. A. Siebbeles and M. A. Ratner, J. Phys. Chem. B, 2010, 114, 14564–14571.
38. C. B. George, I. Szleifer and M. A. Ratner, Chem. Phys., 2010, 375, 503–507.
39. N. Behr and M. B. Raschke, J. Phys. Chem. C, 2008, 112, 3766–3773.
40. T. Yano, T. Ichimura, A. Taguchi, N. Hayazawa, P. Verma, Y. Inouye and S. Kawata, Appl. Phys. Lett., 2007, 91, 121101.
41. M. Futamata, Y. Maruyama and M. Ishikawa, J. Phys. Chem. B, 2003, 107, 7607–7617.
42. R. M. Roth, N. C. Panoiu, M. M. Adams, R. M. Osgood, C. C. Neacsu and M. B. Raschke, Opt. Express, 2006, 14, 2921-2931.
43. K. J. Savage, M. M. Hawkeye, R. Esteban, A. G. Andrei G. Borisov, J. Aizpurua and J. J. Baumberg, Nature, 2012, 491, 574-577.
44. Z. Zhang, M. Sun, P. Ruan, H. Zheng and H. Xu, Nanoscale, 2013, 5, 4151–4155.

4.4 Single molecule level plasmonic catalysis - a dilution study of p-nitrothiophenol on gold dimmers

Author contributions

Single molecule level plasmonic catalysis – a dilution study of p- nitrothiophenol on gold dimers, Chem. Commun., 51, 3069-3072, 2015 https://doi.org/10.1039/C4CC09008J				
	Zhenglong Zhang	Tanja Deckert-Gaudig	Pushkar Singh	Volker Deckert
Conceptual research design	X			X
Planning of research activities	X	X		X
Data collection	X		X	
Data analyses and interpretation	X	X	X	X
Manuscript writing	X	X	X	X
Suggested publication equivalence value			0.25	

Reprinted with kind permission from the Royal Society of Chemistry.

[PS4] Zhenglong Zhang, Tanja Deckert-Gaudig, Pushkar Singh and Volker Deckert, "Single molecule level plasmonic catalysis – a dilution study of p-nitrothiophenol on gold dimers" Chem. Commun., 51, 3069-3072, 2015.

ChemComm

COMMUNICATION

View Article Online
View Journal | View Issue

Cite this: *Chem. Commun.*, 2015, **51**, 3069

Received 11th November 2014,
Accepted 6th January 2015

DOI: 10.1039/c4cc09008j

www.rsc.org/chemcomm

Single molecule level plasmonic catalysis – a dilution study of *p*-nitrothiophenol on gold dimers†

Zhenglong Zhang,[a] Tanja Deckert-Gaudig,[a] Pushkar Singh[a] and Volker Deckert*[ab]

Surface plasmons on isolated gold dimers can initiate intermolecular reactions of adsorbed *p*-nitrothiophenol. At the single molecule level when dimerization is not possible an intramolecular reaction can be observed. Experimental evidence indicates that plasmon-induced hot electrons provide the required activation energy.

In the presence of surface plasmons molecular chemical reactions can be investigated at the nanoscale, as it has been demonstrated for a variety of catalyzed systems.[1–19] Recently, plasmon catalyzed dimerization of *p*-nitrothiophenol (*p*NTP) to 4,4-dimercaptoazobenzene (DMAB) has been realized using surface-enhanced Raman spectroscopy (SERS) and tip-enhanced Raman spectroscopy (TERS).[2–6] For any dimerization the distance between the reactants is decisive. If the distance between *p*NTP molecules gets too large a dimerization reaction cannot occur. In this case the question arises, whether surface plasmons can initiate a further intramolecular reaction like dissociation or rearrangement. To address this issue, a detection sensitivity of signals from a few or ultimately even a single educt molecule is required. In our experiments we employed SERS, which is widely used for noninvasive detection, biological and chemical sensing.[20–25] In SERS laser irradiation of silver or gold nanoparticles induces localized surface plasmon resonances at the nanostructured surface generating enhanced electromagnetic fields.[25] If molecules are brought in closest vicinity to such nanoparticles (*e.g.* by adsorption) a large enhancement of the Raman scattering signal can be observed. Using the junctions or gaps of nanoparticles, so-called "*hot spots*", very high enhancement factors ($\sim 10^8$) can be achieved, providing sufficient signal enhancement for single molecule detection. Therefore such junctions are ideally suited for the intended reactivity detection.[23–27]

In previous studies, it was found that the plasmon catalyzed intermolecular reaction of *p*NTP (adsorbed on gold or silver nanoparticles) to DMAB can be controlled by laser intensity.[3,4] A higher laser intensity generates a stronger plasmon resonance with higher kinetic energy yielding an increased reaction rate. If the concentration, however, is low enough to prevent clustering and self-assembly, the distance of *p*NTP molecules adsorbed on the nanoparticles should become too large for an intermolecular reaction and no reaction should occur even at high laser powers. Then, any detected SERS signal can be related to single or only a few isolated and non-interacting separated molecules.

In this communication, single gold nanoparticle dimers were employed for SERS detection of *p*NTP molecules. In the presented experiments a so far unknown behavior of *p*NTP could be monitored, which strongly differs from previous reports as separated *p*NTP molecules exclusively reacted to thiophenol (TP), and is a new finding in surface catalyzed experiments. In addition, a step-like signal intensity change during the process strongly indicates that the dissociation reaction of *p*NTP to TP occurs at or close to a single molecule level.

As shown in Fig. 1, SERS active gold nanoparticle dimers (GDs) were prepared using a wet chemistry method.[28] Further experimental details can be found in the ESI.† In order to achieve SERS of separated molecules, three different concentrations of aqueous *p*NTP solutions (5×10^{-7}, 10^{-8} and 10^{-9} M) were mixed with

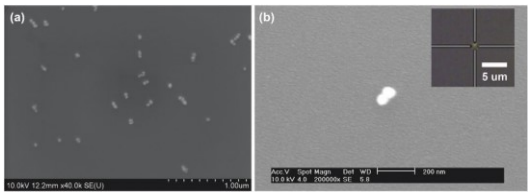

Fig. 1 (a) SEM image of gold nanoparticle dimers spin-coated onto a silicon wafer, (b) a single gold nanoparticle dimer on glass as used in the SERS measurement (inset: optical image of the selected nanoparticle dimer, which is placed in the center of the laser focus).

[a] *Leibniz Institute of Photonic Technology, Albert-Einstein-Str. 9, 07745 Jena, Germany. E-mail: volker.deckert@ipht-jena.de*
[b] *Institute of Physical Chemistry and Abbe Center of Photonics, Friedrich-Schiller University Jena, Helmholtzweg 4, 07743 Jena, Germany*

† Electronic supplementary information (ESI) available: Experimental details and Fig. S1–S3. See DOI: 10.1039/c4cc09008j

This journal is © The Royal Society of Chemistry 2015

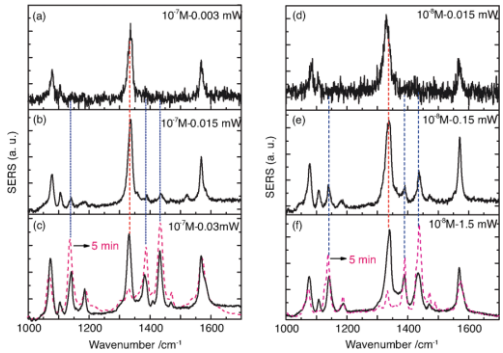

Fig. 2 (a)–(c) SERS spectra of 10^{-7} M *p*NTP excited at 3, 15 and 30 μW laser power, respectively. (d)–(f) SERS spectra of 10^{-8} M *p*NTP excited at 0.015, 0.15 and 1.5 mW laser power, respectively. The dotted red curves in (c) and (f) refer to spectra after continuous irradiation for 5 minutes.

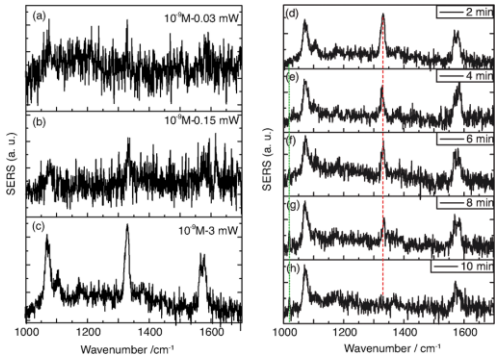

Fig. 3 (a)–(c) Laser intensity dependent SERS spectra excited at 0.03, 0.15 and 3 mW laser power, respectively. (d)–(h) Time dependent SERS spectra at 3 mW laser at the sample.

a gold nanoparticle dimer colloidal solution. The dimerization of *p*NTP to DMAB is characterized by the disappearance of the Raman band at 1332 cm^{-1} (ν_{NO_2}), and the appearance of new Raman bands around 1140 (β_{C-H}), 1387 ($\nu_{NN} + \nu_{CC} + \nu_{C-N}$) and 1432 ($\nu_{NN} + \nu_{CC} + \beta_{C-H}$) cm^{-1}, which are related to the –N=N– unit of DMAB.[2]

First, SERS experiments of the 10^{-7} M *p*NTP–GD mixture were made with increasing laser intensity. Starting with 3 μW (see Fig. 2(a)) only the three main peaks of *p*NTP were detected in the SERS spectrum. Increasing the laser power to 15 μW and 30 μW, respectively, dimerization of *p*NTP to DMAB was verified by the afore-mentioned bands at 1140, 1387 and 1432 cm^{-1} (Fig. 2(b)). Fig. 2(b) and (c) indicate also that an increased laser power yields a higher reaction rate. After continuous irradiation for 5 min almost all *p*NTP molecules in the laser spot have reacted to DMAB (see dotted red curve in Fig. 2(c)).

In the next experiment the 10^{-8} M *p*NTP–GD mixture were investigated, all other experimental parameters except the laser power as stated below remained unchanged. The corresponding SERS spectra are shown in Fig. 2(d)–(f). Similar to the previous experiment, a dimerization of *p*NTP to DMAB occurred, however, higher laser intensities (150 μW) were needed to initiate the reaction. The results of both experiments demonstrate that with 10^{-7} M and 10^{-8} M *p*NTP solutions the gold surface is still densely covered with *p*NTP molecules enabling a dimerization.

For the final experiment a 10^{-9} M *p*NTP solution was used. The resulting SERS spectra are shown in Fig. 3(a)–(c). During these measurements no dimerization of *p*NTP to DMAB was observed. Even at highest laser power (3 mW) for one hour (see Fig. 3(d)–(h) and for the full trace ESI,† Fig. S1) no DMAB signals could be detected. It was concluded that the distance between *p*NTP molecules in the plasmonic *hot-spot* of the GD was indeed too large to allow intermolecular reactions under these conditions. That the reaction of *p*NTP to DMAB could not be initiated even after 1 hour of continuous irradiation, indicates that SERS signals from only a few separated molecules in the *hot-spot* were acquired. This finding is in accordance with the estimated molecular coverage n of *p*NTP on a single gold dimer that was estimated as follows:

$$n = \frac{n_M}{n_{GD}} = \frac{c_M}{c_{GD}} = c_M \Big/ \frac{m_{Au}}{m_{GD} \cdot N_A \cdot V} \quad (1)$$

where c_M and c_{GD} are the molarity of *p*NTP and GD nanoparticles, m_{Au} and m_{GD} refer to the mass of Au and one single GD nanoparticle, respectively. N_A is Avogadro's constant; V is the volume of GDs solution in the preparation process. According to the SEM images the diameter of gold nanoparticles is about 40 nm, and the molarity of the GDs solution is about 3.7×10^{-10} M. Consequently, there are approximately 1000, 100 and 10 molecules absorbed on a single nanoparticle dimer for the respective 10^{-7}, 10^{-8} and 10^{-9} M solutions. Since not all molecules can be absorbed on GDs in the experiment, the actual number of molecules on average will be even lower in the experiments. From the absence of dimerization in the low concentration case we can also conclude that the molecules do not cluster and are statistically absorbed on the GD surface. The average distance d between two molecules can be estimated as

$$d = R\sqrt{8\pi/n}. \quad (2)$$

R is the radius of the gold nanoparticle and n is the number of molecules absorbed on single nanoparticle dimer, which can be calculated by eqn (1). The calculated distances between two molecules of 10^{-7} and 10^{-8} M are ~3 nm and 10 nm, respectively, which is either close enough for two *p*NTP molecules to dimerize to DMAB or, more likely, at such distances collisions happen often enough for a dimerization. But for the 10^{-9} M solution, the average distance between two molecules is ~32 nm, which is obviously preventing the dimerization of two *p*NTP molecules. Thus, SERS spectra of separated *p*NTP and the absence of DMAB molecules at the lowest concentration used here can be explained.

Probably the most striking observation in the SERS experiments of *p*NTP at 10^{-9} M was an intensity decrease of the dominating band at 1332 cm^{-1} (ν_{NO_2}) over time. This peak disappeared after 10 min, simultaneously a new peak at 1017 cm^{-1} was detected after 5 min, as shown in Fig. 3(d)–(h). Since the NO_2 mode of *p*NTP disappeared, we hypothesize that the nitro group was cleaved from the benzene

 This journal is © The Royal Society of Chemistry 2015

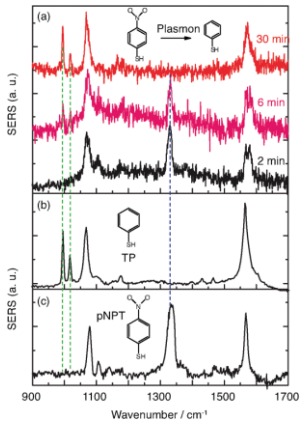

Fig. 4 (a) Time dependent SERS spectra of reacting *p*NTP ($c = 10^{-9}$ M) at 3 mW laser at 2, 6 and 30 min. (b) and (c) normal SERS spectra of TP and *p*NTP, respectively.

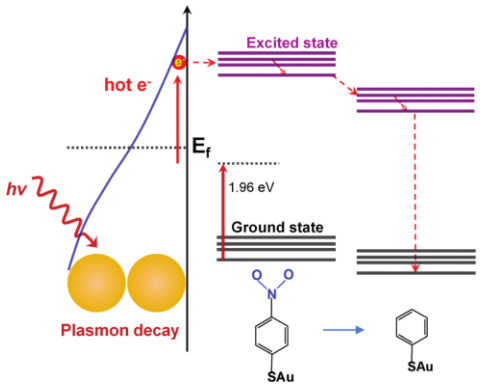

Fig. 5 Proposed mechanism of plasmon (hot electron) catalyzed dissociation of *p*NTP to TP.

ring in the *hot-spot* of the gold dimer resulting in the formation of thiophenol (TP). Comparing SERS spectra of neat TP (Fig. 4(b)) with "*p*NTP on GDs" spectra from late stages (see Fig. 4(a) and also Fig. 3(h)) it is obvious that the new bands at 995 (β_{CCC}) and 1017 (β_{CH}) cm^{-1} as well as the bands at 420 and 685 cm^{-1} in the low wavenumber region match those of TP strikingly well (see also ESI,† Fig. S3). The necessary hydrogen atom for the formation of TP was most probably abstracted from the surrounding water layer that was ubiquitously present since *p*NTP was adsorbed from aqueous solution and the experiment was performed under ambient conditions.

The experimental data demonstrate that a dissociation of *p*NTP to TP proceeds under our special SERS conditions at a concentration of 10^{-9} M (corresponding to a surface coverage of ~10 *p*NTP molecules per dimer). These results clearly differ from the dimerization reaction of *p*NTP to DMAB. The light induced dissociation of nitro substituted aromatic molecules is not new but usually requires drastic conditions. For example, the $-NO_2$ group in nitrobenzene and nitrophenol can be cleaved using UV excitation.[29–31] The required dissociation energy of the C–N bond is ~3.03 eV,[29] which is higher than the energy provided by the incident photon of 632.8 nm (1.96 eV). The power dependent experiments in Fig. 3 show no nonlinear increase of the products, so nonlinear optical effects including two/multi-photon absorption can be ruled out. Hence, the activation energy is too large to be simply overcome by the excitation laser. However, localized surface plasmons excited on silver or gold nanoparticle surfaces can decay non-radiatively into hot electrons with an energy between the vacuum energy and Fermi level (~−5 eV).[32–34] Hot electrons can scatter into an excited state of the absorbed molecules, triggering a chemical reaction by reducing the activation energy.[34] Applied to the present reaction our hypothesis is that plasmon-induced hot electrons initiate $-NO_2$ cleavage from the phenyl ring. A scheme of the proposed mechanism is shown in Fig. 5. Initially, hot electrons generated from plasmon decay on the nanoparticle surface, soon lose coherence and form a nonequilibrium Fermi–Dirac type distribution.[8] The hot electrons in the high energy level have sufficient energy to transfer to the excited state of *p*NTP molecule, creating a transient negative ion of *p*NTP. This negative ion "travels" to the excited state of TP and transfers the electron back to the GD surface, where it returns to the ground state of TP and dissociates.

It should be noted that the simultaneous detection of *p*NTP and TP in Fig. 4(a) – spectrum at 6 min – actually points to the presence of at least two molecules in the hot spot. Although the experiment was performed at a very low concentration it cannot be regarded as "single molecule" SERS in the classical sense. According to the time dependent SERS spectra, the peak intensity change *vs.* time is shown for the *p*NTP band at 1332 cm^{-1}, and the TP band at 1017 cm^{-1} in Fig. 6, respectively. It was found that three clear steps can be discerned: first, some molecules of *p*NTP were detected in the first 5 min of the measurement; after 5 min, half of the *p*NTP molecules reacted to TP; the remaining *p*NTP molecules reacted after 8 min. After that no significant change occurred in the remaining experiment (60 min). Consequently, it can be assumed that two distant, non-interacting molecules were detected in the hotspot of a single GD because both *p*NTP and TP were detected between 5–8 min. Apparently, the two molecules were too far apart from each other for an intermolecular reaction, and instead an intramolecular reaction was initiated. Because of the step-like reaction process, the other possibilities of having 4-2-0, 6-3-0, or 8-4-0 molecules synchronously reacting seem very unlikely. The involvement of even more molecules can be ruled out, as at 10 times higher concentration dimerization already starts.

In summary, we present the detection of a new plasmon catalyzed reaction of *p*NTP near the single molecule level. A dissociation of *p*NTP to TP was detected at low concentration where the distance between *p*NTP molecules adsorbed on single isolated gold dimer became too large for a dimerization reaction. In combination with the results with higher concentrations this further confirms a dimerization reaction of *p*NTP to DMAB. In accordance with previous reports we assume that plasmon-induced hot electrons provide the activation energy necessary for such a dissociation of *p*NTP. The tracked step-like

This journal is © The Royal Society of Chemistry 2015

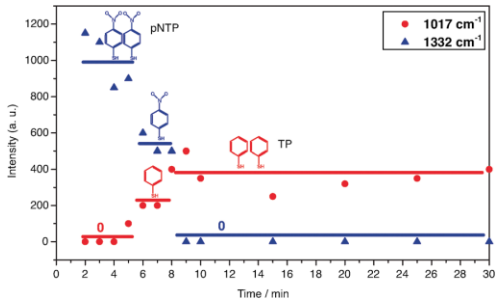

Fig. 6 Step-like process of the dissociation of *p*NTP to TP.

process of the dissociation of *p*NTP to TP strongly indicates a single molecule behavior. The results demonstrate that irradiation of an adsorbate in a gold nanoparticle gap can decrease the activation energy barrier such, that a reaction usually requiring UV light can be triggered in the visible.

We gratefully acknowledge support from the Deutsche Forschungsgemeinschaft (DEP4TERS, FR 1348/19-1) and the Thüringer Aufbau Bank (No. 2011SE9048). Z. Zhang acknowledges financial support from the Alexander von Humboldt foundation.

Notes and references

1 P. Christopher, H. L. Xin and S. Linic, *Nat. Chem.*, 2011, **3**, 467–472.
2 B. Dong, Y. R. Fang, X. W. Chen, H. X. Xu and M. T. Sun, *Langmuir*, 2011, **27**, 10677–10682.
3 E. M. van Schrojenstein Lantman, T. Deckert-Gaudig, A. J. G. Mank, V. Deckert and B. M. Weckhuysen, *Nat. Nanotechnol.*, 2012, **7**, 583–586.
4 M. T. Sun, Z. L. Zhang, H. R. Zheng and H. X. Xu, *Sci. Rep.*, 2012, **2**, 647.
5 V. Joseph, C. Engelbrekt, J. D. Zhang, U. Gernert, J. Ulstrup and J. Kneipp, *Angew. Chem., Int. Ed.*, 2012, **51**, 7592–7596.
6 M. T. Sun and H. X. Xu, *Small*, 2012, **8**, 2777–2786.
7 J. Lee, S. Mubeen, X. L. Ji, G. D. Stucky and M. Moskovits, *Nano Lett.*, 2012, **12**, 5014–5019.
8 S. Mukherjee, F. Libisch, N. Large, O. Neumann, L. V. Brown, J. Cheng, J. B. Lassiter, E. A. Carter, P. Nordlander and N. J. Halas, *Nano Lett.*, 2013, **13**, 240–247.
9 W. Xie, B. Walkenfort and S. Schlucker, *J. Am. Chem. Soc.*, 2013, **135**, 1657–1660.
10 M. T. Sun, Z. L. Zhang, Z. H. Kim, H. R. Zheng and H. X. Xu, *Chem. – Eur. J.*, 2013, **19**, 14958–14962.
11 K. Ueno and H. Misawa, *J. Photochem. Photobiol., C*, 2013, **15**, 31–52.
12 Z. L. Zhang, M. T. Sun, P. P. Ruan, H. R. Zheng and H. X. Xu, *Nanoscale*, 2013, **5**, 4151–4155.
13 S. Mukherjee, L. A. Zhou, A. M. Goodman, N. Large, C. Ayala-Orozco, Y. Zhang, P. Nordlander and N. J. Halas, *J. Am. Chem. Soc.*, 2014, **136**, 64–67.
14 E. M. v. S. Lantman, O. L. J. Gijzeman, A. J. G. Mank and B. M. Weckhuysen, *ChemCatChem*, 2014, **6**, 3342–3346.
15 Z. L. Zhang, S. X. Sheng, H. R. Zheng, H. X. Xu and M. T. Sun, *Nanoscale*, 2014, **6**, 4903–4908.
16 P. Singh and V. Deckert, *Chem. Commun.*, 2014, **50**, 11204–11207.
17 C. L. Wang and D. Astruc, *Chem. Soc. Rev.*, 2014, **43**, 7188–7216.
18 M. J. Kale, T. Avanesian and P. Christopher, *ACS Catal.*, 2014, **4**, 116–128.
19 X. J. Lang, X. D. Chen and J. C. Zhao, *Chem. Soc. Rev.*, 2014, **43**, 473–486.
20 D. L. Jeanmaire and R. P. Vanduyne, *J. Electroanal. Chem.*, 1977, **84**, 1–20.
21 P. L. Stiles, J. A. Dieringer, N. C. Shah and R. R. Van Duyne, *Annu. Rev. Anal. Chem.*, 2008, **1**, 601–626.
22 L. Li, T. Hutter, A. S. Finnemore, F. M. Huang, J. J. Baumberg, S. R. Elliott, U. Steiner and S. Mahajan, *Nano Lett.*, 2012, **12**, 4242–4246.
23 S. M. Nie and S. R. Emery, *Science*, 1997, **275**, 1102–1106.
24 K. Kneipp, Y. Wang, H. Kneipp, L. T. Perelman, I. Itzkan, R. Dasari and M. S. Feld, *Phys. Rev. Lett.*, 1997, **78**, 1667–1670.
25 H. X. Xu, J. Aizpurua, M. Kall and P. Apell, *Phys. Rev. E: Stat. Phys., Plasmas, Fluids, Relat. Interdiscip. Top.*, 2000, **62**, 4318–4324.
26 T. Deckert-Gaudig, E. Kammer and V. Deckert, *J. Biophotonics*, 2012, **5**, 215–219.
27 R. Zhang, Y. Zhang, Z. C. Dong, S. Jiang, C. Zhang, L. G. Chen, L. Zhang, Y. Liao, J. Aizpurua, Y. Luo, J. L. Yang and J. G. Hou, *Nature*, 2013, **498**, 82–86.
28 Z. L. Zhang, P. F. Yang, H. X. Xu and H. R. Zheng, *J. Appl. Phys.*, 2013, **113**, 033102.
29 M. L. Hause, N. Herath, R. S. Zhu, M. C. Lin and A. G. Suits, *Nat. Chem.*, 2011, **3**, 932–937.
30 B. Chen, C. Yang and N. K. Goh, *J. Environ. Sci.*, 2005, **17**, 598–604.
31 Y. M. Li, J. L. Sun, H. M. Yin, K. L. Han and G. Z. He, *J. Chem. Phys.*, 2003, **118**, 6244–6249.
32 M. W. Knight, H. Sobhani, P. Nordlander and N. J. Halas, *Science*, 2011, **332**, 702–704.
33 I. Goykhman, B. Desiatov, J. Khurgin, J. Shappir and U. Levy, *Nano Lett.*, 2011, **11**, 2219–2224.
34 A. O. Govorov, H. Zhang and Y. K. Gun'ko, *J. Phys. Chem. C*, 2013, **117**, 16616–16631.

 This journal is © The Royal Society of Chemistry 2015

Supporting Information

Single Molecule Level Plasmonic Catalysis - Dilution Study of p-Nitrothiophenol on Gold Dimers

Zhenglong Zhang,[a] Tanja Deckert-Gaudig,[a] Pushkar Singh,[a] Volker Deckert[a,b]*

[a]*Leibniz Institute of Photonic Technology, Albert-Einstein-Str. 9, 07745 Jena, Germany.*

[b]*Institute of Physical Chemistry and Abbe Center of Photonics, Friedrich-Schiller University Jena, Helmholtzweg 4, 07743 Jena, Germany.*

* Corresponding authors.

Email: volker.deckert@ipht-jena.de

Experimental details and 3 Figures.

Experimental details

Sample preparation. SERS active gold nanoparticle dimers were prepared using a wet chemistry method (J Appl Phys, 2013, 113, 033102.). 200 µl of GD colloid solutions were added to 200 µl of pNTP in aqueous solution ($c = 5 \times 10^{-7} – 10^{-9}$ M) for 2 hours. Then, 20 µl of the mixture were spin-coated onto cleaned glass slides marked with position indicators, then dried in vacuum.

Measurements. SERS measurements were performed on an inverted microscope with a ×100 objective (NA=0.9, Olympus, Japan), using 632.8 nm laser excitation with a laser spot size of ~1 µm. All spectra were obtained from a single nanoparticle dimer placed in the center of the laser spot. A notch filter was placed in front of the entrance of the spectrometer (SP2750i, Princeton Instruments, USA), and Raman spectra were detected using a CCD detector (PIXIS400, Princeton Instruments, USA) with an acquisition time of 10 s. All spectra shown are raw and untreated data, only a linear baseline correction was applied for presentation.

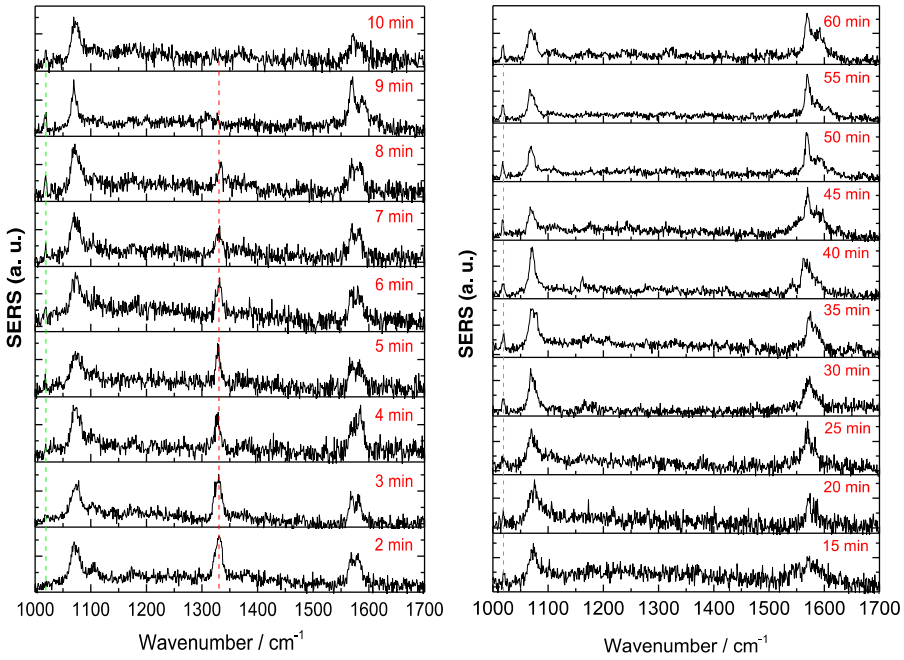

Figure S1. Time dependent SERS spectra of pNTP (c=10^{-9} M). The dominating band at 1332 cm^{-1} (ν_{NO2}) decreased and disappeared within 10 min, simultaneously, a new peak at 1017 cm^{-1} was detected after 5 min.

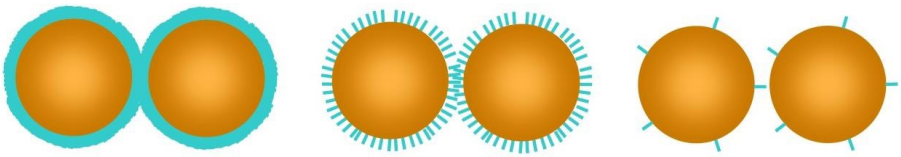

5×10^{-7}M **5×10^{-8}M** **5×10^{-9}M**

Figure S2. Representation of number of molecules absorbed on gold dimers. About 1000, 100, and 10 molecules absorbed on a gold dimer for the concentrations of 5×10^{-7}, 10^{-8} and 10^{-9} M, respectively.

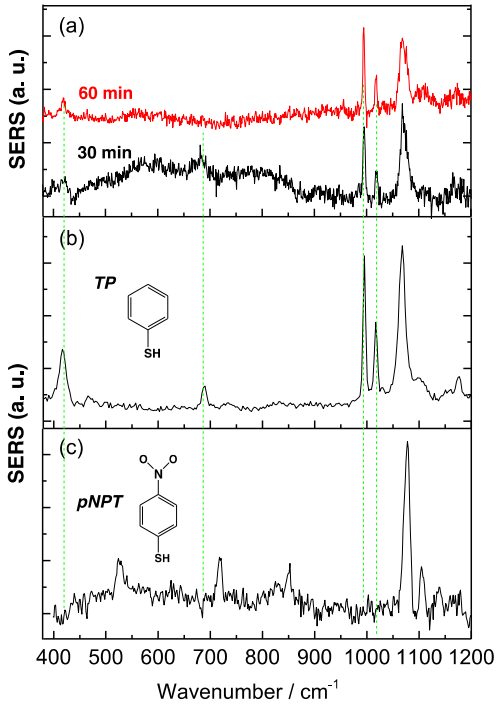

Figure S3. Comparison of low wavenumber SERS spectra of pNTP and TP with spectra recorded during the experiment on a single gold dimer. (a) time dependent SERS spectra of reacted pNTP (c = 10^{-9} M) at 3 mW laser at 30 and 60 min. Normal SERS spectra and corresponding molecular structures of TP and pNTP are shown in (b) and (c), respectively.

4.5 Further Publications

[PS05] T. Deckert-Gaudig, D. Kurouski, M. A. B. Hedegaard, P. Singh, I. Lednev, V. Deckert, Spatially resolved spectroscopic differentiation of hydrophilic and hydrophobic domains on individual insulin amyloid fibrils, *Sci. Rep.,* **6**, 33575 (2016).

[PS06] D. Gangopadhyay, P. Sharma, S. K. Singh, P. Singh, V. Deckert, J. Popp and R. K. Singh, Surface Enhanced Raman Scattering based reaction mechanism of in vitro decyclization of creatinine →creatine, *RSC. Adv.,***6**, 58943 (2016).

[PS07] O. Prakash, S. Kumar, P. Singh, V. Deckert, S. Chatterjee, A.K. Ghosh and R. K. Singh, Surface-enhanced Raman scattering characteristics of CuO:Mn/Ag heterojunction probed by methyl orange: Effect of Mn^{2+} doping, *J. Raman Spectrosc.*, **47**, 813 (2016).

[PS08] A. Gopal, A. H. Woldegeorgis, P. Singh, S. Herzer, W. Ziegler, T. May and G. G. Paulus, Smith–Purcell radiation in the terahertz regime using charged particle beams from laser–matter interactions*, Laser Part. Beams*, **34**, 187 (2016).

[PS09] V. Deckert, T. Deckert-Gaudig, M. Diegel, I. Götz, L. Langelüddecke, H. Schneidewind, G. Sharma, P. Singh, P. Singh, S. Trautmann, M. Zeisbergera and Z. Zhang, Spatial resolution in Raman spectroscopy, *Faraday Discuss.,* **177**, 9-20 (2015).

[PS10] O. Prakash, P. Gautam, S. Kumar, P. Singh, R. K. Dani, M. K. Bharty, N. K. Singh, A. K. Ghosh, V. Deckert and R. K. Singh, Surface enhanced Raman scattering investigation of two novel piperazine carbodithioic acids adsorbed on Ag and ZnO nanoparticles, *RSC Adv.,* **5,** 5571-5579 (2015).

[PS11] D. Gangopadhyay, P. Sharma, S. Singh, P. Singh, N. Tarcea, V. Deckert, J. Popp and R. Singh, Raman spectroscopic approach to

monitor the in vitro cyclization of creatine → creatinine, *Chem. Phys. Lett.,* **618**, 225-230 (2015).

[PS12] P. Sharma, D. Gangopadhyay, P. Singh, P. C. Mishra, V. Deckert, J. Popp and R. K. Singh, In vitro monitoring of ring opening of leflunomide: A surface enhanced Raman scattering and DFT based approach, *Chem. Phys. Lett.*, **613**, 127-132 (2014).

[PS13] A. Gopal, P. Singh, S. Herzer, A. Reinhard, A. Schmidt, U. Dillner, T. May, H.-G. Meyer, W. Ziegler, and G. G. Paulus, Characterization of 700 μJ T rays generated during high-power laser solid interaction, *Opt. Lett.,* **38**, 4705-4707 (2013).

[PS14] A. Gopal, S. Herzer, A. Schmidt, P. Singh, A. Reinhard, W. Ziegler, D. Brömmel, A. Karmakar, P. Gibbon, U. Dillner, T. May, H. G. Meyer, and G. G. Paulus**,** Observation of Gigawatt-Class THz Pulses from a Compact Laser-Driven Particle Accelerator, *Phys. Rev. Lett.,* **111**, 074802 (2013).

4.6 Acknowledgement

First, I would like to thank my supervisor Prof. Volker Deckert for giving me an opportunity to make this work within his group. He opened the door to the wonderful field of nano-spectroscopy and provided me freedom in the investigations of interesting research problems. He not only provided insightful discussions about the research but also continuous support throughout this work.

I would specially like to thank Dr. Tanja Deckert-Gaudig for answering not only scientific questions but also multiple personal questions. I thank her for introducing me to TERS instrument and also spending a significant amount of time in helping me to improve the text of my manuscripts and thesis.

I thank Prof. Jürgen Popp for his support during this work in IPHT and IPC and PD Dr. Wolfgang Fritzsche for being my second supervisor.

I like to thank Dr. Zhenglong Zhang for his intuition in the single molecule level plasmonic reaction experiment and for the very stimulating discussions.

I also like to thank Dr. Marko Diegel for helping me to develop multicolor TERS setup, especially for organizing the optical components.

I thank Dr. Henrik Schneidwind and Mr. Konstantin Kirsch for coating the TERS tips and SERS substrates for different measurements.

Many thanks to all my colleagues from nanospectroscopy group, both past and present, for the support and cooperation. I sincerely acknowledge my office colleagues Lucas Langelüddecke, Steffen Trautmann, Gaurav Sharma, Isabell Götz, Robert Meyer and Dr. Ludovic Roussille for the pleasant working atmosphere; Dr. D. Bender for his help with computers; Mr. W. Fähndrich, Mr. F. Lange and Mr. M Schmäche for their help with mechanics; Mrs. B. Schäfer and Ms. A. Raabe for their help with administrative duties.

Last but most importantly, special thanks to my whole family: my wife Prabha, son Lavlesh, daughter Aahana, parents and brother for their love, support throughout the years, and help me to achieve my goals.

4.7 Further Outlook

As future work, there are many research directions for extending the presented work. There are some ideas which should be pursued, For example;

Since number of molecules and experimental geometry is different in SERS and TERS so one cannot directly compare the results, two different strategies can be used for the direct comparison of data

1) Keep the experimental geometry same and change the number of plasmon excited molecule.
2) Change the experimental geometry and keep the number plasmon excited molecules.

Very fast protonation and deprotonation in TERS compared to SERS need further investigation to understand the time correlation with the geometry of experiment and also for the precise determination of reaction time required in a particular TERS experiment. For the rate determination pico- or femtosecond time resolved experiment are needed which can provide further detail about fundamental physics involved in such processes.

The multicolor lab allows to measure the TERS signal from five different laser wavelengths, in particular the preparation time for an experiment will be considerably reduced by adjustable optical parts. As plasmon induced reaction are very sensitive to incident light wavelength, multicolor lab could be used to determine the wavelength dependent reaction threshold to initiate the reaction. This will provide a pathway for improving the efficiency of plasmon induced reactions.

Curriculum Vitae

Pushkar Singh
Bartning Str. 15
64289, Darmstadt
Germany

Employment

06.2016- Present	**Mitarbeiter,** JASCO Deutschland GmbH, Darmstadt, Germany
09.2012-05.2016	**Wissenschaftlicher Mitarbeiter**, Leibniz-Institut for Photonic Technology, Jena, Germany
03.2012- 08.2012	**Wissenschaftlicher Mitarbeiter**, Department of Physics**,** Friedrich-Schiller-Universität Jena, Germany
06.2005- 12.2010	**Research Assistant,** Max-Born-Institute, Berlin, Gemany
07.2003- 05.2005	**Physicist**, Department of Physics and Material Science, Jaypee Institute of Information Technology Noida, India

Education

07.2001- 06.2003	**Master of Technology** (Optoelectronics and Optical Communication**)** Indian Institute of Technology, New Delhi, India
07.1998- 06.2000	**Master of Science** (Physics**)** Indian Institute of Technology**,** Roorkee, India

Achievements

- Ministry of Human Resource Development (MHRD) fellowship during Master of Technology program, Indian Institute of Technology Delhi, India
- Qualified Graduate Aptitude Test in Engineering (GATE) 2000, organized by Indian Institute of Technology Kanpur, India
- Qualified National Eligibility Test (NET), organized by Council of Scientific & Industrial Research, Government of India

Selbständigkeitserklärung

ich erkläre, dass ich die vorliegende Arbeit selbständig und unter Verwendung der angegebenen Hilfsmittel, persönlichen Mitteilungen und Quellen angefertigt habe.

Ort, Datum, Unterschrift des Verfassers

Erklärung zu den Eigenanteilen

Die Co-Autorinnen/-Autoren der in dieser kumulativen Dissertation verwendeten Manuskripte sind sowohl über die Nutzung, als auch über die oben angegebenen Eigenanteile der weiteren Doktorandin-nen/Doktoranden als Co-Autorinnen/-Autoren an den Publikationen und Zweitpublikationsrechten bei einer kumulativen Dissertation informiert und stimmen dem zu.

Die Anteile der Promovendin/des Promovenden sowie der weiteren Doktorandinnen/Doktoranden als Co-Autorinnen/Co-Autoren an den Publikationen und Zweitpublikationsrechten bei einer kumulativen Dissertation sind in der Anlage aufgeführt.

Name der Promovendin/ des Promovenden	Datum	Ort	Unterschrift

Ich bin mit der Abfassung der Dissertation als publikationsbasierte Dissertation, d.h. kumulativ, einver-standen und bestätige die vorstehenden Angaben.

Name Betreuerin/ Betreuer	Datum	Ort	Unterschrift

Name Betreuerin/ Betreuer	Datum	Ort	Unterschrift